



# **R-type currents in *Arabidopsis* guard cells: properties and molecular nature.**

(R-type Ströme in *Arabidopsis* Schließzellen: Eigenschaften und molekularer Hintergrund.)

Dissertation on the attainment of a doctorate in natural sciences  
Julius-Maximilians-Universität Würzburg,  
submitted by

**JUSTYNA JOANNA JAŚLAN**

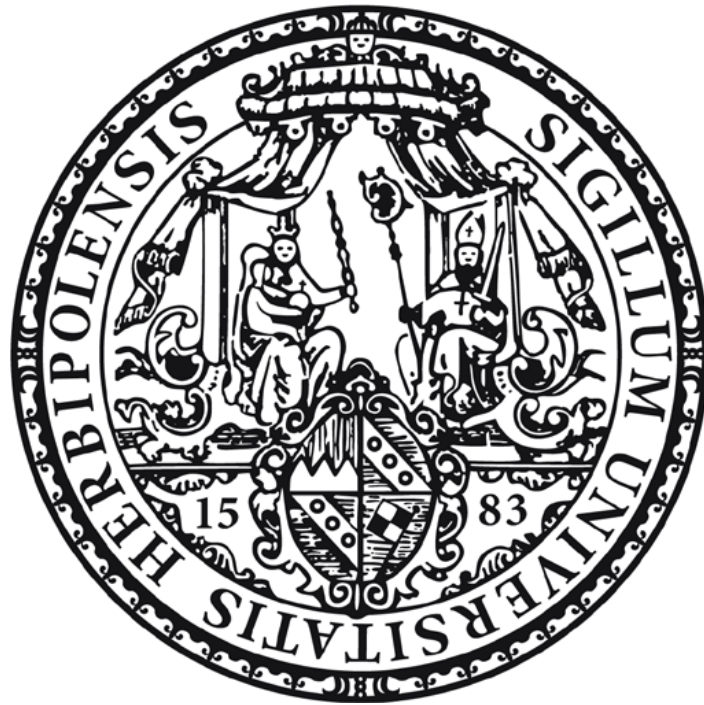
from

**Lublin**

Würzburg 2019







# **R-type currents in *Arabidopsis* guard cells: properties and molecular nature.**

(R-type Ströme in *Arabidopsis* Schließzellen: Eigenschaften und molekularer Hintergrund)

Dissertation on the attainment of a doctorate in natural sciences  
Julius-Maximilians-Universität Würzburg,  
submitted by

**JUSTYNA JOANNA JAŚLAN**

from

**Lublin**

Würzburg 2019



**Submitted on:** .....

Office stamp

**Members of the *Promotions committee*:**

**Chairperson:** .....

**Primary referee:** Prof. Dr. Rainer Hedrich

**Second referee:** Prof. Dr. Erhard Wischmeyer

**Date of Public Defence:** .....

**Date of Receipt of Certificates:** .....

**“One, remember to look up at the stars and not down at your feet.  
Two, never give up work. Work gives you meaning, and purpose and life is empty without it.  
Three, if you are lucky enough to find love, remember it is there and don’t throw it away.”**

**Stephen Hawking**

# Table of contents

1. Introduction.....	1
1.1. Mouths of the leaves - stomata.....	1
1.2. Stomatal movements are regulated by multiple factors .....	2
1.3. Potassium transport across plasma membrane .....	6
1.4. Anion transport across plasma membrane .....	8
1.4.1. The SLAC1 family.....	10
1.4.2. The ALMT family .....	12
2. Aim of the study .....	17
3. Material and methods.....	19
3.1. Plant material .....	19
3.1.1. Growth conditions .....	19
3.1.2. Isolation of guard cell protoplasts .....	19
3.2. Patch clamp technique .....	21
3.2.1. Patch clamp configurations .....	21
3.2.2. Patch clamp set-up.....	23
3.2.3. Measuring and reference electrodes.....	24
3.2.4. Preparation of the measuring glass microelectrode .....	25
3.2.5. Running the patch clamp measurements.....	26
3.2.6. Sign convention for ionic currents.....	26
3.2.7. Liquid junction potential.....	27
3.2.8. Voltage pulse protocol.....	27
3.2.9. Data analysis .....	28
3.2.10. Measuring patch clamp solutions.....	31

3.3. Quantitative Real-Time PCR .....	34
3.3.1. Enzymatic isolation of guard cell protoplasts .....	34
3.3.2. RNA isolation from plant material .....	34
3.3.3. Reverse Transcription .....	35
3.3.4. Quantitative real-time polymerase chain reaction (qRT-PCR) .....	35
3.3.5. Primers for Quantitative Real-time Polymerase Chain Reaction.....	37
3.3.6. Cyclor-Program for Quantitative Real-time Polymerase Chain Reaction.....	38
3.4. Genotyping loss-of-function mutants.....	38
3.4.1. DNA Isolation .....	39
3.4.2. Cyclor-Program for Polymerase Chain Reaction.....	41
4. Results .....	42
4.1. Residual R-type anion currents in the <i>almt12</i> mutant.....	42
4.1.1. Basic characterization of residual R-type anion currents .....	42
4.1.2. ATP affects R-type background currents .....	45
4.1.3. Calcium-dependent behavior of QUAC-like currents .....	47
4.1.4. ALMT genes expressed in guard cells of Col0 and the <i>almt12</i> mutant .....	49
4.2. <i>almt12/13</i> and <i>almt12/14</i> double loss-of-function mutants .....	50
4.3. Differences between Col0 and WS R-type currents .....	53
4.3.1. Expression of prominent R- and S- type channels in Col0 and WS.....	54
4.3.2. Calcium-dependent QUAC current in the WS ecotype.....	55
4.3.3. Chloride currents in <i>Arabidopsis thaliana</i> guard cell protoplasts .....	56
4.3.4. ATP and its derivative AMP-PNP blocks R-type anion channels.....	58
5. Discussion .....	61
5.1. <i>ALMT13</i> and <i>ALMT14</i> as genes involved in the generation of R-type anion currents..	61
5.2. A rise in cytosolic ATP reduces R-type anion currents in <i>A.thaliana</i> guard cells .....	63
5.3. Residual QUAC current in the <i>almt12</i> mutant is dependent on cytosolic calcium.....	66



5.4. Chloride permeability of <i>A. thaliana</i> R-type anion channels in the native environment .....	69
5.5. Col0 versus WS - features of anion currents associated with expression of the S- and R-type channels .....	71
5.6. The role of ALMT12-14 in stomatal closure during drought stress.....	73
6. Summary.....	75
7. Zusammenfassung.....	77
8. Table list .....	79
9. Figure list .....	80
10. References.....	81
11. Glossary .....	104
12. Supplementary information .....	106
13. Curriculum Vitae.....	111
14. Publication list .....	112
15. Acknowledgements .....	113
16. Affidavit in English and German .....	114

# 1. Introduction

## 1.1. Mouths of the leaves - stomata

Stomata are defined as microscopic holes located on plant epidermis, which enable the communication between the interior and exterior plant environment. They allow plants to regulate gas exchange and control water loss in response to environmental signals (Sirichandra C. et al., 2009, Voss L. J. et al., 2018). Due to their role in water loss control, stomata were indispensable for plant landfall during plant evolution. They were found in plants fossils dated over 400 million years ago. The most primitive plants with stomata living on Earth today are the mosses and hornworts (Paton J. A. and Pearce J. V., 1957, Raven J. A., 2002, Hetherington A. M. and Woodward F. I., 2003, Susmilch F. C. et al., 2018). Stomata are built by two specialized epidermal cells, which create the stomatal pore. The so-called „guard cells” are formed in the late stages of leaf and cotyledon differentiation, as a result of asymmetric division of some epidermal mother cells (Willmer C. M. and Fricker M., 1996, Geisler M. et al., 2003, Nadeau J. and Sack F., 2003). In the plant kingdom, there are a few different types of stomata. The two most representative types are the **Graminean** and the **Amaryllis** types. The **Graminean type (Figure 1)** is present in grasses and some monocotyledons. The Graminean stoma type has dumb-bell shaped guard cells, which are narrow in the middle and have wider vesicular ends (Willmer C. M. and Fricker M., 1996, Hetherington A. M. and Woodward F. I., 2003). These stomata are surrounded by subsidiary cells that support their movement (Raschke K. and Fellows M. P., 1971, Wilson J. A. et al., 1978, Willmer C. M. and Fricker M., 1996, Franks P. J. and Farquhar G. D., 2007). The **Amaryllis stomata type** is present in dicotyledons and remaining monocotyledons, gymnosperms, mosses and ferns. This type of stomata (**Figure 1**) has kidney-shaped guard cells, which are surrounded by the epidermal pavement cells rather than by subsidiary cells (Willmer C. M. and Fricker M., 1996, Hetherington A. M. and Woodward F. I., 2003). Stomatal distribution on the leaf surface depends on the environment in which plants are growing. Monocotyledons and some dicotyledons (e.g. Caryophyllaceae) have amphistomatic leaves with stomata on both sides of leaves. The majority of dicotyledons have hypostomatic leaves. In this leaf type

stomata are present on the abaxial (lower) surface. However, water plants have epistomatic leaves with stomata only on the adaxial (upper) surface (Willmer C. M. and Fricker M., 1996, Muir C. D., 2015, Richardson F. et al., 2017).

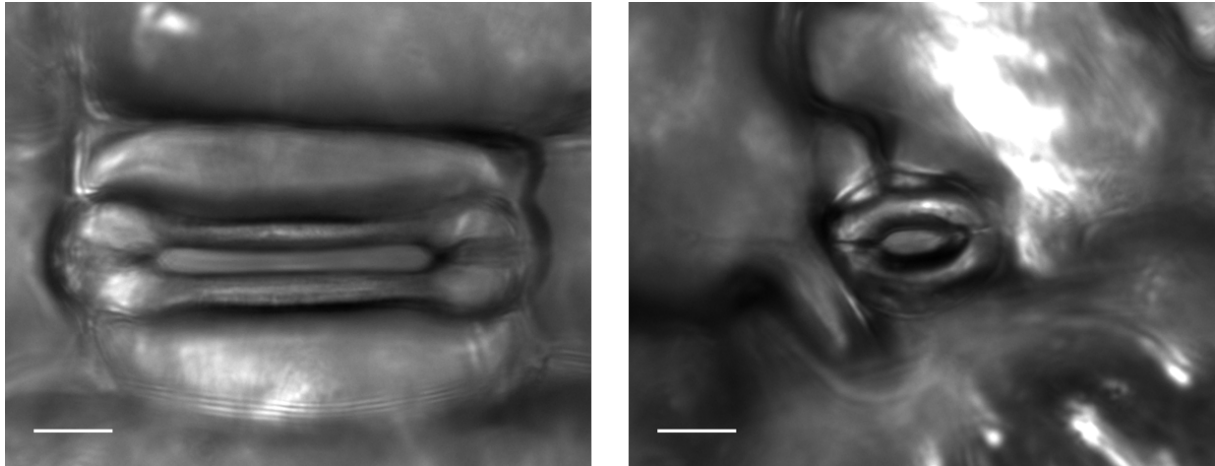


**Figure 1. Morphological types of stomata.**

Picture located on the left side present Graminean type of stoma from Barley (*Hordeum vulgare*). The right picture shows Amaryllid stomata type present in *Arabidopsis thaliana*. Scale bar = 10  $\mu$ M.

## 1.2. Stomatal movements are regulated by multiple factors

The stomata pore width is regulated by variation in light intensity, relative humidity, temperature, atmospheric CO<sub>2</sub> concentration and plant hormones, such as ABA (abscisic acid). This ability allows plants to adapt to variable environmental conditions (Hetherington A. M. and Woodward F. I., 2003, Kopcewicz J. and Lewak S., 2002, Shope J. et al., 2003, Gao X-Q. et al., 2005, Roelfsema M. R. G. and Hedrich R., 2016).

**Light promotes stomata opening.** Blue and red light can be detected by several photoreceptors (Franklin K. A. et al., 2005, Christie J. M. et al., 2007). Red light is a trigger and an energy source. It can induce stomatal opening by driving photosynthesis in mesophyll and guard cell chloroplasts (Wang Y. et al., 2014). Blue light acts only as a trigger of stomata movement. Zeiger and Hepler demonstrated, that all components necessary for stomatal response to blue light are present in guard cells (Zeiger E. and Hepler R., 1977). Short blue-light pulse (30 to 60 s) is enough to induce stomatal opening in C<sub>3</sub> and C<sub>4</sub> plants (Iino M.

et al., 1985, Lee D. M. and Assmann S. M., 1992). The blue light pulse is absorbed by the blue-light receptors phototropin 1 (PHOT1) and phototropin 2 (PHOT2), which are light-responsive serine/threonine protein kinases (Christie J.M. et al., 1999, Briggs W. R. et al., 2001, Kinoshita T. et al., 2001). After light absorption PHOT1 and PHOT2 activates itself via autophosphorylation and reversibly binds to a 14-3-3 protein (Kinoshita T. et al., 2001, Kinoshita T. et al., 2003, Christie J. M. et al., 2007). An active phototropin-14-3-3 complex transmits the blue light signal to the plasma membrane H<sup>+</sup>-ATPase (Kinoshita T. et al., 2001, Christie J. M. et al., 2007, Shimazaki K. et al., 2007). The protein phosphatase 1 (PP1) which belongs to the PPP (phosphoprotein phosphatase) family of serine/threonine protein phosphatases, can mediate signals between phototropins and H<sup>+</sup>-ATPases, which has been studied in *Vicia faba* guard cells (Takemiya A. et al., 2006). To activate H<sup>+</sup>-ATPases, two factors are necessary: phosphorylation of the threonine residue in the C-terminus of the pump and a binding of a 14-3-3 protein to the phosphorylation site (Kinoshita T. et al., 1999, Emi T. et al., 2001). The ATP is delivered as an energy source for H<sup>+</sup>-ATPase proton pumps. They generate the proton gradient and hyperpolarise the plasma membrane of guard cells. Inward-rectifying K<sup>+</sup> channels activate in hyperpolarized ranges of plasma membrane and allow K<sup>+</sup> ions to flow into the guard cells (Roelfsema M. R. G. and Hedrich R., 2005). At the same time anions such as Cl<sup>-</sup> and NO<sub>3</sub><sup>-</sup> are acquired from the apoplast through anion/H<sup>+</sup> symporters (Schroeder J. I. et al., 2001). Furthermore, malate is synthesized in the cytosol (MacRobbie E. A. C., 1980, Raschke K., 1979, Raschke K., 1988, Roelfsema M. R. G. and Hedrich R., 2005). Due to the accumulation of potassium, chloride and malate ions, the water potential in guard cells decreases (MacRobbie E. A. C., 1980, Raschke K., 1979). This causes the osmotic flow of water into the guard cells, which results in an increased volume by approximately 40% (value determined for *Vicia faba*) and finally stomatal opening (MacRobbie E. A. C., 1980, Shope J. C. et al., 2003, Gao X. Q. et al., 2005, Roelfsema M. R. G. and Hedrich R., 2005).

**Effect of tropospheric ozone** on stomatal movement was for the first time demonstrated in 1999 by Thorsethaugen G. and colleagues. With the help of the patch clamp technique they could show that O<sub>3</sub> inhibits inward-potassium channels which mediate K<sup>+</sup> influx into the cell during stomatal opening (Thorsethaugen G. et al., 1999). This phytotoxic pollutant enters the leaf mainly via open stomata (Brosché M. et al., 2010). In the apoplast, O<sub>3</sub> is degraded into reactive oxygen species, which are involved in several signalling pathways leading to stomatal

closure (Vahisalu T. et al., 2010, Wilkinson S. et al., 2012, Kollist H. et al., 2014). The toxic influence of ozone on plants trigger fast stomatal closure (within 10 min) or impaired control of stomatal movement, called “stomatal sluggishness” (Kollist H. et al., 2007, Vahisalu T. et al., 2010, Hoshika Y. et al., 2017). This allows plants to reduce the amount of ozone entering and acclimate to its concentration (Vaultier M -N. et al., 2014). Depending on the concentration, O<sub>3</sub> can lead to chronic or acute plant stress (Vaultier M -N. et al., 2014). The visible effect of ozone induced acute stress are injuries on the leaf surface such as chlorosis and necrosis (Wilkinson S. et al., 2012).

**Elevated atmospheric CO<sub>2</sub> caused reduction in stomatal aperture.** This finding was for the first time described by Freudenberger H. and Heath O. V. S. (Freudenberger H., 1940, Heath O. V. S., 1948). Later Fitzsimons P. and Weyers J. demonstrated that isolated guard cell protoplasts can change turgor by shrinking and swelling in response to CO<sub>2</sub> concentration. Low atmospheric CO<sub>2</sub> leads to stomatal opening. The opposite effect - stomatal closure - was observed under conditions of high atmospheric CO<sub>2</sub> (Fitzsimons P. J. and Weyers J. D. B., 1986, Engineer C. B. et al., 2016). The work of Fitzsimons P. and Weyers J. was one of the first which showed that all components of the CO<sub>2</sub> signalling pathway are present in guard cells (Fitzsimons P. J. and Weyers J. D. B., 1986, Engineer C. B. et al., 2016). More specifically, this response depends on intercellular CO<sub>2</sub> concentration, which is determined by atmospheric CO<sub>2</sub> concentration and the mesophyll assimilation rate (Mott 1988, Vavasseur A. and Raghavendra A. S., 2005).

**Abscisic acid (ABA)** is a plant stress hormone. In terms of its chemical structure - ABA is a 15-carbon, weak, organic acid (C<sub>15</sub>H<sub>20</sub>O<sub>4</sub>) and belongs to the sesquiterpenes class (Geiger D. et al., 2011, Finkelstein R., 2013). Abscisic acid is synthesized in the mevalonic acid pathway or by the oxidative carotenoid degradation in the vasculature, guard cells of the vegetative part of the plants and all seed tissues (Finkelstein R., 2013, Boursiac Y. et al., 2013). It was isolated for the first time in 1963 by Frederick Addicott from cotton fruit (Zeevaart J. A. D., 1999). ABA transport occurs via diffusion and by ABA transporters, like e.g. AtABCG25 and AtABCG40, which belong to the ATP-binding cassette (ABC) transporters family (Boursiac Y. et al., 2013). ABA can be transported via the xylem from roots to shoots or via phloem from leaves to roots (McAdam S. A. M. et al., 2016, Li W. et al., 2017). It regulates physiological and

developmental processes, including response to biotic and abiotic stress e.g. drought, salinity, cold, pathogens (Finkelstein R., 2013).

This plant stress hormone (ABA) can activate  $\text{Ca}^{2+}$ -permeable channels, which allow  $\text{Ca}^{2+}$  translocation from the apoplast and intracellular reservoirs (i.e. vacuole) into the cytoplasm (McAinsh M. R. et al., 1990, Schroeder J. I. et al., 2001, Roelfsema M. R. G. and Hedrich R., 2004, Jammes F. et al., 2011, Bauer H. et al., 2013). Increased  $\text{Ca}^{2+}$  concentration in the cytoplasm inhibits the  $\text{H}^+$ -ATPase proton pumps and inward-rectifying  $\text{K}^+$  channels (Kinoshita T. et al., 1995, Schroeder J. I. et al., 2001). Moreover, both ABA and  $\text{Ca}^{2+}$  ions promotes activity of anion channels, which depolarize the guard cells plasma membrane and activate outward-rectifying  $\text{K}^+$  channels. Active outward-rectifying  $\text{K}^+$  channels mediate  $\text{K}^+$  efflux from guard cells, which is promoted by cytosolic alkalisation (approximately 0.2 pH units), related to a rise in ABA levels (Schroeder J. I. et al., 1987, Schroeder J. I. and Hagiwara S., 1989, Keller B. U. et al., 1989, Hedrich R. et al., 1990, Irving H. R. et al., 1992, Linder B. and Raschke K., 1992, Schroeder J. I. et al., 1992, Blatt M. R. and Armstrong F., 1993, Roelfsema M. R. G. et al. 2004). Release of  $\text{K}^+$ ,  $\text{Cl}^-$  and organic ions (for example malate<sup>2-</sup>) results in increased water potential, water efflux from guard cells and finally stomatal closure (Hedrich R. et al., 1990, Pandey S. et al., 2007).

During drought, ABA induces two signalling pathways in guard cells, which leads to stomatal closure (Geiger D. et al., 2011). The slow signalling pathway lasts from several minutes to hours. It is related to gene expression responsible for plant adaptation to drought conditions (Kline K. G. et al., 2010, Geiger D. et al., 2011). The fast signalling pathway lasts a few seconds to several minutes and ends with stomatal closure by activation of R-type (ALMT12) and S-type anion channels (SLAH3 and SLAC1) as well as the blocking of inward-rectifying  $\text{K}^+$  channels (KAT1) (Geiger D. et al., 2011). ABA participates in S-type anion channel activation by stimulating its phosphorylation process via the  $\text{Ca}^{2+}$ -dependent and  $\text{Ca}^{2+}$ -independent kinases, which has been shown independently for *Arabidopsis thaliana* (Pei Z-M. et al.,1997), *Vicia faba* (Schwarz M. and Schroeder J. I., 1998, Leonhardt N. et al., 1999, Li J. et al., 2000) and *Nicotiana tobacco* (Grabov A. et al., 1997). The fast signalling pathway (**Figure 2**) starts with ABA perception in the cytoplasm by the Pyr/Pyl/RCAR receptors (**Py**rabactin Resistance / **PYR1** Like / **R**egulatory **C**omponent of **A**BA **R**eceptor; **Figure 2**) (Park S. Y. et al.,2009, Geiger D. et al., 2009, 2010, 2011, Peterson F. C. et al., 2010, Hedrich R., 2012). Subsequently, active

Pyr/Pyl/RCAR receptors deactivate the ABI1 and ABI2 (**ABA-insensitive 1** and **2**) proteins (Ma Y, et al., 2009, Park S-Y. et al., 2009). These proteins belong to the type **2C** protein phosphatase (PP2C) family and inhibit autophosphorylation of **Ca<sup>2+</sup>-dependent protein kinases** (CPKs) and OST1 (**O**pen **S**tomata **1**), which is a Ca<sup>2+</sup>-independent kinase (Geiger D. et al., 2009, 2010, 2011, Hedrich R., 2012). Active CPKs and OST1 phosphorylate S-type anion channels in a calcium-dependent and calcium-independent manner respectively (Geiger D. et al., 2011).

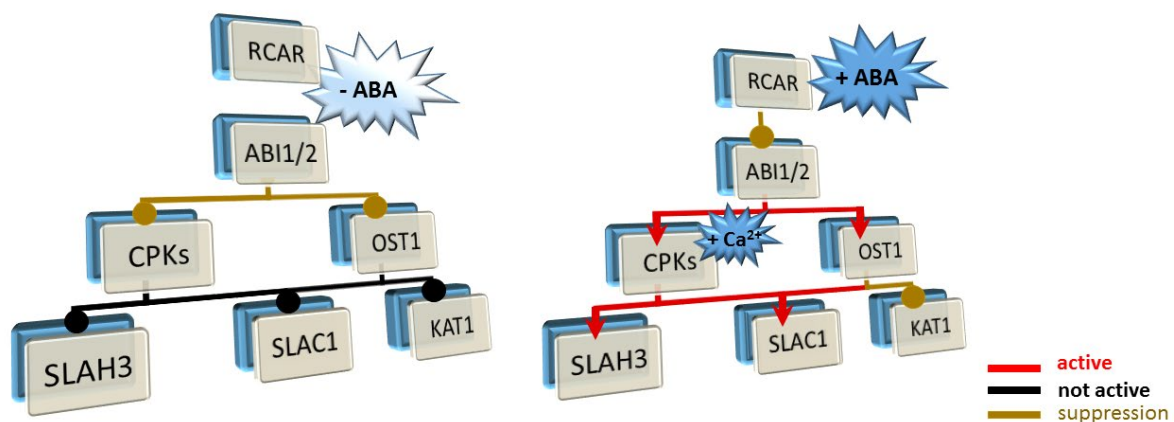


**Figure 2. Protein cascade of quick ABA response leading to stomatal closure.**

ABI1 and ABI2 phosphatases are responsible for negative regulation of ABA signalling. ABA deactivate ABI1 and ABI2 phosphatases what result in CPKs and OST1 autophosphorylation and S-type anion channels – SLAH3 and SLAC1 – activation (Hedrich R., 2012). Figure has been prepared based on Geiger D. et al., 2011.

### 1.3. Potassium transport across plasma membrane

Potassium ions are the main ingredient of the plant cytosol. They are used for osmoregulation and control of the cell membrane potential (Lebaudy A et al., 2007). In the *Arabidopsis thaliana* genome, at least 35 genes encode the cellular system of K<sup>+</sup> transport (Lebaudy A. et al., 2007). Inward and outward-rectifying K<sup>+</sup> channels enable the cell to take up and release K<sup>+</sup> ions during stomatal opening and closure (Schroeder J. I., 1988). These multimeric proteins consist of transmembrane domains and cytosolic N- and C-terminal parts. In the functional

channel, four pore domains form a pore region of the potassium channel, containing a highly selective filter (Lebaudy A. et al., 2007). Considering the gene sequence, structure and function of the proteins, the Shaker family K<sup>+</sup> channels can be subdivided into 5 groups (**Figure 3**). Four groups comprise inward-rectifying potassium channels: e.g. AKT1, KAT1, AKT2 and regulatory subunit AtKC1, which are expressed in the guard cells of *Arabidopsis thaliana* plants (Szyroki A. et al., 2001).

The first and second group includes genes coding some of the first potassium channels identified in *Arabidopsis thaliana* in 1992 - AKT1 (*A*rabidopsis *t*haliana **K**<sup>+</sup> **T**ransporter **1**) and KAT1 (**K**<sup>+</sup> Channel *A*rabidopsis *t*haliana **1**) (Sentenac H. et al., 1992, Anderson J. A. et al., 1992). These inward-rectifying potassium channels are active at negative potentials during cell membrane hyperpolarization. They are conducting potassium ions into the cell and their gating is largely independent of potassium ion concentration (Schroeder J. I. et al., 1987, Kourie J. and Goldsmith M. H., 1992, Schachtman D. P. et al., 1992, Hedrich R., 2012). KAT1 is highly expressed in *Arabidopsis thaliana* guard cells. It has been shown, that knockout of the KAT1 channel decreased potassium inflow into the guard cells by 50% (Szyroki A. et al., 2001). However, the KAT1 knockout mutant does not show any significant difference in light-, ABA- or CO<sub>2</sub>-dependent stomatal opening, compared to wild type. These results demonstrated that KAT1 is not crucial for stomatal opening (Szyroki A. et al., 2001). A few years later, the AKT2 gene (*A*rabidopsis *t*haliana **K**<sup>+</sup> **T**ransporter **2**), a member of group number three, was discovered (Cao Y. et al., 1995). Due to the function, AKT2 was placed in a separate branch within the plant Shaker family. AKT2 is a weakly inward-rectifying potassium channel, which allows potassium flow not only into a cell, but also out of the cell into the apoplast. However, its voltage-independent form can be switched to a voltage-dependent inward-rectifier form via phosphorylation of the voltage sensor domain (Michard E. et al., 2005). The fourth group consists of AtKC1 (*A*rabidopsis *t*haliana **K**<sup>+</sup> Rectifying **C**hannel **1**), which acts as a regulatory subunit of the inward-rectifying channels and form together with them heteromeric structures.

The fifth group consists of channels conducting potassium ions out of the cell (Lebaudy A. et al., 2007). Two channels belong to this group in plants: SKOR (**S**tellar **K**<sup>+</sup> **o**utward **r**ectifier) and GORK (**G**uard cell **o**utward **r**ectifying **K**<sup>+</sup> channel) (Lebaudy A. et al., 2007, Ward J. M. et al., 2009, Hedrich R., 2012). They are activated during membrane depolarization. SKOR was



cloned in 1998 from *Arabidopsis thaliana* stelar tissues (xylem parenchyma cells) as the first discovered outward-rectifying potassium channel (Gaymard F. et al., 1998). Shortly after that (in 2000) the *Arabidopsis thaliana* gene coding for the GORK channel, expressed in guard cells and root hairs, was cloned and characterized (Ache P. et al., 2000). Research showed that GORK is the main outward-rectifying channel in guard cells and participate in stomatal closure in response to ABA or darkness (Hosy E. et al., 2003, Lebaudy A et al., 2007).

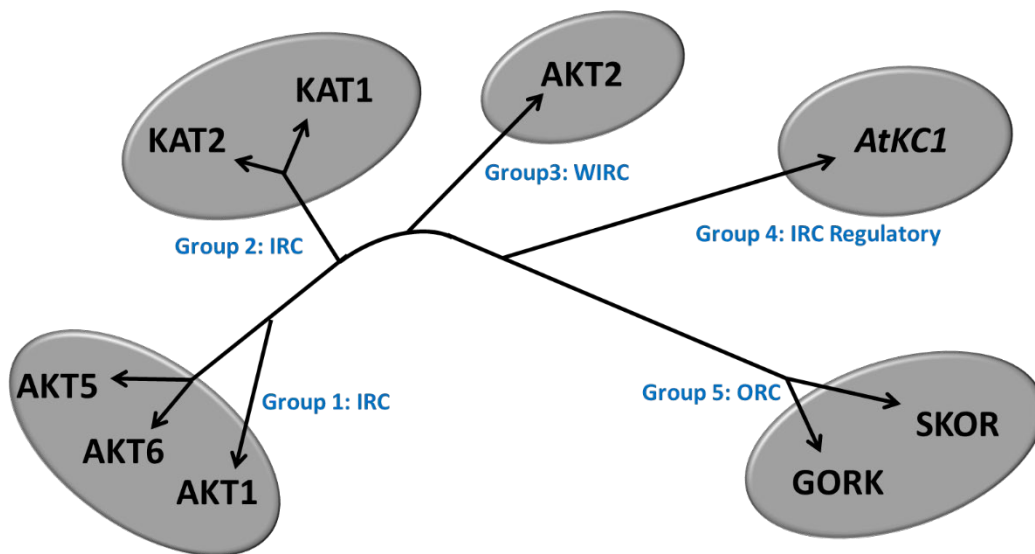


**Figure 3. Phylogenetic tree of the Arabidopsis thaliana Shaker family potassium channels.**

Meaning of the abbreviations used in this Figure: IRC – inward rectifying conductance; WIRC – weakly inward rectifying conductance; ORC – outwardly rectifying conductance; IRC Regulatory – regulatory subunit involved in IRC formation. Figure has been prepared based on Lebaudy A. et al., 2007.

### 1.4. Anion transport across plasma membrane

In plant cells, several inorganic and organic anions such as sulphate, chloride, nitrate or phosphate, as well as malate and citrate are present (Barbier-Brygoo H. et al., 2011). These anions are used as a counterbalance of a charge for cationic groups and osmoregulation (Barbier-Brygoo H. et al., 2011). Moreover, sulphate, nitrate and phosphate are nutritious providing sulphur, nitrogen and phosphorus, which are necessary for the synthesis of biomolecules. Malate and citrate are required for carbohydrate metabolism and involved in

cellular pH regulation (Barbier-Brygoo H. et al., 2011). The first studies of anion transport across plasma membrane were done by Epstein in barley roots (Epstein E., 1953, Barbier-Brygoo H. et al., 2011). Since then, it has been proven that anion channels and transporters play a key role in plant physiology. There are several anion channels and transporter families responsible for anion transport across the plasma membrane (Barbier-Brygoo H. et al., 2011). In the early 90s, two anion channel types were found in the guard cells of *Vicia faba* and referred to as slow-type (S-type) and rapid-type (R-type) channels (Keller B. et al., 1989, Schroeder J. I. and Hagiwara S., 1989, Hedrich R. et al., 1990, Linder B. and Raschke K., 1992, Schroeder J. I. and Keller B. U., 1992). S-type anion channels are characterized by slow activation and deactivation kinetics in the scope of 10 seconds, as well as weak voltage dependence (Barbier-Brygoo H. et al., 2011). On the contrary, R-type anion channels activate and deactivate quickly (within milliseconds) and their activity is dependent on plasma membrane voltage. Furthermore, their current-voltage relationship is described by a characteristic V-shape (Hedrich R. et al., 1990). Both channel types in *Vicia faba* are activated during plasma membrane depolarization and are permeable to chloride and nitrate (Linder B. and Raschke K., 1992, Schroeder J. I. and Keller B. U., 1992, Hedrich R. and Marten I., 1993, Hedrich R. et al., 1994, Schmidt C. and Schroeder J. I., 1994, Dietrich P. and Hedrich R., 1998). Additionally, R-type anion channels can conduct sulphate across the membrane and in *Vicia faba* they are activated by cytosolic calcium and nucleotides, such as ATP (Hedrich R. et al., 1990, Dietrich P. and Hedrich R., 1998, Frachisse J. M. et al., 1999, Barbier-Brygoo H. et al., 2011). Both channel types play a crucial role in stomatal closure via conduction of anion efflux (Schroeder J. I. and Hagiwara S., 1989, Schmidt C. and Schroeder J. I., 1994, Kim T. H. et al., 2010, Meyer S. et al., 2010, Barbier-Brygoo H. et al., 2011). Recently, it has been discovered that S-type anion channels are encoded by genes from the SLAC1 (**S**low **A**nion **C**hannel **1**) family, and R-type anion channels by genes from the ALMT (**A**luminium activated **M**alate **T**ransporter) family (Vahisalu T. et al., 2008, Sasaki T. et al., 2010, Meyer S. et al., 2010).

### 1.4.1. The SLAC1 family

SLAC1 was the first gene of the SLAC1-type family, found in the *Arabidopsis thaliana* genome (**Figure 4**) (Negi J. et al., 2008, Vahisalu T. et al., 2008). SLAC1 as a functional channel is a trimer (Chen Y-H., et al., 2010). Each SLAC1 subunit consist of 10 transmembrane  $\alpha$ -helices (Chen Y-H., et al., 2010). This topology is similar to the structure of the dicarboxylate transporter from *Schizosaccharomyces pombe* and the bacterial tellurite resistance protein TehA (Walter E. G. et al., 1991, Grobler J. et al., 1995). Four homologues of SLAC1 (SLAH1 – 4) belonging to the SLAC1-type family, were found in the *Arabidopsis thaliana* genome (**Figure 4**) (Negi J., et al., 2008, Vahisalu T. et al., 2008). SLAH3, similarly to SLAC1, is expressed in guard cells (Negi J., et al., 2008, Geiger D. et al., 2011). Transcripts of SLAH1 and SLAH2 genes were found in *Arabidopsis thaliana* roots (Maierhofer T. et al., 2014, Cubero-Font P. et al., 2016). SLAH4 expression was notified in soybean and *Arabidopsis thaliana* roots (de Sá M.E. et al., 2012, Zheng X. et al., 2015). SLAC1, as well as SLAH1 – 3 proteins are located in the plasma membrane (Negi J., et al., 2008). So far there is no information about SLAH4 protein localization.



**Figure 4. Phylogenetic tree of the *Arabidopsis thaliana* S-type gene family.**

The phylogenetic tree was constructed using Clustel Omega (<https://www.ebi.ac.uk/Tools/msa/clustalo/>).

In 2008, two independent research groups published results indicating that SLAC1 is the major component of S-type anion current (Negi J. et al., 2008, Vahisalu T. et al., 2008). This channel presents typical S-type anion currents and gating characteristics reflected by slow activation and deactivation and weak voltage dependence (Linder B. et al., 1992, Schroeder J. I. et al., 1992, Schmidt C. et al., 1994). In SLAC1 knockout mutants, a lack of slow anion currents has been observed (Vahisalu T. et al., 2008). Moreover, mutant plants showed no response to

factors causing stomatal closure such as ABA, increased CO<sub>2</sub> levels, darkness, drought, and ozone (Negi J. et al., 2008, Vahisalu T. et al., 2008, Barbier-Brygoo H. et al., 2011). It has been complicated to prove that SLAC1 and SLAH genes encode functional anion channels and not channel regulators. The first attempts of SLAC1 and SLAH protein expression in a heterologous expression system did not bring positive results. It has been concluded that these channels require an activating regulator and they are inactive when these factors are absent (Barbier-Brygoo H. et al., 2011). It was postulated based on electrophysiological studies that S-type anion channels may be activated in the presence of free calcium in the cytosol and that they are controlled by phosphorylation processes (Schmidt C. et al., 1995, Schroeder J. I. and Hagiwara S., 1989). Both increased free cytosolic calcium levels and phosphorylation processes, are also related to the ABA signalling pathway that leads to stomatal closure (Kim T. H. et al., 2010). In 2009, two research groups discovered independently that OST1 kinase, which is an ABA signalling pathway regulator in guard cells, interacts physically with SLAC1 (Geiger D. et al., 2009, Lee S. C. et al., 2009). Voltage clamp experiments in the heterologous expression system also showed that in the presence of OST1, SLAC1 is activated and generates current with S-type anion current characteristics. These data explicitly showed that SLAC1 encodes an S-type anion channel (Mustilli A. C. et al., 2002, Geiger D. et al., 2009, Lee S. C. et al., 2009). Geiger and colleagues further found two calcium-dependent kinases (CPKs), CPK21 and CPK23, which activated SLAC1. Both *ost1* and *cpk23* loss-of-function mutants showed decreased activity of S-type anion channels. These results revealed two possibilities of S-type anion channel regulation in guard cells: through calcium-dependent and calcium-independent signalling pathways (Geiger D. et al., 2009, 2010). An electrophysiological approach showed some differences in the properties of SLAC1 and SLAH3. Both channel types are activated during depolarization of plasma membrane. However, they differ in their anion permeability: SLAC1 is permeable for chloride and nitrate, while SLAH3 is preferentially a nitrate-permeable channel (Geiger D. et al., 2009, Roelfsema M. R. et al., 2004). Additionally, extracellular nitrate is a gating modifier of SLAH3 and can increase its activity (Geiger D. et al., 2011). Recently published results showed that expression of SLAH1 and SLAH3 together leads to the creation of SLAH1/SLAH3 heteromers. These heteromers are permeable for chloride and nitrate and their activation is independent from the nitrate concentration (Cubero-Font P. et al., 2016). Furthermore, SLAH1 and SLAH3 can fulfill the SLAC1 function in the stomatal closure process in guard cells of the *slac1* loss-of-function mutant (Negi J., et al., 2008).

### 1.4.2. The ALMT family

The *Arabidopsis thaliana* ALMT (Aluminium activated Malate Transporters) family consists of 14 genes (Figure 5). Based on the similarity in the amino acid sequence they have been segregated into three clades (Figure 5, Kovermann P. et al., 2007). *AtALMT1*, 2, 7, 8 and 10 (At1g08430, At1g08440, At2g27240, At3g11680 and At4g00910, respectively) have been assigned to the first clade. Clade II consists of *AtALMT3*, 4, 5, 6 and 9 (At1g18420, At1g25480, At1g68600, At2g17470 and At3g18440, respectively). The remaining *AtALMT* genes *AtALMT11*, 12, 13, 14 (At4g17585, At4g17970, At5g46600, At5g46610, respectively) belong to clade III (Kovermann P. et al., 2007). So far, only *AtALMT1*, *AtALMT4*, *AtALMT6*, *AtALMT9* and *AtALMT12* have been characterized. Three of them - *AtALMT4*, *AtALMT6* and *AtALMT9* - are located in the vacuole membrane, while *AtALMT1* and *AtALMT12* are localized in the plasma membrane (Hoekenga O. A. et al., 2006, Meyer S. et al., 2010, Sasaki T. et al., 2010, Meyer S. et al., 2011, DeAngeli A. et al., 2013, Eisenach C. et al., 2017). Two other ALMTs – ALMT2 and ALMT5 - has been characterized in different species: ALMT2 in *Zea mays* (Zm), ALMT5 in *Glycine max* (Gm) and *Solanum lycopersicum* (Sl) (Ligaba A. et al., 2012, Sasaki T. et al., 2016, Peng W. et al., 2018).

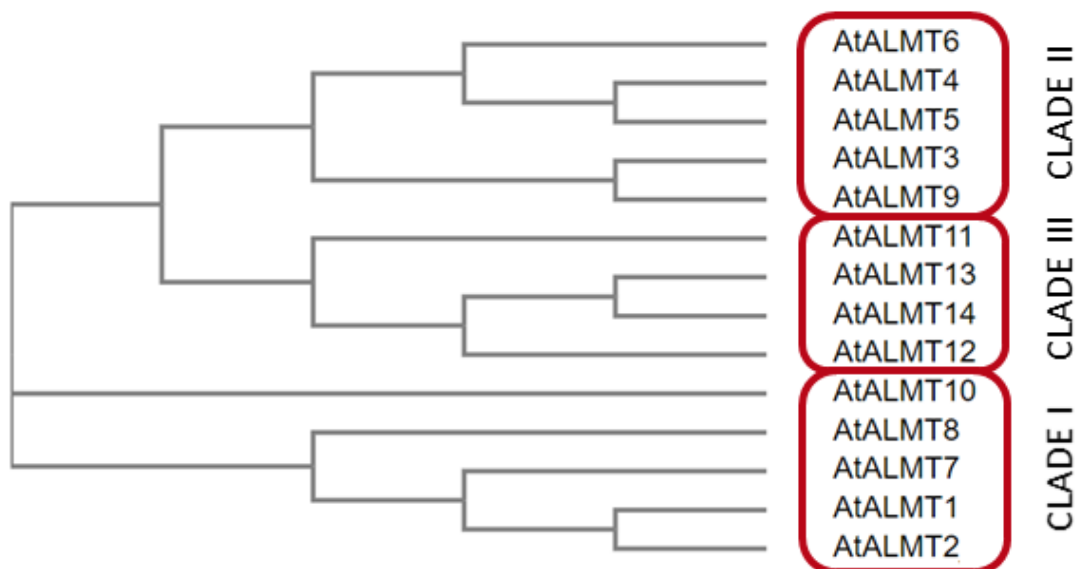


**Figure 5. Phylogenetic tree of the *Arabidopsis thaliana* ALMT family.**

The phylogenetic tree was constructed using Clustel Omega (<https://www.ebi.ac.uk/Tools/msa/clustalo/>). Gens were segregated into three clades based on Kovermann P. et al., 2007.

Gene expression of **AtALMT1**, the first characterized member of the *Arabidopsis thaliana* *ALMT* family, was detected in plant roots and can be positively modulated by  $\text{Al}^{3+}$  ions (Yamaguchi M. et al., 2005, Hoekenga O. A. et al., 2006). AtALMT1 is localized in the plasma membrane and not regulated by membrane potential. However, the presence of  $\text{Al}^{3+}$  ions in soil can increase its activity (Hoekenga O. A. et al., 2006). AtALMT1 share a 44% similarity in amino acid sequence to TaALMT1 (Sasaki T. et al., 2004, Pineros M. A. et al., 2008, Barbier-Brygoo H. et al., 2011). Electrophysiological study showed that  $\text{Al}^{3+}$ -activation of AtALMT1 and TaALMT1 channels is correlated with malate release from roots to the soil (Sasaki T. et al., 2004, Hoekenga O. A. et al., 2006).

Many of AtALMT1 homologs like BnALMT1 and BnALMT2 (*Brassica napus*), GmALMT1 (*Glycine max*) or ScALMT1 (*Secale*) show similar localization and functionality. In all these species, the ALMT1 gene is expressed in the plasma membrane of the root tip, functions as an aluminium-activated protein, and mediates malate efflux from the roots into the soil (Hoffland E. et al., 1989, Ligaba A. et al., 2006, Fontecha G. et al., 2007, Collins N. C. et al., 2008). However, in some other species ALMT1 homologs play a different function. ZmALMT1 (*Zea mays*) protein does not contribute to plant aluminium resistance. Permeation of ZmALMT1 is higher for inorganic (sulphate, nitrate) than for organic (malate, citrate) anions. High permeability of the ZmALMT1 to inorganic anions suggest a role of this channel in mineral nutrition and inorganic anion homeostasis (Pineros M. A. et al., 2008). HvALMT1 (*Hordeum vulgare*) also is not involved in plant  $\text{Al}^{3+}$ -tolerance. It is localized in the plasma membrane of guard cells and mature root cells. The physiological role of HvALMT1 is conductance of malate efflux and influx, which likely supports turgor regulation and osmolality balance in roots and guard cells (Gruber B. D. et al., 2011, Xu M. et al., 2015).

AtALMT2 is still not characterized, however, some data are available for its homolog **ZmALMT2**. It is localized in the plasma membrane of mature root cells and vascular tissue (Ligaba A. et al., 2012). ZmALMT2 was studied in two heterologous systems: *Xenopus oocytes* and transgenic *Arabidopsis thaliana* plants. Both of them showed malate, citrate,  $\text{Cl}^-$  and  $\text{NO}_3^-$  permeability corresponding with ALMT2 expression. Extracellular  $\text{Al}^{3+}$  had no influence on transport activity of ZmALMT2 expressed in the *Xenopus oocyte* system (Ligaba A. et al., 2012). ZmALMT2 is proposed to be responsible for providing solubilisation of soil nutrients. This

protein could be also involved in transport of organic ions or mineral anions in the xylem (Ligaba A. et al., 2012).

**AtALMT3** as well as its homolog LjALMT3, is localized in the vacuolar membrane (Zhang J., 2014, Takanashi K. et al., 2016). Nevertheless, in addition to the location, these channels have not been yet characterized.

The next channel from the ALMT family - **AtALMT4** is localized in the vacuolar membrane and participates in stomatal closure. The *Atalmt4* loss-of-function mutant revealed increased water loss in response to ABA treatment and drought compared to wild type. Phosphorylated AtALMT4 is not active. During ABA-dependent stomatal closure AtALMT4 is activated via dephosphorylation and mediates Mal<sup>2-</sup> release from the vacuole into the cytosol (Eisenach C. et al., 2017). ALMT4 protein was also identified in *Lotus japonicus*, where it is highly expressed in nitrogen fixing nodules. Studies performed in the *Xenopus laevis* oocyte system showed that LjALMT4 mediates efflux of dicarboxylates (malate, fumarate, succinate). Based on this study, Takanashi K. and co-workers concluded, that LjALMT4 mediate efflux and influx of dicarboxylates and inorganic ions in nodule vasculatures (Takanashi K. et al., 2016).

Previously **AtALMT5** was reported to be localized in the endoplasmic reticulum and for this reason not further characterized (Kovermann P. et al., 2007). However, recently it was published that this channel is localized in the vacuolar membrane (Zhang J., 2014). Tonoplast localization was also reported for its homolog – LjALMT5, which is expressed in *Lotus japonicus* nodules (Takanashi K. et al., 2016). Both channels are not yet characterized. In contrast, GmALMT5 is localized in the plasma membrane of the root cells. Overexpression of GmALMT5 in *Arabidopsis thaliana* results in increased malate efflux to the rhizosphere compared to the wild type plants. Furthermore, enhanced expression of GmALMT5 was noticed in soybean seedlings grown under low phosphate conditions. Combining both facts, Peng W. and co-workers concluded that GmALMT5 plays a role in mobilization of inaccessible phosphate sources, by release of malate from root cells to the rhizosphere (Peng W. et al., 2018). Another ALMT5 homolog was identified in *Solanum lycopersicum*. It is localized in the ER. Expression of SIALMT5 in the *Xenopus* oocyte system allowed the measurement of the response to malate, chloride and nitrate perfusion, but not to citrate perfusion. However, overexpression of SIALMT5 in tomato results in increased content not only of malate, but also of citrate in mature seeds (Sasaki T. et al., 2016).

**AtALMT6** is localized in the vacuolar membrane. The analysis of the gene expression revealed AtALMT6 transcripts in guard cells and flower tissues. However, there was no difference in the stomatal movement between the *Atalmt6* loss-of-function mutant and wild type plants. Furthermore, these plant lines also respond similarly to drought stress. Using the patch clamp technique, Meyer S. et al. (2011) demonstrated that AtALMT6 is a calcium-, voltage- and time-dependent channel that mediates malate fluxes. Depending on vacuolar pH and vacuolar membrane potential, AtALMT6 can mediate malate influx from the cytosol into the vacuole or malate release from the vacuole (Meyer S. et al., 2011).

**AtALMT9** is ubiquitously expressed in plant tissue. It is worth noticing that the highest level was observed in mesophyll cells (Kovermann P. et al., 2007). This seems to be related to stomatal opening kinetics, which is slowed down in the *Atalmt9* loss-of-function mutant compared to wild type plants (De Angeli A. et al., 2013). Additionally, *Atalmt9* loss-of-function plants present higher resistance to drought stress and lower water evaporation from the leaf surface (De Angeli A. et al., 2013). Patch clamp measurements in native and heterologous system showed explicitly that this channel is activated by malate and permeable for chloride (De Angeli A. et al., 2013). Just as in the case of AtALMT6, measured currents were bell-shaped, which is characteristic for R-type anion channels. It has been concluded that ALTM9 is involved in stomatal opening but does not influence their closure (De Angeli A. et al., 2013). VvALMT9 (*Vitis vinifera*), the AtALMT9 homolog, is localized in vacuolar membrane of the berry mesocarp tissue and is upregulated during fruit maturation. Patch clamp studies revealed that VvALMT9 mediates selective influx of malate and tartrate into vacuole (De Angeli A. et al., 2013).

The **AtALMT12** channel belongs to clade III of the ALMT family (**Figure 5**). It is predominantly expressed in guard cells and located in the plasma membrane (Meyer S. et al., 2010, Sasaki T. et al., 2010). Stomatal aperture measurements showed that the *Atalmt12* loss-of-function mutant does not close its stomata as effectively as wild type (Col0) in response to ABA, increased CO<sub>2</sub> concentration, darkness and calcium (Meyer S. et al., 2010, Sasaki T. et al., 2010). Additionally, water loss experiments showed that the *Atalmt12* loss-of-function mutant lost water faster than wild type (Sasaki T. et al., 2010). These data indicate that AtALMT12 plays a role in stomatal movement. Malate activated R-type currents have been measured after ALMT12 expression in *Xenopus* oocytes (Meyer S. et al., 2010). Furthermore, AtALMT12



is strongly voltage-dependent, i.e. it is activated by plasma membrane depolarization (Meyer S. et al., 2010). These properties have been observed also in native system during patch clamp measurements (Meyer S. et al., 2010, Sasaki T. et al., 2010).

## 2. Aim of the study

The anion release and further depolarization of the guard cells plasma membrane activate the outward-rectifying potassium channels, resulting in stomatal closure (Roelfsema M. R. and Hedrich R., 2005). In the early 90s, R-type anion channels were discovered to be a component involved in stomatal closure, studied and characterized in *Vicia faba* (Hedrich R. et al., 1990, Hedrich R. and Marten I., 1993, Hedrich R. et al., 1994, Dietrich P. and Hedrich R., 1998). Prof. Rainer Hedrich and other researchers showed their fast activation and strong voltage dependence manifested in characteristic bell-shaped current (Hedrich R. et al., 1990). However, the genes underlying these were not identified. The first data outlining the R-type anion currents in *Arabidopsis thaliana* were published in 2010 (Meyer S. et al., 2010, Sasaki T. et al., 2010). Researchers showed that AtALMT12 - a homolog of TaALMT1, is involved in stomatal closure (Meyer S. et al., 2010, Sasaki T. et al., 2010). Prof. Hedrich R. and Prof. Martinoia E., proved that the ALMT12 channel, localized in the guard cells plasma membrane, is involved in the generation of R-type anion currents (Meyer S. et al., 2010). Interestingly, the *almt12* loss-of-function mutant still shows a high level of R-type-like currents, which could suggest that the ALMT12 channel is not the only component of the R-type currents coded by the *ALMT* gene family (Meyer S. et al., 2010). *ALMT11*, *ALMT13* and *ALMT14*, which belong to the same clade of the *ALMT* gene family as *ALMT12*, are promising candidates to encode another QUAC (quick-activating anion channel) current component (Kovermann P. et al., 2007). Moreover, Brosché M. and co-workers observed variation in O<sub>3</sub>-induced leaf injury for *Arabidopsis thaliana* ecotypes (Brosché M. et al., 2010). Ozone is an air pollutant entering the plant leaf mostly via open stomata so the magnitude of leaf injury could be correlated with stomatal closure in different *Arabidopsis thaliana* accessions and possibly expression of genes from the *ALMT* family (Kerstiens G. and Lenzian K. J., 1989, Brosché M. et al., 2010).

Thereby, my aim was to elucidate the members of the *ALMT* family that mediate the entire QUAC current in *Arabidopsis thaliana* guard cell protoplasts. Additionally, I aimed to evaluate QUAC current and *ALMT* gene expression in Col0 and WS ecotypes as a possible explanation of difference in stomatal response to O<sub>3</sub>. To achieve this, I aimed to apply the patch clamp technique to guard cell protoplasts isolated from *Arabidopsis thaliana* wild type lines (Col0

and WS) and the *almt12* loss-of-function mutant to characterize QUAC currents and background QUAC-like currents at various cytosolic and apoplastic conditions. Additionally, I planned to quantify the expression of genes from the *ALMT* family (or other genes of interest– e.g. SLAC1, SLAH3). I aimed to then relate the expression patterns of the *ALMT* family genes to the QUAC currents in *Arabidopsis thaliana* ecotypes and background QUAC-like currents in the *almt12* mutant or possible double loss-of-function mutants from the *ALMT* family.

## 3. Material and methods

### 3.1. Plant material

#### 3.1.1. Growth conditions

The different *Arabidopsis thaliana* ecotypes Columbia (*Col0*), Wassilewskija (*WS*) as well as loss-of-function mutants *almt12*, *almt12/almt13*, *almt12/almt14* were cultivated in plastic flowerpots ( $\varnothing = 7$  cm) filled with Profi Substrat soil (Einheitserde Werkverband e.V.) inside a growth chamber. Short-day conditions (8 hours of light and 16 hours of darkness) were used during plant cultivation. The temperature in the chamber was maintained at 22°C and 16°C, respectively, in the light and dark period. Plants were illuminated by fluorescent tubes (Osram L58W/77 FLUORA; Philips TLD 58W/840), which generated approximately  $150 \mu\text{mol s}^{-1} \text{m}^{-2}$  of light intensity. The relative humidity in growth chamber was kept at about 60%. Five to six weeks old plants were used for the experiments.

#### 3.1.2. Isolation of guard cell protoplasts

An enzymatic method was applied to isolate guard cell protoplasts from the epidermis. For this purpose, the lower epidermis of the mature *Arabidopsis* leaf was peeled off with tweezers and immediately placed into petri dish filled with enzyme solution. The patch clamp experiments required samples prepared from one plant, while for the analysis of gene expression (**Section 3.3**) one protoplasts sample came from five plants. Four to six leaves were detached from one plant. Enzyme solution used for protoplasts isolation contained the following components:

- 0.65% cellulase R-10 (Serva Electrophoresis GmbH, Heidelberg, Germany)
- 0.35% Macerozyme R-10 (Serva Electrophoresis GmbH, Heidelberg, Germany)

- 0.25% BSA - bovine serum albumin (Serva Electrophoresis GmbH, Heidelberg, Germany)
- 0.05 mM KCl
- 0.05 mM CaCl<sub>2</sub>
- 5 mM ascorbic acid
- 0.05% kanamycin sulphate
- 10 mM MES adjusted to pH = 5.5 with Tris
- $\pi = 400 \text{ mosm kg}^{-1}$  adjusted with D-sorbitol

The plant material was incubated in the enzyme solution for 16 hours at 18°C without shaking. Subsequently, the sample was filtered through a moistened nylon filter (mesh  $\varnothing = 50 \mu\text{m}$ ) by washing with about 50 ml of wash solution in order to remove debris from the suspension. The wash solution consisted of:

- 20 mM CaCl<sub>2</sub>
- 5 mM MES adjusted to pH = 5.6 with Tris
- $\pi = 400 \text{ mosm kg}^{-1}$  adjusted with D-sorbitol

The filtrate was then centrifuged (Eppendorf 5810R Eppendorf AG, Hamburg, Germany) for 14 minutes at 4°C and a speed of  $69 \times g$  (without acceleration or braking). After the supernatant was decanted, 50  $\mu\text{l}$  of the remaining protoplasts suspension was placed in a patch clamp measuring chamber, filled with 250  $\mu\text{l}$  of wash solution. Such filled measuring chambers were kept for at least one hour on ice before patch clamp experiments were conducted.

## 3.2. Patch clamp technique

The patch clamp technique is a popular electrophysiological technique. This method was invented by Erwin Neher and Bert Sakmann in the late 1970s and provided for high-resolution current recordings. The patch clamp technique is commonly used and highly suited to examine the function of different types of transport proteins like ion channels, pumps and carriers in various cell types. With the help of it small currents arising from ions passing the membrane through single ion channels can be measured (Neher E. and Sakmann B., 1976, Hamill O. P. et al., 1981). In 1984 the patch clamp technique was applied for the first time to a plant system by two independent groups. They studied ion channels in the plasma membrane of wheat protoplasts (Moran N. et al., 1984) and guard cell protoplasts of *Vicia faba* (Schroeder J. I. et al., 1984).

### 3.2.1. Patch clamp configurations

In principle, patch clamp experiments can be carried out in four different experimental modes (**Figure 6**): cell attached, whole cell, outside-out patch and inside-out patch. First of all, the "cell-attached" configuration has to be established. It is the first step to achieve all others. (**Figure 6**). For this purpose, a glass measuring pipette (so-called "patch pipette") has to be gently placed on the cell membrane. Subsequently, a slight suction is applied to the membrane via the patch pipette, while constantly monitoring the variability of the pipette resistance. The "cell-attached" configuration is successfully established, when the pipette resistance reaches the level of several G $\Omega$ , indicating that the contact between membrane and glass pipette becomes very tight. This formation is known as the so-called "*gigaseal*". The piece of membrane, which covers the tip of the pipette is electrically isolated from the remaining cell membrane. It is suited to record single channels, while the cell remains intact. The "inside-out" configuration is directly formed from the "cell-attached" configuration by gentle pulling the pipette away from the membrane (**Figure 6**). When the pipette moves, the membrane breaks, but the small piece of it that is directly attached to the pipette remains intact. In this experimental mode the internal side of the membrane patch is exposed to the bath solution, that fills the patch clamp chamber. Similarly, to "cell-attached" configuration, "inside-out" mode is used for single channels recordings, however the ionic conditions on both sides of the membrane patch are specified with the help of the perfusion system. Similar

to the "inside-out" mode, the "whole-cell" configuration (**Figure 6**) is also directly established from the "cell-attached mode". To achieve this configuration, a short suction impulse is applied to disrupt the cell membrane inside the rim made by the tip of the glass pipette. The destructive effect of the suction pulse could be promoted by simultaneous application of a short electrical pulse (e.g. +/- 700 mV). Achieving access to the interior of the cell is equivalent to forming the "whole-cell" configuration. In this configuration, the pipette solution can equilibrate with the internal solutes of the measured cell, and measurements can be carried out under controlled solute conditions on both sides of the membrane. Patch clamp experiments performed in the "whole-cell" configuration provide electrical access to the entire cell membrane and this, in turn, enables the recording of whole-cell membrane currents at certain membrane voltages. The fourth patch clamp mode - "outside-out" can be reached directly from the "whole-cell" configuration (**Figure 6**). To achieve it, the glass pipette should be slightly withdrawn from position in "whole-cell" mode. During this process, the tip of the pipette becomes closed by the patch of the membrane, which exposes its outside face to bath solution in the measuring chamber. The generation of these configurations can be followed by visual control and recording of changes in the resistance of the patch pipette.

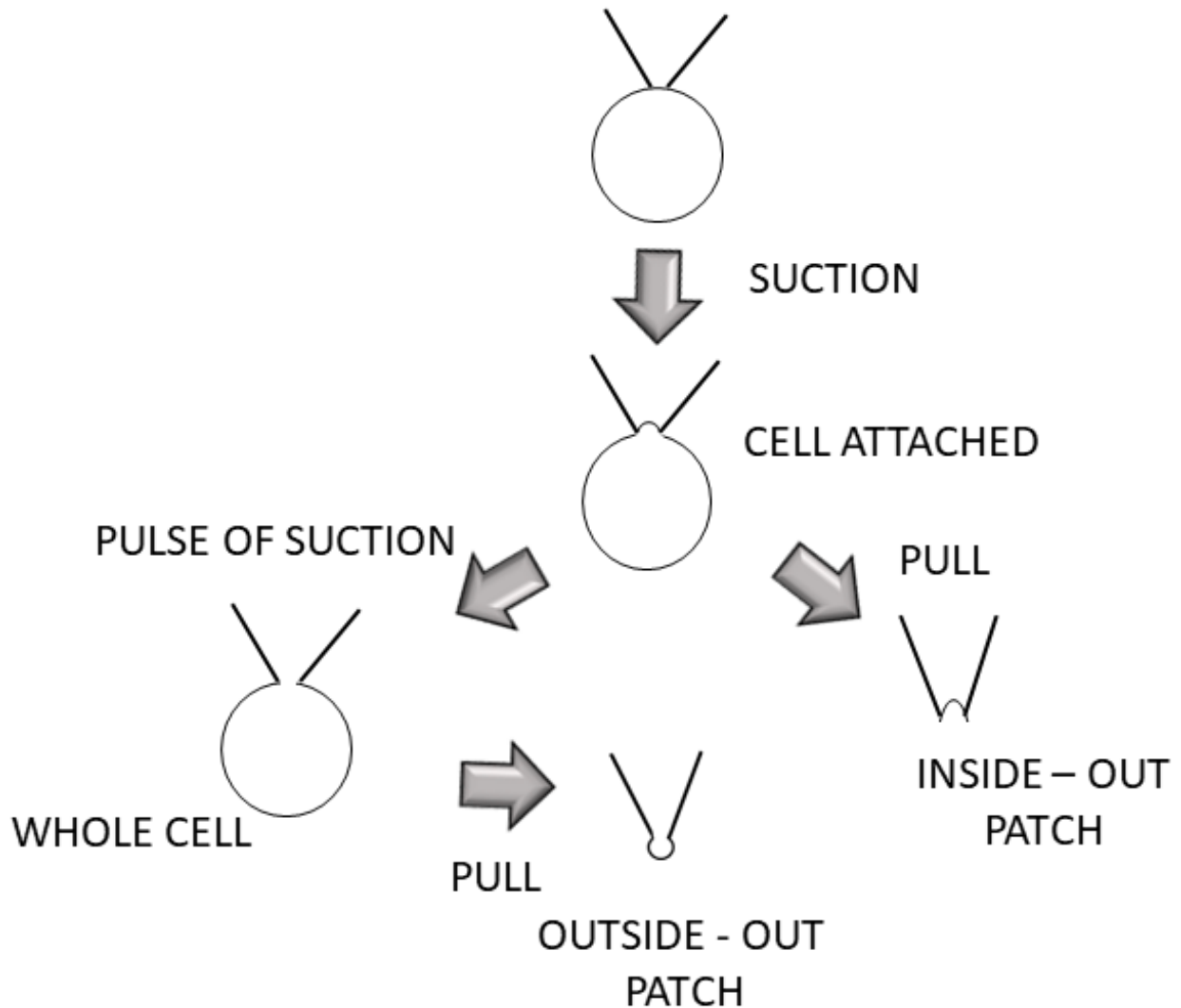


**Figure 6. Generation of the four experimental patch clamp configurations.**

A detailed description is found in the main text. The drawing has been prepared based on Hamill O. P. et al. (1981).

### 3.2.2. Patch clamp set-up

The working station used for the patch clamp studies was surrounded by a Faraday cage. The cage shielded the equipment from electric fields caused by external electrostatic charges or electromagnetic disturbances to reduce the recording noise. Inside the cage was an inverted microscope (Axio Observer.A1, Carl Zeiss, Jena, Germany) with a movable top plate (Scientifica, England), mounted on a pneumatic table (Technical Manufacturing Corporation, Peabody, Massachusetts, USA). The pneumatic table protected the microscope and movable



top plate from possible mechanical vibrations caused by motions of the floor. In the centre of the microscope top plate, the patch clamp chamber with the protoplasts was placed. On the right side of the measuring chamber, a motorized micro-manipulator (PatchStar Micromanipulator, Scientifica, England) was mounted, enabling spatial manipulation and stable placement of the measuring electrode. The preamplifier was installed at the manipulator and directly held the patch clamp electrode. The reference electrode, which was stably placed in the patch clamp chamber containing the bath medium was connected to the preamplifier via a silver wire. To allow perfusion of the bath medium within the measuring chamber, peristaltic pumps (Ismatec, Glattbrugg, Switzerland) were connected to it by polyethylene tubes (Ismatec, Wertheim, Germany and Hartenstein GmbH, Würzburg, Germany). The hosepipes delivered and drained the bath solution to ensure stable ion concentration in the measuring chamber. Before solution was delivered to the patch clamp chamber, it flew through glass olives, which were inside covered with Sigmacote® (Sigma, Munich, Germany). Application of the olives avoided electrical connection between pumps and measuring chamber. The voltage clamp experiments were performed with an EPC7 amplifier (HEKA, Lambrecht, Germany), connected to a computer through an AD/DA (analog-to-digital/digital-to-analog) converter (ITC – 16, Instrutech Corp, Elmont, NY, USA). Before transferring to the AD/DA converter, signals measured with sampling rate 100  $\mu$ s passed a low-pass filter (NP1, Tamm, Germany) and were filtered to 1 kHz. The EPC7 amplifier was operated by the software program Pulse (HEKA, Lambrecht, Germany). In order to avoid further electromagnetic disturbances, the EPC7 amplifier, the AD/DA converter, the low-pass filter, the computer as well as the power supply of the microscope, micromanipulator and the peristaltic pumps were placed outside the Faraday cage.

### **3.2.3. Measuring and reference electrodes**

Two crucial elements with a high impact on the quality of the current recordings were the measuring electrode and the reference electrode. Both were made of silver wire (WPI, Sarasota, USA). Before the patch clamp measurements were started, both electrodes were coated with a fresh silver chloride layer in a galvanizing process using a 3 M KCl solution and a 6 V alkaline battery as a direct voltage source. Each electrode (one after another) was submerged in the KCl solution with applied DC (direct current) voltage and performed the

anode function. Another silver wire which was fixed to the power supply played the function of the cathode.



When the galvanizing process was completed, the silver/silver chloride wire of the measuring electrode was rinsed with water to wash off remaining 3 M KCl solution and then dried before the electrode was assembled and mounted on the preamplifier.

After coating the reference electrode was placed in a polyethylene tube filled with 3 M KCl solution. The side of the tube that was placed into the bath medium was closed with a 2% agarose plug prepared with 3 M KCl solution. The agarose plug ensured that the concentrated KCl solution and silver ions from the electrode did not leak out into the bath medium.

#### **3.2.4. Preparation of the measuring glass microelectrode**

The measuring patch pipettes were made of capillary tubes produced from borosilicate glass (internal diameter 1.05 mm, external diameter 1.5 mm, length 80 mm, GB150T-8P, Science Product, Hofheim, Germany). For this, the glass capillary tube was placed in a vertical pipette puller (Narishige PP-83, Narishige Scientific Instruments, Tokio, Japan). By using the force of gravity and high temperature, two glass pipettes were formed in a two-stage process. Next the glass pipette was placed in a holder mounted at a microscope (Zeiss ID03, Carl Zeiss, Jena, Germany) to cover the end of the pipette close to the tip with a hydrophobic silicone material under optical control (Sylgard 184 silicon elastomer kit, Dow Corning Corporation, Midland, MI, USA). After this step, the silicone layer was hardened by hot air. The silicone coat was applied to reduce electrostatic charging of the glass pipette. Finally, the patch pipette tip was suitably shaped by exposure to a heated platinum–iridium wire. Once prepared, the glass pipette was filled to 2/3 of its length with the pipette solution and pulled over the silver/silver chloride wire of the measuring electrode holder. The measuring pipette used for patch clamp measurements presented in this thesis had a resistance in the range of 3 – 5 MΩ for all used solutions.

### **3.2.5. Running the patch clamp measurements**

In order to establish the "whole-cell" configuration, a patch pipette under optical control was placed in a measuring chamber filled with bath medium. A test pulse of +/-10 mV (hold for 10 ms) was continuously applied to the patch pipette. Accordingly, changes in the patch pipette resistance could be observed, enabling the determination of whether a Giga-ohmic seal resistance had been established and to differentiate between different patch clamp modes. Subsequently, the offset potential compensation was performed. Whereupon, the patch pipette tip was positioned near to the selected guard cell protoplast. In response to constant and gentle suction applied via the patch pipette, the plasma membrane of the selected guard cell protoplast was sucked to the pipette tip. The giga-ohmic seal resistance visualized obtained "cell-attached" configuration. In order to achieve "whole-cell" configuration, constant and gentle suction was continued. The "whole cell" mode was recognized by capacitive spikes that occurred in the suction process. Before compensating them, the appropriate holding potential was established. To eliminate the capacitive spikes, built-in components of the amplifier were used. Fast compensation ( $C_{fast}$ ) eliminated capacitive currents originating from the electrostatic charge accumulated on components of the measuring chamber. The slow compensation ( $C_{slow}$ ) eliminated capacitive current transients caused by charging/discharging the entire plasma membrane. To achieve a defined conditions inside the cell, 7 minutes was given for ionic exchange between the pipette solution and the internal solutes of the protoplast. Afterwards, appropriate voltage pulse protocols were applied, and corresponding currents were recorded.

### **3.2.6. Sign convention for ionic currents**

Since 1992, a set sign convention for ionic currents in electrophysiological study has been used. This sign convention unifies the position of the electrical potential at the cytoplasmic side of the plasma membrane simultaneously defining the outer membrane side as 0 mV. Accordingly, a negative measured current (inward current) can be created either by anions flowing from the cytosol to the outside compartment or by cations flowing into the cytosol. Analogously, a positive current (outward current) can be generated by the movement of cations or anions in the opposite direction (Bertl A. et al., 1992, Nelson M. and Rinzel J., 1998).

### 3.2.7. Liquid junction potential

Handling of patch clamp experiments under certain bath and pipette ionic conditions generate discrepancies between the voltage applied on a cell membrane and the voltage recognized by the cell membrane. Erwin Neher explained and described it in his article titled "Correction for Liquid Junction Potential in Patch Clamp Experiments" (Neher E., 1992). He named this difference as Liquid Junction Potential. It exists when the composition of the solutes in pipette and the bath solution varies significantly. When the patch pipette is placed in the bath medium, both solutions come into contact with each other at the pipette tip. As a result, ions will diffuse between the solutions in order to balance the different concentrations. Movement of the ions, which have different mobility, creates the Liquid Junction Potential. In the beginning of the patch clamp experiment, after the tip of the measuring pipette is in contact with the bath solution, compensation is made for the difference in the electrical potential of the patch pipette and reference electrode ( $V_{\text{offset}}$ ). This compensation includes also the Liquid Junction Potential. When "whole-cell" configuration is achieved, the Liquid Junction Potential no longer exists, because the pipette solution is no longer in contact with the bath solution. Due to the offset compensation, the applied voltage needs to be corrected offline by the Liquid Junction Potential.

Liquid Junction Potential value was experimentally determined according to Neher E. (1992). Furthermore, applied pulse protocols were corrected according to the equation:

$$V_M = V_{\text{cmd}} - V_{\text{LJP}}$$

( $V_M$  – membrane potential,  $V_{\text{cmd}}$  – potential applied by amplifier on the membrane,  $V_{\text{LJP}}$  – Liquid Junction Potential).

The Liquid Junction Potential measured for a sulphate-based pipette solution in the following thesis were equal to -10 mV.

### 3.2.8. Voltage pulse protocol

Two voltage pulse protocols were used to record R-type anion currents. As illustrated in **Figure 7**, both protocols were composed of three segments. During the first segment, the plasma membrane was clamped at -170 mV (**Figure 7A**) or +70 mV (**Figure 7B**) for 200 ms in both

voltage protocols. The second segment (which lasted 800 ms) differed in both protocols. In the first protocol (**Figure 7A**), voltages were applied in the range of -170 mV to +70 mV in 10-mV increments, while in the second voltage pulse protocol (**Figure 7B**), voltages were applied in the range from +90 mV to -240 mV in 10-mV decrements from the holding voltage. In the last segment, the membrane was instantaneously clamped to -170 mV (**Figure 7A**) or +70 mV (**Figure 7B**) for 200 ms. After each 3-segment voltage pulse, a break period took place. During the break period, the membrane was kept at the holding voltage of -170 mV or +70 mV respectively for a further 2 s without recording the membrane currents. Thus, one total voltage pulse lasted for 3.2 s. The effect of ATP was investigated with the help of the protocol showed in **Fig. 7B**. All other experiments were carried out using protocol showed in **Fig 7A**.

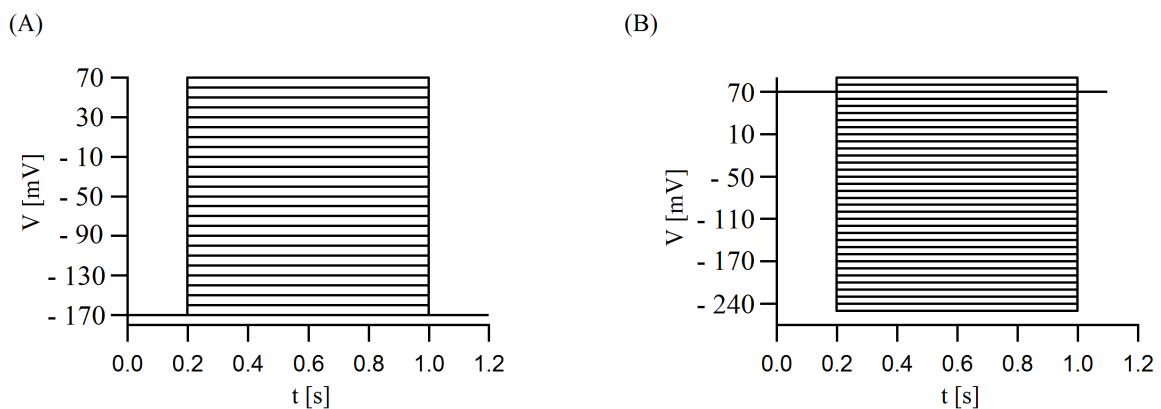


**Figure 7. Voltage pulse protocols used for measurements of R-type anion channel currents.**

### 3.2.9. Data analysis

To perform off-line analysis, IGOR Pro 6.6 software (Wave Metrics Inc., Lake Oswego, USA) was used. The acquired data stored on the set-up computer were exported in IGOR text data format. For data analyses, steady-state currents ( $I_{ss}$ ) were determined (**Figure 8A** red lines). This provides information about the number of activated channels and the corresponding current amplitudes, which are not changing over time and allow us to measure the maximum current values at respective voltages.

Steady-state currents were determined for each experiment and at each clamped membrane voltage as a mean of the last 10 ms from ongoing 800 ms voltage pulse. In order to eliminate

the influence of protoplast size on the current amplitudes, the steady-state currents were normalized to the membrane capacitance ( $C_m$ ), which reflects the membrane surface. The  $C_m$  value was read out from the amplifier during membrane capacitance compensation. Finally, normalized steady-state currents ( $I/C_m$ ) were plotted against the corresponding membrane voltages (**Figure 8B**). For each experimental condition, the mean of at least 3 experiments, performed for different protoplasts, were calculated and presented with corresponding SEM (standard error).

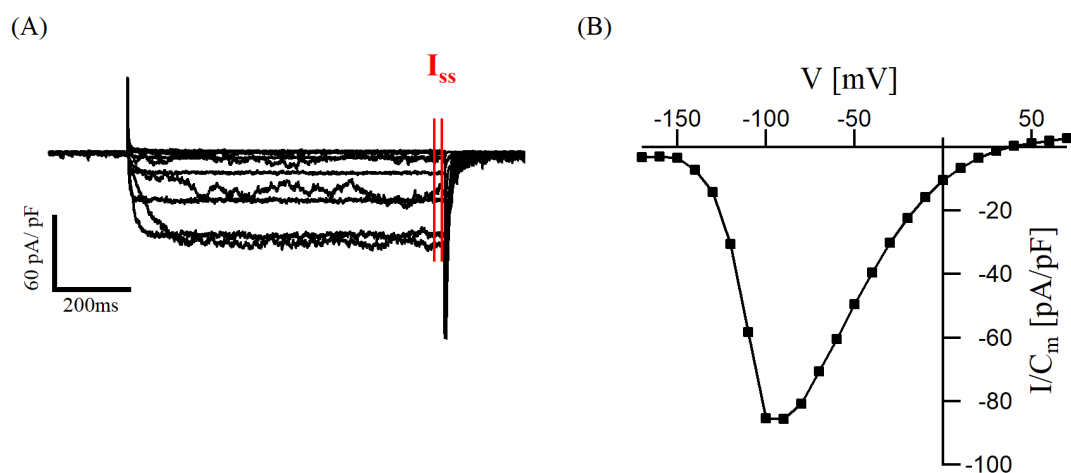


**Figure 8. Analysis of R-type current measurements.**

(A) Example of current traces recorded in response to applied voltages. The space between red lines represents steady state currents ( $I_{ss}$ ) that were used for analyses. (B) Measured steady state currents ( $I_{ss}$ ) were normalized to the size of the cell ( $C_m$ ) and plotted versus corresponding voltages.

Furthermore, so-called "tail currents", recorded in the third segment of the pulse protocol, were used to determine the relative voltage-dependent open probability (rel.  $P_o(V)$ ) of R-type currents.

The change of applied voltage on a membrane enforces instantaneous change of driving forces and thus also ion flow, however conformational protein rearrangements are not so fast and need time. A delay in channel reaction (slow switch between open and closed state) to the voltage applied on the membrane allow us to record "tail currents". If we assume that the number of functional channel proteins localized in the membrane is constant, we will be able to determine the relative voltage-dependent open probability at different voltage-prepulses

via the "tail current" analysis:  $(I_{\text{tail}}(V)/I_{\text{tail max}}(V)) = G/G_{\text{max}} = \text{rel. } P_o(V)$ . To record "tail currents" after each prepulse-voltage in the range of -170 mV to +70 mV (segment 2), plasma membrane was instantaneously clamped to -170 mV (segment 3) (**Figure 7, Section 3.2.7**). From the recorded data, the instantaneous tail current density was determined (**Figure 9**), plotted against corresponding voltages and normalized to the maximal predicted tail current density. To determine  $\text{rel. } P_o(V)$ , the slope of the data points was fitted with the Boltzmann equation:

$$\text{rel. } P_o(V) = P_{\text{max}} / (1 + \exp(-z_q * (x - V_{1/2}) / 25.26))$$

( $P_{\text{max}}$  – maximum open probability,  $V_{1/2}$  – midpoint voltage for activation,  $z_q$  – value which describes equivalent gating charges corresponding with the movement of charge(s) during transition between the open and closed channel state,  $25.26 = \frac{F}{RT}$ ;  $F$  – Faraday constant,  $R$  – gas constant,  $T$  – temperature).

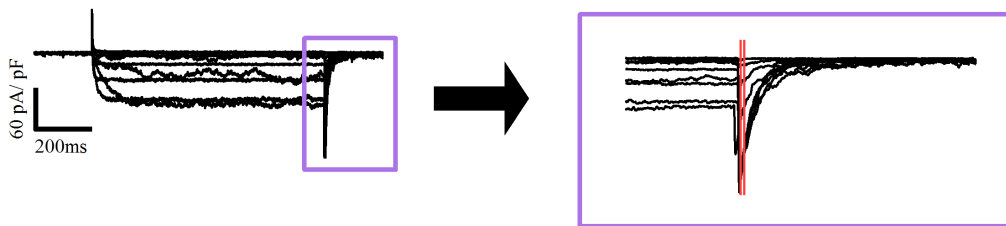


**Figure 9. Analysis of R-type tail currents**

Example of data analysis for one measurement. The graph on the left-hand-side presents examples of current traces recorded in response to applied voltages. The graph on the right-hand-side presents magnified region where instantaneous tail current amplitudes were determined in the range labelled by red lines.

To perform statistical analyses, OriginPro 2018b software (OriginLab Corporation, Northampton, USA) was used. Data comparisons were performed with the use of one-way analysis of variance (One-Way ANOVA) or two-way analysis of variance (Two-Way ANOVA) followed by Bonferroni test.

### 3.2.10. Measuring patch clamp solutions

The measuring patch clamp solutions applied for data acquisition were composed of chemical substances purchased from AppliChem GmbH (Darmstadt, Germany), Carl Roth GmbH (Karlsruhe, Germany), Merck KGaA (Darmstadt, Germany), Serva Electrophoresis GmbH (Heidelberg, Germany) and Sigma – Aldrich Chemie GmbH (Steinheim, Germany). The pH value of all solutions was adjusted by titration under the control of a calibrated digital 646 Calimatic pH-meter (Knick Elektronische Messgeräte GmbH & Co.KG Berlin, Germany). The H<sup>+</sup> concentration of bath and pipette solutions was adjusted to pH 5.6 by using 10 mM MES/Tris buffer and pH 7.1 by using 10 mM HEPES/Tris, respectively. The osmolality was measured with an osmometer (Vapor Pressure Osmometer 5520, Wescor, Vapro) and adjusted to 400 or 440 mosm kg<sup>-1</sup> using D-sorbitol. The WEBMAXC STANDARD program ([www.stanford.edu/~cpatton/webmaxcS.htm](http://www.stanford.edu/~cpatton/webmaxcS.htm)) was used to calculate the free calcium concentration of the pipette solution, which was adjusted with EGTA to 195 nM or 1850 nM as indicated. Additionally, the calcium concentration was controlled with the Fura-2 fluorescent technique (Kong S. K. and Lee C. Y., 1995). Mg-ATP and AMPPNP (adenylyl-imidodiphosphate) were added during pipette solution preparation from 5 mM Mg-ATP or 5 mM AMPPNP dissolved in 0.5 M Tris respectively.



**Table 1. Composition of bath solution.**

---

<b>R – type anion channels</b>
20 mM Ca (OH) <sub>2</sub>
20 mM DL – Malic Acid
2 mM MgCl <sub>2</sub>
0.5 mM LaCl <sub>3</sub>
10 mM MES
pH = 5.6 adjusted with Tris
$\pi = 400 \text{ mosm kg}^{-1}$ with D-sorbitol

---

**Table 2. Composition of sulphate-based pipette solutions.**

---

<b>R1.</b>	<b>R2.</b>
<b>Ca<sup>2+</sup><sub>cyt free</sub> = 195 nM</b>	<b>Ca<sup>2+</sup><sub>cyt free</sub> = 1850 nM</b>
3 mM CaCl <sub>2</sub>	1.1 mM CaCl <sub>2</sub>
10 mM EGTA	1.45 mM EGTA
<hr/>	
75 mM Cs <sub>2</sub> SO <sub>4</sub>	
2 mM MgCl <sub>2</sub>	
5 mM Mg-ATP	
pH = 7.1 adjusted with Tris	
$\pi = 440 \text{ mosm kg}^{-1}$ with D – sorbitol	

---

**Table 3. Composition of chloride-based pipette solutions.**

<b>R3.</b>	<b>R4.</b>	<b>R5.</b>
<b>„75 mM Cl<sup>-</sup>“</b>	<b>„75 mM Cl<sup>-</sup> + 1mM SO<sub>4</sub><sup>2-</sup>“</b>	<b>„75 mM Cl<sup>-</sup> + 1 mM Malate“</b>
-----	1 mM Cs <sub>2</sub> SO <sub>4</sub>	1 mM DL-Malic Acid
	75 mM CsCl	
	2 mM MgCl <sub>2</sub>	
	5 mM Mg-ATP	
	3 mM CaCl <sub>2</sub>	
	10 mM EGTA	
	pH = 7.1 adjusted with Tris	
	$\pi = 440 \text{ mosm kg}^{-1}$ with D-sorbitol	

**Table 4. Pipette solution composition used to study ATP effect on R-type anion channels**

<b>R6.</b>	<b>R7.</b>	<b>R8.</b>
<b>„0 mM ATP“</b>	<b>„5 mM ATP“</b>	<b>„5 mM AMPPNP“</b>
0 mM Mg-ATP	5 mM Mg-ATP	5 mM AMPPNP
	75 mM Cs <sub>2</sub> SO <sub>4</sub>	
	2 mM MgCl <sub>2</sub>	
	3 mM CaCl <sub>2</sub>	
	10 mM EGTA	
	pH = 7.1 adjusted with Tris	
	$\pi = 440 \text{ mosm kg}^{-1}$ with D-sorbitol	

### 3.3. Quantitative Real-Time PCR

In order to determine the expression of *ALMT* genes, mRNA was isolated from enzymatically-isolated guard cell protoplasts (**Section 3.3.1**) of *Arabidopsis thaliana* plants. The plant material was harvested from wild type plants (Col, WS) and diverse loss-of-function mutants (*almt12*; *almt12/13*; *almt12/14*), which were cultivated under controlled growth conditions as specified in **Section 2.1.1**. After the isolation, mRNA was converted into cDNA (complementary DNA) with reverse transcriptase. The gene expression was quantified by quantitative real-time polymerase chain reaction (qRT-PCR). The number of molecules of a given gene was normalized to 10,000 AtActin 2/8 molecules using DNA standard curves calculated for the individual PCR products.

#### 3.3.1. Enzymatic isolation of guard cell protoplasts

Five weeks old *Arabidopsis thaliana* plants were used for enzymatic isolation of guard cell protoplasts as described in **Section 3.1.2**. One sample of protoplasts was derived from five plants. Plant material was incubated in the bath solution containing 20 mM malate (**Table 1, Section 3.2.10**) for 1 hour at room temperature after enzymatic isolation. Subsequently, plant material was centrifuged and decanted in the same way as described in **Section 3.1.2**. The samples placed in the reaction tube was immediately frozen in liquid nitrogen and lysed with TissueLyser II (5 min shaking at 30 Hz; Qiagen).

#### 3.3.2. RNA isolation from plant material

According to the manufacturer's instructions ([www.qiagen.com](http://www.qiagen.com)), total RNA was extracted from the homogenized samples using the RNeasy Plant Micro Kit (Qiagen). An additional DNA digestion was been performed after total RNA was extracted. Ribonucleic acids were handled with the use of sterile materials and RNase-free solutions. Water used for preparation contained 0.1 % (v/v) DEPC (Diethylpyrocarbonate) and was autoclaved.

### 3.3.3. Reverse Transcription

cDNA synthesis from mRNA was carried out essentially as described by Biemelt S. et al. (2004). In the first step, mRNA was dissolved in 14  $\mu\text{l}$  of DEPC water (RNase-free water), afterwards 6.3  $\mu\text{l}$  of Master Mix was added. The Master Mix contained:

- 0.8  $\mu\text{l}$  Oligo – dT – Primer (100  $\mu\text{M}$ )
- 1  $\mu\text{l}$  dNTPs (10 mM)
- 4  $\mu\text{l}$  RT – Buffer (5x, Promega)
- 0.5  $\mu\text{l}$  RNase inhibitor

In the next step, the mixture was incubated for 2 min at 70°C and then cooled down on ice in order to add thermolabile 0.8  $\mu\text{l}$  MMLV RT (Moloney Murine Leukemia Virus Reverse Transcriptase, Promega, Mannheim, Germany, 100 U/ $\mu\text{l}$ ). The reverse transcriptase MMLV-RT enables single-strand cDNA synthesis, using Oligo-dT-Primer connected to the 3'-polyA ends of the mRNA. The sample was further incubated for 60 min at 42°C. The obtained cDNA was stored at -80°C, and later used for qRT-PCR reaction.

cDNA from previously isolated *Arabidopsis thaliana* guard cell protoplasts was generated by the technical assistant of Prof. Dr. Georg Nagel (University of Würzburg).

### 3.3.4. Quantitative real-time polymerase chain reaction (qRT-PCR)

To quantify expression levels of different genes, qRT-PCR was performed. Quantitative real-time polymerase chain reaction allows the direct analysis of the reaction kinetics using fluorescent dyes (SYBR®Green I, ABgene®, Thermo Fisher Scientific Inc.). These dyes bind to or intercalate in the DNA double helix. Therefore, the direct quantity of the gene expression is reflected via a proportional increase in fluorescence (Rasmussen R. et al., 1998). Moreover, analysis of the melting curve of the product helps to differentiate between the specific DNA product from by-products of the PCR reaction.

cDNA used as a template for qRT-PCR was diluted 20 times in water containing tRNA (HPLC H<sub>2</sub>O from Carl Roth GmbH, Karlsruhe, Germany with 10 ng/ $\mu\text{l}$  tRNA Sigma-Aldrich Chemie GmbH, Steinheim, Germany), which prevents cDNA binding to the walls of the measuring

plates. Dilution is necessary for adjusting cDNA concentration to the measuring buffers. After dilution the reaction mixture was prepared, which consist of following:

- 10.00 µl Absolute QPCR SYBR® Green Capillary Mix
- 0.12 µl Primer fwd (50 µM)
- 0.12 µl Primer rev (50 µM)
- 7.76 µl HPLC H<sub>2</sub>O
- 2.00 µl Template

The reaction mixture was placed on 96-well plates (Twin-TEC, Eppendorf). Then, the product was multiplied, and its quantity was determined in real time with the usage of Real-Time-Thermocycler Realplex-x4 (Eppendorf AG, Hamburg, Deutschland). Additionally, a series of standard solutions for selected genes with specified DNA concentrations (10, 1, 0.1 and 0.01 fg/µl) was prepared. The fluorescence measured for each sample was referenced to these gene standards, allowing the calculation of the number of selected gene transcripts in the tested samples. The same series of standard solutions was also prepared for reference genes. The following genes were used for reference: *AtActin2* (AT3g18780) and *AtActin8* (AT1g49240) – *AtACT2/8*. The number of molecules for measured samples was normalized to these reference genes and determined per 10,000 molecules of *AtACT2/8*.

Quantification of *ALMT3*, *ALMT4*, *ALMT5*, *ALMT6*, *ALMT9*, *SLAC1* and *SLAH3* expression levels was performed by the technical assistant of Dr. Peter Ache (University of Würzburg). Data of *ALMT3*, *ALMT4*, *ALMT5*, *ALMT6*, *ALMT9*, *SLAC1* and *SLAH3* expression were analysed by Dr. Heike Müller (University of Würzburg).

### 3.3.5. Primers for Quantitative Real-time Polymerase Chain Reaction

For the Quantitative Real-time Polymerase Chain Reaction, the following primers were used:

*Table 5. Primers for the Quantitative Real-time Polymerase Chain Reaction.*

<b>Gen</b>	<b>Forward Primer 5' → 3'</b>	<b>Reverse Primer 3' → 5'</b>
<b>ALMT1</b>	CTATACGAGAAGTCGGA	TGCCCATTACTTAATGT
<b>ALMT2</b>	CCGTGGGTGCATTACT	TTCGACTTAGACGGCT
<b>ALMT3</b>	CTAGGGTTAGGGATTTGAC	CTGTAACATACTTCCCG
<b>ALMT4</b>	AATGATTCTCAGCTATGGA	GTGTCTCGCTAACTTGT
<b>ALMT5</b>	GAGCCGCTTCAAGATGCTAGTA	ATGACTTCTTCAAACCTCTCCTGCT
<b>ALMT6</b>	GATGAATCTCAGATATGGG	TTGATCCACTACGTTAAG
<b>ALMT7</b>	CCTGTAAATCACTCACC	CGTCTACATGCGTATCA
<b>ALMT8</b>	CACACATTGACAACTCC	ACATGACATGAGCTATT
<b>ALMT9</b>	ACCTAATCCGGATCTTAGTCGAT ACT	TCACCGAATAAAGTGGAAGCTC AG
<b>ALMT10</b>	GATTTCTGGTGTTTGA	GTTGTTTAGTGTTGTTGTC
<b>ALMT11</b>	GACGATAAGCGAGAAAGTAAT	AGTATGGCTGGTTAAGGAC
<b>ALMT12</b>	AGGAGGATGTTACGGC	GGTTTTCGCATCGGAC
<b>ALMT13</b>	GGCCACGTTTCATATTAC	ACCTCCACAGTCTTATC
<b>ALMT14</b>	AGGAAATAGCGGTAGAC	CTCAGAATCTTTCTTTCGT
<b>ACT2/8</b>	GGTGATGGTGTGTCT	ACTGAGCACAATGTTAC

### 3.3.6. Cyclor-Program for Quantitative Real-time Polymerase Chain Reaction

*Table 6. Cyclor-Program for Quantitative Real-time Polymerase Chain Reaction.*

Process	Temperature	Duration	
<b>1. Step:</b>			
„Hot Start “	95°C	15 min	
<b>2. Step:</b>			
Denaturation	95°C	15 s	This step is repeated 40 - 45 times
Annealing	60°C	20 s	
Elongation	72°C	20 s	
Detection	79°C	10 s	
<b>3. Step:</b>			
Melting point of	95°C	10 s	
product analysis	60°C	15 s	
	$\Delta T_m$ (60°C→95°C)	[0.3°C/s]	
	95°C	5 s	
<b>End</b>	40°C	2 min	

### 3.4. Genotyping loss-of-function mutants

The genotype of all loss-of-function R-type anion channels mutants, used for electrophysiological studies, was checked with the PCR technique (polymerase chain reaction). The result of two types of PCR reactions for each mutant were necessary to evaluate that plants are homozygotes with the tDNA insertion. The first reaction type (called in this thesis a gene reaction) used the primer pairs gene reaction forward and gene reaction reverse, which were placed at the beginning and at the end of a tested gene. Gene reaction PCRs were intended to check whether the plant was a homozygote. To prove the presence of the tDNA insertion, the second reaction type (called in this thesis a tDNA reaction) used the primer pairs tDNA reaction forward and tDNA reaction reverse, which were placed at the beginning of a gene and in the tDNA insertion region.

### 3.4.1. DNA Isolation

In order to show the correct genotype of the examined plants, DNA of loss-of-function mutants (*almt12*, *almt12/almt13*, *almt12/almt14*), as well as wild type (Col0) was isolated. For this, five weeks old plants, cultivated as described in **Section 2.1.1.**, were used. One detached leaf was placed in a 1.5 ml reaction tube (Eppendorf) filled with sterile metal balls. Then, the reaction tube was put into liquid nitrogen. After freezing, plant material was homogenized for 1 min at a frequency of 30 Hz with the use of the TissueLyser II (Qiagen). After homogenization, plant material was again frozen in liquid nitrogen. 250 µl of Edwards Buffer was added to the frozen material. Edwards Buffer was composed of:

- 200 mM Tris HCl/pH = 7.5
- 250 mM NaCl
- 25 mM EDTA pH = 8.0
- 0.5% SDS
- solution filled up with distilled water to end volume of 50 ml

Then, the mixture was heated at 90°C for 5 min and placed on ice. Subsequently, a reactive mixture was prepared from the following ingredients:

- 12.5 µl water for PCR
- 4 µl Reaction Buffer
- 1 µl Primer forward (10 µM)
- 1 µl Primer reverse (10 µM)
- 0.4 µl dNTPs
- 0.2 µl Phusion
- 1.5 µl DNA

This mixture was placed in a PCR tube (Eppendorf). Afterwards a PCR was carried out with the use of a Mastercycler personal (Eppendorf). For PCR, the following primers were used:



*Table 7. Primers used for genotyping loss-of-function mutants.*

<b>Gen</b>	<b>Forward Primer 5' → 3'</b>	<b>Reverse Primer 5' → 3'</b>
<b>ALMT12</b>	GTTGTGCAAAGGGCTTAATAGAG	CAAGAAGGCTCATGAAAAGACAG
gene reaction		
<b>ALMT12</b>	GTTGTGCAAAGGGCTTAATAGAG	TACGAATAAGAGCGTCCATTTTAGAGT
tDNA reaction		
<b>ALMT13</b>	GGCGGATTTAGAATCCAAAAC	TAATAAAGCGGAATTGGAACG
gene reaction		
<b>ALMT13</b>	GGCGGATTTAGAATCCAAAAC	TTCATAACCAATCTCGATACAC
tDNA reaction		
<b>ALMT14</b>	TTGAAACAGTGCTATTTGGG	TGAGGCCGAAAGTATAAAAAGC
gene reaction		
<b>ALMT14</b>	TTGAAACAGTGCTATTTGGG	ATTTTGCCGATTCGGAAC
tDNA reaction		

### 3.4.2. Cyclor-Program for Polymerase Chain Reaction

*Table 8. Cyclor-program for genotyping loss-of-function mutants.*

<b>Process</b>	<b>Temperature</b>	<b>Duration</b>	
<b>Initialization step</b>	98°C	5 min	
<b>Denaturation step</b>	98°C	15 s	
<b>Annealing step</b>	52°C (ALMT12)	15 s	This step was repeated 35 times
	55°C (ALMT13, ALMT14)		
<b>Elongation step</b>	72°C	40 s	
<b>Final elongation</b>	72°C	7 min	
<b>Final hold</b>	4°C	-----	

## 4. Results

### 4.1. Residual R-type anion currents in the *almt12* mutant

#### 4.1.1. Basic characterization of residual R-type anion currents

Anion mobilization plays a crucial role in the volume regulation of guard cells. The rapid- (R-type) and slow- (S-type) activating anion channels conduct anion efflux from the cytosol to apoplast which results in cell shrinking (Schroeder J. I. and Keller B. U., 1992, Raschke K. et al., 2003). R-types known also as a quick-activating anion channel (QUAC) were mostly characterized in *Vicia faba*. Studies revealed that activation of *Vicia faba* R-type anion currents are dependent on cytoplasmic  $Ca^{2+}$  and nucleotides, such as ATP (Hedrich R. et al., 1990, Dietrich P. and Hedrich R., 1998). However, the molecular nature of R-type currents in *Vicia faba* were not discovered. The first protein generating QUAC current was found in *Arabidopsis thaliana*. A tDNA insertion in the *ALMT12* gene decreased *Arabidopsis thaliana* R-type anion currents by 40%, which resulted in impaired stomatal closure compared to wild type (Meyer S. et al., 2010).

**To better understand R-type-like background current** in the *almt12* mutant (remaining 60% of wild type R-type anion currents), in the present doctoral thesis, the electrical features of QUAC-like anion currents were electrophysiologically studied and compared to wild type. For this purpose, a series of patch clamp experiments were performed on guard cell protoplasts isolated from the *Arabidopsis thaliana* ecotype (Col0) and the *almt12* mutant. They were carried out in the presence of 20 mM CaMalate in standard bath solution and 75 mM  $SO_4^{2-}$  in pipette solution, which additionally contained 195 nM of free  $Ca^{2+}$  (**standard bath solution and pipette solution R1, Table 1 and 2 respectively, Section 3.2.10**). During experiments, the negative holding potential of -170 mV was used (**Section 3.2.8**). When the regular pulse protocol, ranging from -170 mV to +70 mV with 10 mV steps, was applied, fast-activated current responses were recorded. R-type channels revealed inward currents as a result of the  $SO_4^{2-}$  ions fluxes out of the cell, when depolarized voltages were applied.

Observed currents instantaneously declined after coming back to a negative holding potential (**Figure 10A**). Wild type and *almt12* revealed noticeable inward anion currents when the membrane potential was clamped to -150 mV, which vanished at more positive voltages than +30 mV (**Figure 10B**). Recorded currents were normalized to the size of the protoplasts ( $C_m$ ). The steady-state current density responses from each voltage pulse were plotted against the respective voltages. This allowed the visualization of strong, bell-shaped voltage dependence, typical for R-type anion channels, with peak-current density observed around -90 mV (**Figure 10B**). Furthermore, a significant difference in the peak-current densities between the Col0 ecotype and the *almt12* loss-of-function mutant at low cytosolic calcium concentration was noticed with means of  $-86 \pm 6$  pA/pF and  $-52 \pm 4$  pA/pF, respectively (**Figure 10B**). To carefully evaluate the voltage dependency of Col0 and the *almt12* mutant and mechanism standing behind reduced peak-current density, tail currents from *almt12* and Col0 were examined. The tail current procedure allowed the equalization of driving forces. Data acquisition was conducted by instantaneous jump from different membrane potentials, in the range of -170 mV to +70 mV, to the holding potential, equal to -170 mV, which stabilized a close state of R-type channels. Recorded current amplitudes were dependant only on the number of open channels activated upon the voltage pulse standing before the holding potential. Therefore, they were used to determine the relative voltage-dependent open-channel probability (rel.  $P_o(V)$ ) (**Figure 10C**). The slope of  $G/G_{max}$  data points derived for the *almt12* mutant and Col0 were described with a single Boltzmann equation. Data did not reveal notable differences in the charge movement ( $z_q \approx 2$ ) and midpoint voltage ( $V_{1/2} \approx 116$  mV) (**Table S1**). Furthermore, relative open probability reaches 1 at -50 mV, which suggests that all R-type channels are open in the positive voltage range (**Figure 10C**).

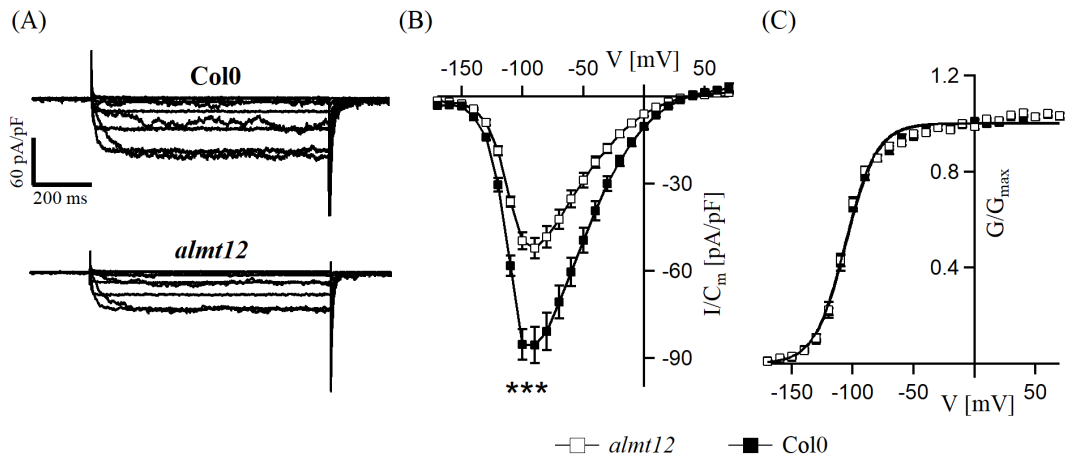


**Figure 10. R-type anion channel response in guard cell protoplasts of Columbia (Col0) and the *almt12* loss-of-function mutant.**

(A) Example of current traces recorded for R-type anion channels of Col0 and the *almt12* loss-of-function mutant in response to applied voltages. (B) Steady-state current density ( $I_{ss}/C_m$ ) plotted against corresponding voltages for Col0 and the *almt12* loss-of-function mutant. Data points represent mean of 6-9 experiments with SEM. Measurements were performed in whole-cell configuration. Present data are significantly different in peak current, \*\*\*,  $P \leq 0.001$ , One-Way Anova followed by Bonferroni test. (C) Relative voltage-dependent open channel probability of Col0 and *almt12*. Conductance-voltage curves ( $G/G_{max}(V)$ ) were determined via instantaneous tail current responses to -170 mV after voltage pre-pulses ranging from -170 mV to +70 mV were applied. After normalization to maximum predicted tail current density the data points were plotted as means ( $\pm$ SEM) of 6-9 experiments against respective voltage. Solid lines give the fits of the data points with the Boltzmann equation.

**Permeability of R-type anion channels** for  $\text{NO}_3^-$ ,  $\text{Cl}^-$ ,  $\text{I}^-$ ,  $\text{Br}^-$  and  $\text{malate}^{2-}$  has been demonstrated for the first time in *Vicia faba* guard cell protoplasts (Hedrich R. and Marten I., 1993). A similar study in *Arabidopsis thaliana* hypocotyls revealed  $\text{NO}_3^-$ ,  $\text{Cl}^-$ ,  $\text{SO}_4^{4-}$  and  $\text{malate}^{2-}$  as possible substrates (Frachisse J. M. et al., 1999). Anion currents measured in *Arabidopsis thaliana* (Col0 and the *almt12* loss-of-function mutant) guard cell protoplasts, in contrast to *Vicia faba* did not reveal bell-shaped R-type currents in chloride-based solution (Schroeder J. I. and Keller B. U., 1992, Sasaki T. et al., 2010). Cytosolic sulphate was reported to be a regulatory factor of the R-type anion channels in *Arabidopsis thaliana* hypocotyls (Frachisse J. M. et al., 1999). Additionally, malate was described as a modulator of the R-type anion channels in *Vicia faba* guard cell protoplasts (Hedrich R. and Marten I., 1993). Therefore, it was a point of interest to check whether supplementation by sulphate or malate chloride-based cytosolic solution will affect chloride permeability of the R-type anion channels in *Arabidopsis thaliana* guard cell protoplasts.

Thus, guard cell protoplasts isolated from the *almt12* mutant and the Col0 ecotype were used. Patch clamp experiments under standard bath solution (**Table 1, Section 3.2.10**) and pipette solution containing 75 mM Cl<sup>-</sup> and 1mM SO<sub>4</sub><sup>2-</sup> or 1mM malate<sup>2-</sup> were carried out (**Table 3 R4 and R5, Section 3.2.10**). Regular pulse protocol and negative holding potential were used under both cytosolic conditions. The presence of 1 mM sulphate in addition to the 75 mM chloride creates a bell-shaped current in both the wild type and mutant upon application of the voltage protocol (**Figure 11A**). Col0 and *almt12* showed similarly located (around -100 mV), significantly different peak currents at  $-4 \pm 1$  pA/pF and  $-16 \pm 3$  pA/pF, respectively (**Figure 11A**). Replacement of sulphate by malate in cytosolic solution revealed only linear current for Col0 as well as the *almt12* mutant (**Figure 11B**).

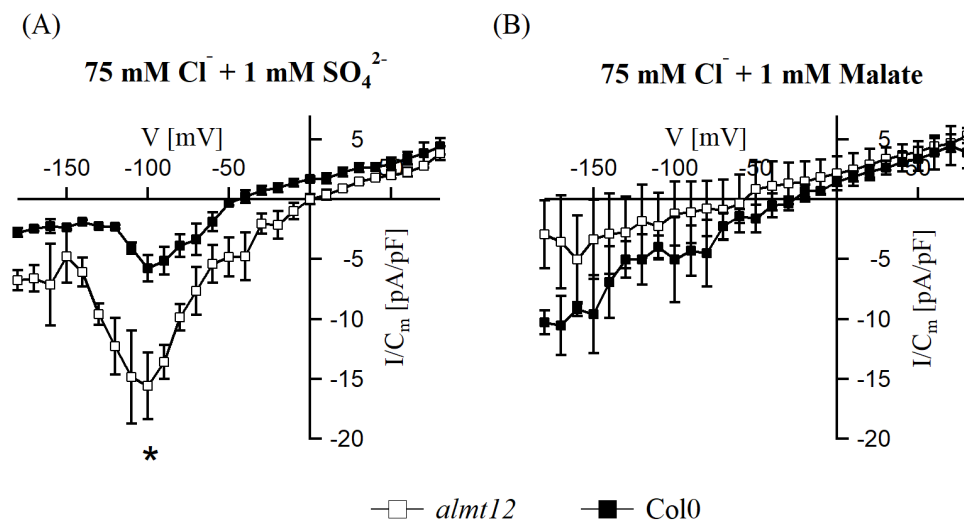


**Figure 11. R-type anion channel response in guard cell protoplasts of Col0 and the *almt12* loss-of-function mutant to different cytosolic conditions.**

(A) and (B) Comparison of steady-state currents density ( $I_{ss}/C_m$ ) plotted against respective voltages, between Col0 and the *almt12* loss-of-function mutant. Data points represent mean of (A) 3 and (B) 3-4 experiments with SEM. Measurement were performed in whole-cell configuration. To quantify significant differences between peak currents in (A) - \*,  $P < 0.05$ , One-Way Anova followed by Bonferroni test were used.

#### 4.1.2. ATP affects R-type background currents

R-type anion currents in *Vicia faba* stay active only in the presence of cytosolic ATP (Hedrich R. et al., 1990). This could also be true in *Arabidopsis thaliana*. However, the AtALMT12 channel that partially creates R-type anion currents belongs to the same family as AtALMT9, which is blocked by ATP (Meyer S. et al., 2010, Zhang J. et al., 2014). Therefore, it was

interesting to check the influence of ATP on *Arabidopsis thaliana* R-type anion currents (Col0) as well as R-type-like anion currents (the *almt12* mutant). The enzymatic release of guard cell protoplasts from Col0 and the *almt12* mutant and the patch clamp method were used to find if there is a difference in QUAC currents in the presence and absence of 5 mM ATP in the pipette solution (**Table 4 R6 and R7, Section 3.2.10**). The absence of cytosolic ATP was confirmed by calculation according to Goh Ch-H. et al. (2002). The pulse protocol in the range of +90 mV to -240 mV with 10 mV steps and holding potential of +70 mV was applied (**Section 3.2.8**). R-type channels under these applied conditions revealed  $\text{SO}_4^{2-}$  ion fluxes out of the cell (**Figure 12A**). The presence of 5 mM ATP kept R-type anion channel conductive in range of -150 mV to +30 mV for *almt12* as well as for wild type (**Figure 12B and C**). The peak current position for the mutant was observed at -90 mV with the registered value of  $-65 \pm 9$  pA/pF (**Figure 12C**). Very similar peak features were observed for the Col0 ecotype (position: -90 mV; current density:  $-63 \pm 11$  pA/pF) (**Figure 12B**). Removal of ATP from the pipette solution shifts R-type-like currents activity in the *almt12* mutant to more negative voltages with the peak current located around -170 mV (**Figure 12C**). Moreover, the aforementioned features of QUAC were not significantly changed compared to the wild type. It is worth noting that the shift of peak current to more negative voltages also caused a rise in current density in a similar way for *almt12* and wild type ( $-148 \pm 17$  pA/pF and  $-169 \pm 30$  pA/pF, respectively) (**Figure 12B and C**). Additionally, in the absence of ATP, the rise in cytosolic calcium did not significantly influence R-type current in either the wild type or mutant (**Figure S1A and B, Section 12**).

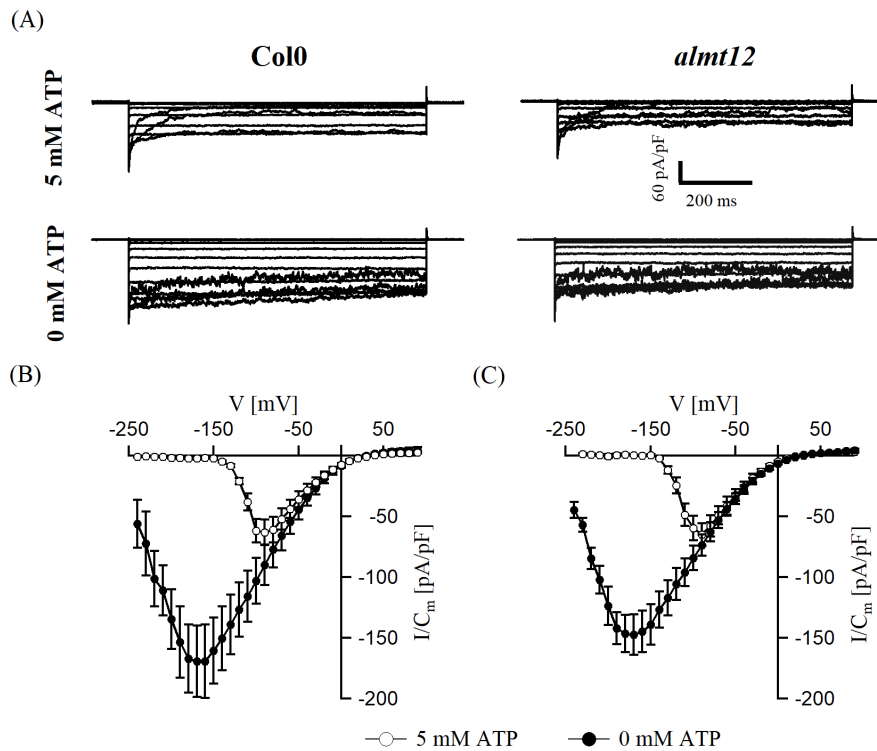


**Figure 12. R-type anion channel response of guard cell protoplasts of the *Columbia* (Col0) ecotype and the *almt12* loss-of-function mutant to cytosolic ATP.**

(A) Example of traces recorded for R-type anion channels of Col0 and *almt12* in response to applied voltages. (B) and (C) Steady-state current density ( $I_{ss}/C_m$ ) plotted against corresponding voltages for (B) Col0 and (C) *almt12*. Data points represent the mean of 3-6 experiments with SEM. Measurements in A, B, and C were performed in whole-cell configuration.

#### 4.1.3. Calcium-dependent behavior of QUAC-like currents

It has been shown that *Vicia faba* R-type anion currents are dependent on cytosolic calcium, but nothing is known about the model plant *Arabidopsis thaliana* (Hedrich R. et al., 1990). To fill this gap, *Arabidopsis thaliana* guard cell protoplasts isolated from the *Columbia* (Col0) ecotype and the *almt12* loss-of-function mutant were used. To examine the influence of free cytosolic  $Ca^{2+}$  concentration on QUAC (wild type) and QUAC-like residual currents present in the *almt12* knockout, two calcium concentration in pipette solution, 195 nM and 1850 nM, were used (Table 2 R1 and R2, Section 3.2.10). The pulse protocol and negative holding potential described in Section 3.2.8 were applied. In response, strongly voltage-dependent and bell-shaped current were recorded at negative voltages in both cytosolic calcium concentrations for the mutant as well as wild type (Figure 13A and B). The rise in cytosolic calcium did not change the position of peak current, which was noticed around -90 mV (Figure



**13A and B**). There were no differences between peak-current densities at low ( $-86 \pm 6$  pA/pF) and high ( $-86 \pm 10$  pA/pF) cytosolic calcium in the Col0 ecotype (**Figure 13A**). The *almt12* loss-of-function mutant presented peak current densities of  $-52 \pm 4$  pA/pF and  $-72 \pm 5$  pA/pF at free cytosolic calcium concentrations of 195 nM and 1850 nM, respectively (**Figure 13B**). Furthermore, tail currents analysis revealed no differences in the voltage midpoint of channel activation and charge movement between plant lines in either calcium concentration ( $V_{\text{half}} \approx -115$  mV,  $z_q \approx 2$ , **Table S1, Section 12**). There is a 1.4-fold significant increase in peak current density associated with the rise in free cytosolic calcium concentration for the *almt12* loss-of-function but not Col0 (**Figure 13C**). Furthermore, a 1.6-fold smaller *almt12* peak current density at 195 nM free cytosolic  $\text{Ca}^{2+}$  become almost equal to wild type after a rise in cytosolic  $\text{Ca}^{2+}$  to 1850 nM (**Figure 13C**).

In conclusion, residual R-type currents present in the *almt12* loss-of-function mutant have very similar features to wild type e.g. strong voltage dependency, voltage range activity, peak current position and blockage by cytosolic ATP. However, their ion selectivity at low sulphate conditions and behavior in response to elevated cytosolic calcium are different.

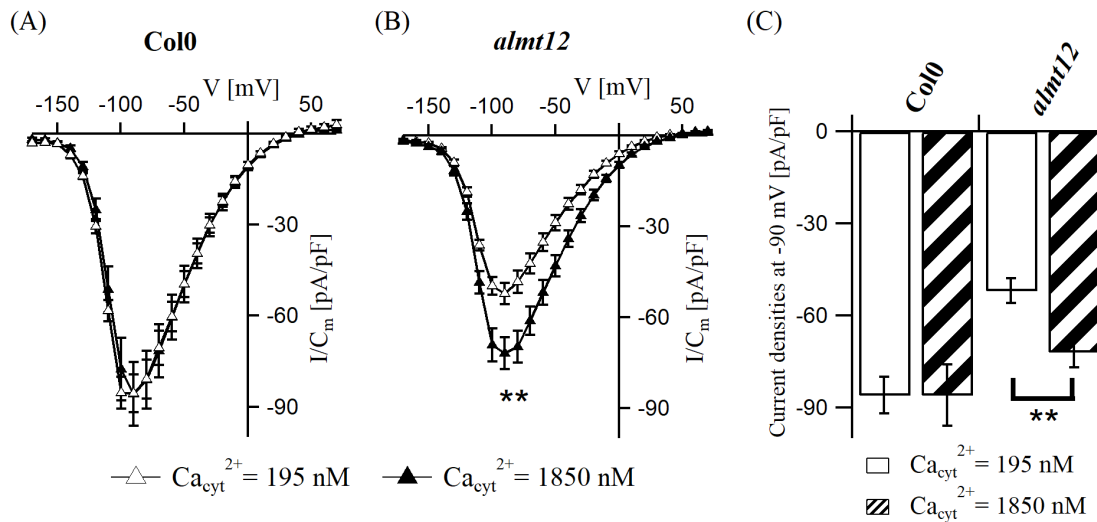


**Figure 13. R-type anion channel response in guard cell protoplasts of Col0 and the *almt12* loss-of-function mutant under different cytosolic calcium conditions.**

(A) and (B) Steady-state current density ( $I_{ss}/C_m$ ) of (A) Col0 and (B) the *almt12* loss-of-function mutant plotted against corresponding voltages recorded under different free cytosolic  $Ca^{2+}$  concentrations. Data points represent mean of (A) 6-10 and (B) 9-12 experiments with SEM. Measurements were performed in the whole – cell configuration. Data showed in B are significantly different in peak current, \*\*,  $P \leq 0.01$ , One-Way Anova followed by Bonferroni test. (C). Peak current density of guard cell protoplasts from Columbia (Col0) and *almt12* under 195 nM and 1850 nM free cytosolic  $Ca^{2+}$ . The steady-state current densities evoked upon a voltage jump from -170 mV to +90 mV were determined. Data represent means  $\pm$  SEM of six to twelve experiments. Current recordings were carried out with sulfate-based ATP-containing pipette solution, adjusted to 195 nM or 1850 nM free  $Ca^{2+}$ . For statistical analysis, One-Way Anova followed by Bonferroni test was performed. Asterisks indicate significant differences:  $P \leq 0.01$  \*\*.

#### 4.1.4. ALMT genes expressed in guard cells of Col0 and the *almt12* mutant

QUAC currents in Col0 and the *almt12* mutant revealed two different features: response to a rise in cytosolic  $Ca^{2+}$  and ion selectivity at low sulphate conditions (Section 4.1.1 and 4.1.3). It is known that AtALMT12 contributes to the generation of *A. thaliana* R-type anion currents (Meyer S. et al., 2010). Thus, the variation could be explained by the expression of different channels from the ALMT family participating in the creation of R-type currents. To test this hypothesis, expression levels of the other ALMT family members were measured by qRT-PCR (Section 3.3). cDNA was prepared from enzymatically isolated guard cell protoplasts from *Columbia* (Col0) and the *almt12* loss-of-function mutant (Section 3.3.3). The expression level was measured for all genes belonging to the ALMT family: ALMT1 - ALMT14. qRT-PCR analysis showed marginal expression ( $10 \pm 3$  transcripts per 10.000 actin) of ALMT1 (which belongs to

clade I of the *ALMT* family) in Col0 but expression was negligible in the *almt12* mutant (**Figure S2, Section 12**). Furthermore, transcripts for genes classified to clade II were found; *ALMT3*, *ALMT4*, *ALMT5*, *ALMT6* and *ALMT9*, were expressed at similar levels in wild type and the *almt12* mutant (**Figure S2 and Table S2, Section 12**). All genes from clade II have vacuolar (*ALMT3/4/5/6/9*) or endoplasmic reticulum (*ALMT5*) localization, so were excluded from further consideration (Kovermann P. et al., 2007, Meyer S. et al., 2011, DeAngeli A. et al., 2013, Zang J., 2014, Eisenach C. et al., 2017). Finally, the Col0 ecotype expressed three genes from clade III of the *ALMT* family - *ALMT12*, *ALMT13*, and *ALMT14* - at respective levels of  $1138 \pm 188$ ,  $114 \pm 25$  and  $60 \pm 20$  molecules per 10.000 actin (**Figure 14**). The *almt12* loss-of-function mutant revealed only *ALMT13* gene expression, which was comparable to the wild type level at  $123 \pm 47$  transcripts per 10.000 molecules of *AtActin 2/8* (**Figure 14**).

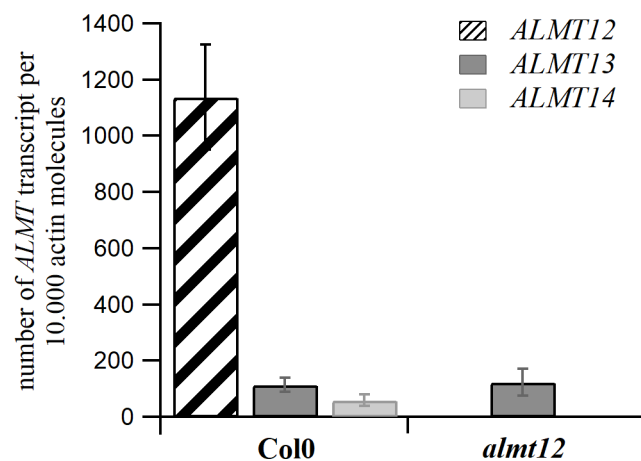


**Figure 14.** Expression of *ALMT12*, *ALMT13* and *ALMT14* in guard cell protoplasts of *Columbia* (Col0) and the *almt12* loss-of-function mutant.

Transcript levels of *ALMT12*, *ALMT13* and *ALMT14* in Col0 and the *almt12* loss-of-function mutant. Data represent mean  $\pm$  SEM. The number of independent biological repetitions was  $n = 3$ . Total number of examined samples was  $n = 7-10$ .

#### 4.2. *almt12/13* and *almt12/14* double loss-of-function mutants

The qRT-PCR analysis revealed that the *Columbia* ecotype guard cell protoplasts expressed *ALMT12*, *ALMT13* and *ALMT14* genes (**Figure 14, Section 4.1.4**). Meyer S. et al. proved that the product of the *ALMT12* gene partly generates R-type anion currents in *Arabidopsis*

*thaliana* (Meyer S. et al., 2010). Furthermore, the *almt12* mutant expressed only the *ALMT13* gene (**Figure 14, Section 4.1.4**). In order to provide further information about the contribution of ALMT13 and ALMT14 channels in *A. thaliana* R-type currents, two double loss-of-function mutants, *almt12/almt14* and *almt12/almt13*, were examined by qRT-PCR and the patch clamp method. qRT-PCR was performed on cDNA prepared from guard cell protoplasts of *almt* double loss-of-function mutants. Subsequently, expression level of genes from clades I to III were examined. Of the genes that belong to clade I only *ALMT1* revealed marginal expression in *almt12/almt14* and *almt12/almt13*, similar to Col0 (**Figure S3 and Table S2, Section 12**). Expression of *ALMT3 - 6* and *ALMT9* located in clade II were not significantly different compared to the *almt12* mutant and Col0 (**Figure S3 and Table S2, Section 12**). The *almt12/almt14* mutant did not show *ALMT11*, *ALMT12* and *ALMT14* transcripts, but *ALMT13* expression level ( $141 \pm 32$  transcripts per 10.000 actin) was similar to wild type ( $114 \pm 25$  transcripts per 10.000 actin) and *almt12* ( $123 \pm 47$  transcripts per 10.000 actin) (**Figure 15A**). The *almt12/almt13* loss-of-function mutant did not express *ALMT11*, *ALMT12* and *ALMT13* gene transcripts, but had 2-fold higher *ALMT14* gene expression level ( $148 \pm 29$  transcripts per 10.000 actin) compared to Col0 ( $60 \pm 20$  transcripts per 10.000 actin) (**Figure 15A**).

The patch clamp measurements of *almt12/almt13* and *almt12/almt14* double knockout mutants were performed in standard bath solution and pipette solution containing 195 nM free  $\text{Ca}^{2+}$  (**Table 1 and Table 2 R1, Section 3.2.10**). Protoplasts kept at negative holding potential were clamped with the pulse protocol described in **Section 3.2.8 (Figure 7A)**. R-type-like background currents were observable in both mutants, starting at -150 mV, with peak current position at around -90 mV (**Figure 15B**). The mean measured peak current density for *almt12/almt13* and *almt12/almt14* was  $-54 \pm 8$  pA/pF and  $-48 \pm 1$  pA/pF, respectively (**Figure 15C**). These values were comparable with the results obtained under the same conditions for guard cell protoplasts isolated from the *almt12* loss-of-function mutant ( $-52 \pm 4$  pA/pF) (**Figure 15C**) and significantly smaller than Col0 ( $-86 \pm 6$  pA/pF) (**Figure 15C**).

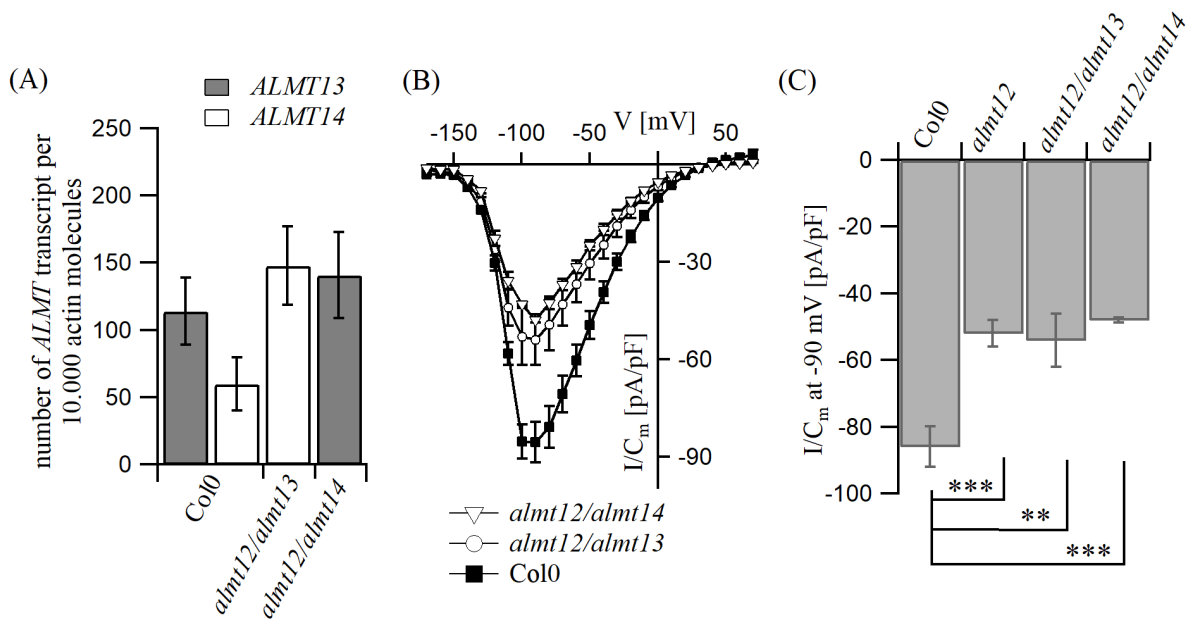


**Figure 15. R-type anion channel response in guard cell protoplasts of Columbia (*Col0*) and *almt12/almt13*, *almt12/almt14* loss-of-function mutants.**

(A) Transcript levels of *ALMT13* and *ALMT14* in *Col0*, *almt12/almt13* and *almt12/almt14* loss-of-function mutants. Data represents means  $\pm$  SEMs. The number of independent biological repetition was  $n = 3$ , total number of examined samples was  $n = 7-8$ . (B) Steady-state current density ( $I_{ss}/C_m$ ) plotted against corresponding voltages for *Col0*, *almt12/almt13*, and *almt12/almt14* loss-of-function mutants. Data points represent means of 4-6 experiments with SEM measured in sulphate-based solution at low cytosolic calcium concentration (195 nM) and 5 mM ATP. (C) Current density at -90 mV measured for *Col0* and different loss-of-function mutants. Values of currents represent mean with SEM for 4-9 experiments. Asterisks indicate significant differences between the peak current of mutants and the control (*Col0*) (One-Way Anova followed by Bonferroni test): \*\*,  $P \leq 0.01$ , \*\*\*,  $P \leq 0.001$ . Measurement in B and C were performed in whole – cell configuration. *almt12/almt13* and *almt12/almt14* mutant lines were kindly provided by Prof. Dr. Hannes Kollist from the University of Tartu, Estonia and Dr. Mikael Brosché from the University of Helsinki, Finland.

R-type current characterization for both *ALMT* double mutants were repeated under high (1850 nM) cytosolic calcium conditions (Table 2 R2, Section 3.2.10). As seen previously for the *almt12* mutant, increased cytosolic calcium concentration did not change the voltage range of R-type-like channel activity (Table S1, Section 12; Figure 16A and B) and peak current position (around -90 mV) (Figure 16A and B). Nevertheless, with the rise in free cytosolic  $Ca^{2+}$  concentrations from 195 nM to 1850 nM, the difference in peak current density of *Col0* ( $-86 \pm 10$  pA/pF) and *almt12/almt13* ( $-62 \pm 6$  pA/pF) decreased from 1.6 to 1.4-fold, while differences in R-type current between *Col0* ( $-86 \pm 10$  pA/pF) and the *almt12/almt14* loss-of-function mutant ( $-73 \pm 3$  pA/pF) became negligible (Figure 16A and B). It is important to notice that calcium has a significant impact on the R-type peak current density in the

*almt12/almt14* loss-of-function mutant, but not in the *almt12/almt13* loss-of-function mutant (Figure 16C). The rise in *almt12/almt14* peak current density is positively correlated with increased cytosolic calcium concentration (Figure 16C).

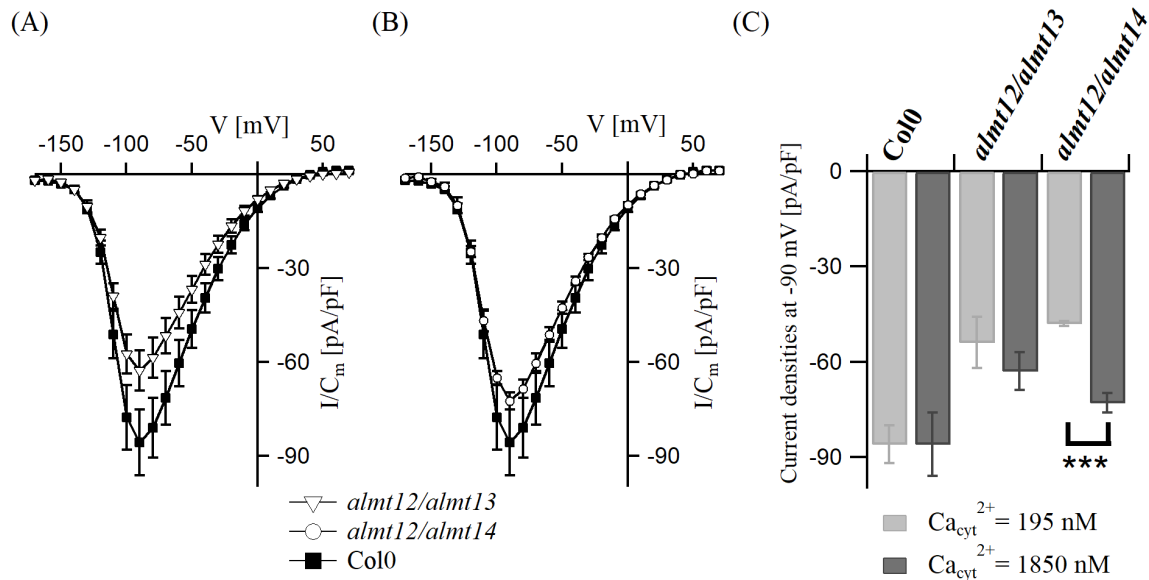


**Figure 16. R-type anion channel response in guard cell protoplasts of Col0 and *almt12/almt13* and *almt12/almt14* loss-of-function mutants under different cytosolic calcium conditions.**

(A) and (B) Steady-state current density ( $I_{ss}/C_m$ ) of Col0 and (A) *almt12/almt13* and (B) *almt12/almt14* loss-of-function mutants plotted against corresponding voltages recorded under 1850 nM free cytosolic  $Ca^{2+}$  concentration. Data points represent mean of (A) 7-10 and (B) 3-10 experiments with SEM. Measurements in A and B were performed in whole-cell configuration. (C) Peak current density of guard cell protoplasts from Columbia (Col0) and *almt12/almt13* and *almt12/almt14* under 195 nM and 1850 nM free cytosolic  $Ca^{2+}$ . Steady-state current densities evoked upon a voltage jump from -170 mV to 90 mV were determined. Data represent means  $\pm$  SEM of three to seven experiments. Current recordings were carried out with a sulfate-based ATP-containing pipette solution adjusted to 195 nM or 1850 nM free  $Ca^{2+}$ . For statistical analysis, One-Way Anova followed by Bonferroni test was performed. Asterisks indicate significant differences:  $P < 0.001$  \*\*\*.

### 4.3. Differences between Col0 and WS R-type currents

Ozone induces stomatal closure (Kollist H. et al., 2007, Vahisalu T. et al., 2008, Vahisalu T. et al., 2010, Hoshika Y. et al., 2018). This phytotoxic air pollutant enters the plant leaf mostly via open stomata, so its uptake is related to stomatal conductance and can also be visualised by leaf injury (Kerstiens G. and Lenzian K. J., 1989, Kollist H. et al., 2000, Kangasjärvi J. et al., 2005, Brosché M. et al., 2010, Hoshika Y. et al., 2018). Recently, differences in leaf injury induced by  $O_3$  between varied *Arabidopsis* natural accessions (e.g. Col0 and WS) was published (Brosché M. et al., 2010).

#### 4.3.1. Expression of prominent R- and S- type channels in Col0 and WS

The S-type and R-type anion channels participate in stomatal closure (Schroeder J. I. and Keller B. U., 1992, Schroeder J. I. et al., 1993, Meyer S. et al., 2010, Sasaki T. et al., 2010, Geiger D. et al., 2011). In order to investigate genes responsible for variable stomatal conductance in response to ozone, cDNA was prepared from enzymatically isolated guard cell protoplasts of *Columbia* (Col0) and *Wassilewskija* (WS) ecotypes (**Section 3.3.3**). Expression level was quantified for the most prominent candidates from the R-type gene family (*ALMT12*, *ALMT13*, *ALMT14*) and the S-type gene family (*SLAC1* and *SLAH3*). All three examined genes from the R-type family (*ALMT12*, *ALMT13*, and *ALMT14*) were found in the Col0 ecotype at respective levels of  $1138 \pm 188$ ,  $114 \pm 25$  and  $60 \pm 20$  molecules per 10.000 actin (**Figure 14**). The WS ecotype had  $1278 \pm 86$  transcripts of *ALMT12* per 10.000 actin,  $793 \pm 234$  transcripts of *ALMT13* per 10.000 actin and no expression of the *ALMT14* gene (**Figure 17A**). qRT-PCR analysis showed *SLAC1* gene expression to be around 8 times higher than *SLAH3* for both ecotypes. Col0 had  $9497 \pm 890$  and  $1299 \pm 166$  of *SLAC1* and *SLAH3* transcripts per 10.000 actin, respectively while WS had  $6394 \pm 1067$  and  $689 \pm 63$  transcripts per 10.000 actin (**Figure 17B**). In summary, Col0 and WS have different expression patterns for S-type and R-type anion channel genes.

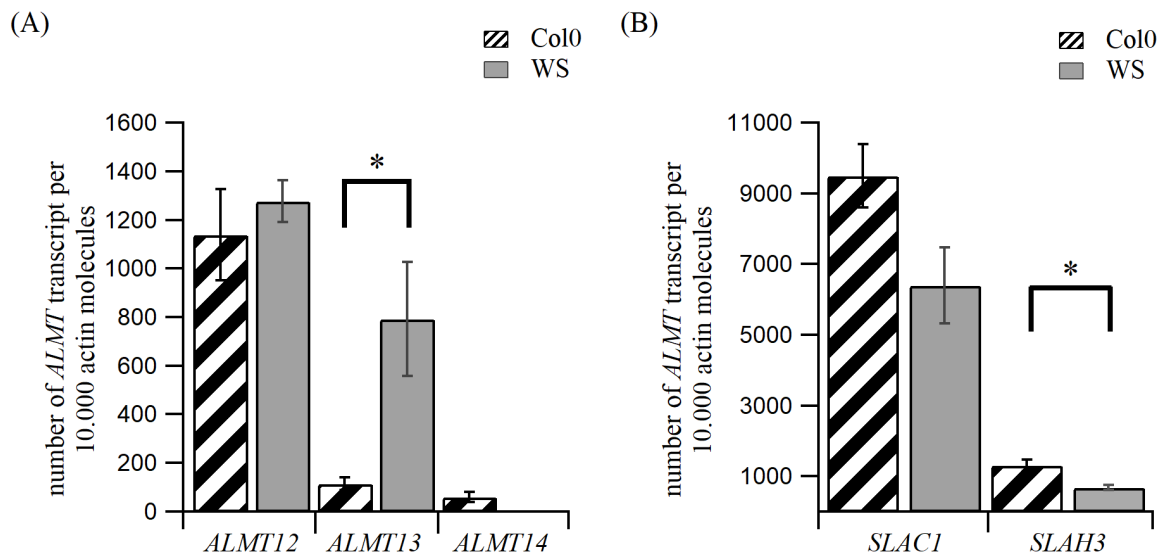


**Figure 17. Expression of *ALMT12*, *ALMT13*, *ALMT14*, *SLAC1* and *SLAH3* in guard cell protoplasts of *Columbia* (Col0) and *Wassilewskija* (WS) ecotypes.**

Transcript level of (A) *ALMT12*, *ALMT13* and *ALMT14* and (B) *SLAC1*, *SLAH3* in Col0 and WS guard cell protoplasts. Data represent mean  $\pm$  SEM values. The number of independent biological repetitions was  $n = 3$ . The total number of examined samples was  $n = 6-10$ . Expression of *ALMT13* and *SLAH3* in WS significantly differ compared to Col0, \*,  $P < 0.05$ , Two-Way Anova followed by Bonferroni test. Data of *SLAC1* and *SLAH3* expression were analysed by Dr. Heike Müller (University of Würzburg).

#### 4.3.2. Calcium-dependent QUAC current in the WS ecotype

Variation in ALMT genes expressed in Col0 and WS ecotypes suggest differences in R-type current between both *Arabidopsis thaliana* ecotypes. Similarly to the previous investigation of residual R-type currents in the *almt12* mutant, the activation threshold, peak current position and size, calcium dependency, selectivity and ATP dependency were examined. The patch clamp measurements were performed on guard cell protoplasts isolated from both ecotypes. They were carried out in the presence of 20 mM CaMalate in the bath solution and 75 mM  $SO_4^{2-}$  in the pipette solution, which additionally contained either 195 nM or 1850 nM free  $Ca^{2+}$  (Table 1 and Table 2 R1 and R2, Section 3.2.10). Negative holding potential and applied pulse protocol from -170 mV to +70 mV allowed recordings of typical fast-activated and deactivated currents, which over the voltage scale showed a characteristic bell-shaped (Figure 18A and B). For both ecotypes and cytosolic calcium concentrations, R-type anion currents have been detected in the range of -150 mV to +30 mV of plasma membrane



potentials (**Figure 18A and B**). Furthermore, peak-current density was observed at -90 mV (**Figure 18A and B**).

The size of peak-current density for the WS ecotype ( $-35 \pm 5$  pA/pF) differs from Col0 ( $-86 \pm 6$  pA/pF) at low cytosolic calcium. Furthermore, a rise in about 66 % to  $-58 \pm 7$  pA/pF at high cytosolic calcium concentration, which did not happen in Col0 (**Figure 18B**). Tail current data analysis revealed a lack of notable calcium- and ecotype-dependent differences in charge movement ( $z_q \approx 2$  for Col0 and WS). Both ecotypes had similar midpoint voltage ( $V_{1/2} \approx 116$  mV) and achieved relative open probability equal to 1 at -50 mV, independently of calcium levels (**Figure S1, Section 12**).

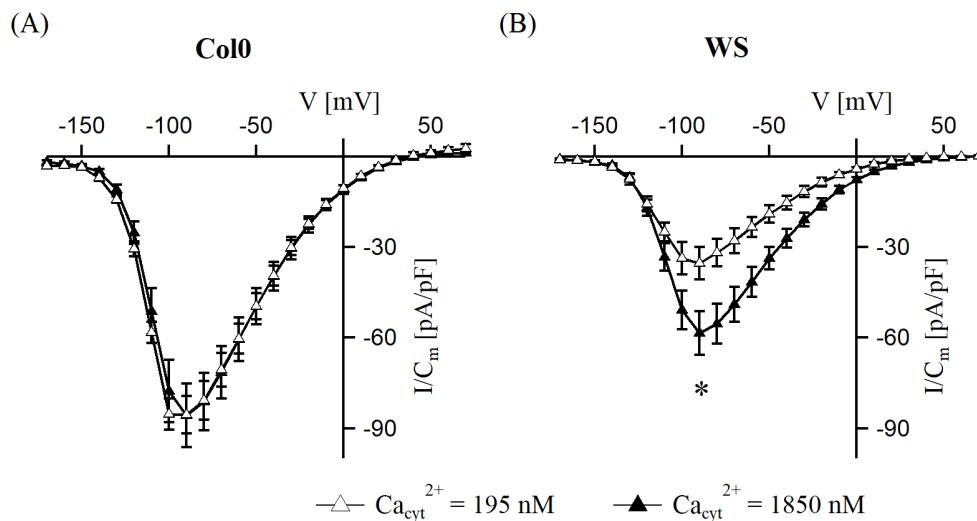


**Figure 18. Voltage-induced macroscopic R-type anion currents of guard cell protoplasts from Columbia (Col0) and Wassilewskija (WS) ecotypes.**

(A) and (B) Steady-state current density ( $I_{ss}/C_m$ ) plotted against corresponding voltages for (A) Col0 and (B) WS. Data points represent mean for 5-10 experiments with SEM. Measurements in A and B were performed in the whole-cell configuration. Data presented in B are significantly different in peak current, \*,  $P < 0.05$ , One-Way Anova followed by Bonferroni test.

#### 4.3.3. Chloride currents in *Arabidopsis thaliana* guard cell protoplasts

It has been shown that *Vicia faba* R-type anion channels are permeable not only for sulphate but also for chloride (Hedrich R. and Marten I., 1993). The same effect was observed for *Arabidopsis thaliana* hypocotyl cells (Frachisse J. M. et al., 1999). Guard cell protoplasts of Col0 did not reveal bell-shaped R-type-like currents in the presence of cytosolic chloride, however linear chloride currents were noticed (Mumm P., 2010). Supplementation of malate,

a possible modulator of the R-type anion channels, did not reveal discernible R-type anion currents in Col0 (**Figure 11B, Section 4.1.1**) (Hedrich R. and Marten I., 1993). Furthermore, linear chloride currents were not affected by the presence of cytosolic malate (**Figure 19C, Section 4.3.3**).

The WS ecotype is interesting due to changed expression level of *ALMT12*, *ALMT13*, *ALMT14* and *SLAH3* compared to the Col0 ecotype (**Figure 17A and B, Section 4.3.1**). In order to check the chloride permeability of the R-type anion channels in the guard cell protoplasts of the WS ecotype, patch clamp experiments were carried out in the presence of cytosolic chloride instead of sulphate (**Table 3 R3, Section 3.2.10**). Application of the regular voltage protocol resulted in voltage-dependent current responses (**Figure 19A and B**). Characteristic bell-shaped R-type currents described in **Section 4.3.2** were recorded when sulphate was present in the pipette solution. Linear, voltage-independent current was noticed in the chloride-based pipette solution (**Figure 19A and B**). Furthermore, linear current present in the Col0 ecotype in negative voltages was higher than the WS ecotype. Current reached at -180 mV was  $-9 \pm 4$  pA/pF for Col0 and  $-2 \pm 1$  pA/pF for WS (**Figure 19A and B**). Supplementation of chloride-based pipette solution with 1mM malate did not evoke bell-shaped R-type currents and caused an increase in the voltage independent current in the WS ecotype ( $-13 \pm 1$  pA/pF at -180 mV) to levels comparable to Col0 ( $-10 \pm 1$  pA/pF at -180 mV) over the whole measured voltage range (**Figure 19C and D**). Additionally, the clear difference in reversal potential noticed for ecotypes in the presence of cytosolic chloride vanished after malate supplementation (**Figure 19C and D**).

Briefly summarizing, the characteristic bell-shaped R-type current is not present for WS or Col0 ecotypes in cytosolic chloride-based solution and malate cannot activate it. However, chloride voltage-independent currents present in the WS ecotype are modulated by cytosolic malate.

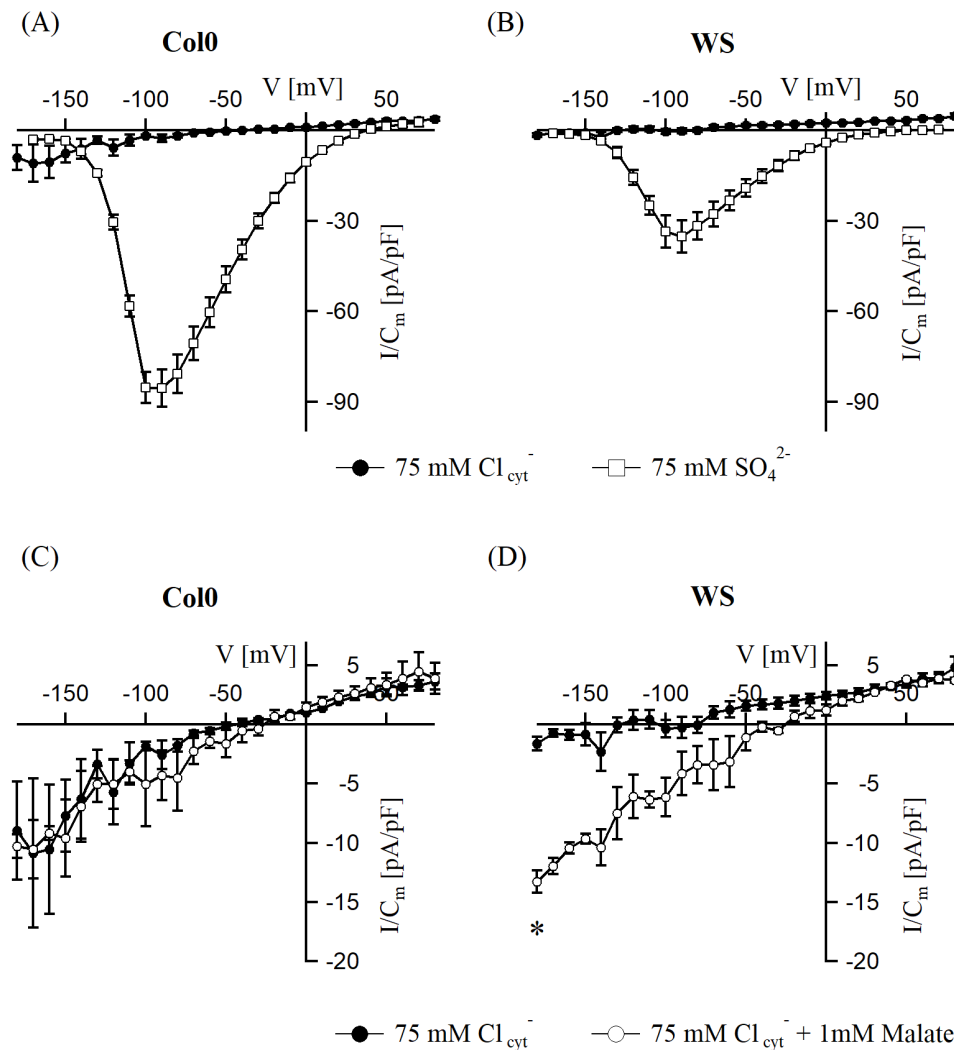


**Figure 19. R-type anion channel response in guard cell protoplasts of Columbia (Col0) and Wassilewskija (WS) ecotypes to different cytosolic conditions.**

(A), (B), (C) and (D) Steady-state current density ( $I_{ss}/C_m$ ) plotted against corresponding voltages for Col0 and WS. Data points represent means of (A) 3-6, (B) 3-5 and (C,D) 3 experiments with SEM. Measurements in A, B, C and D were performed in whole-cell configuration. Data present in D was significantly different at -180 mV, \*,  $P < 0.05$ , Two-Way ANOVA followed by Bonferroni test.

#### 4.3.4. ATP and its derivative AMP-PNP blocks R-type anion channels

Patch clamp experiments presented in Section 4.1.2 revealed that ATP negatively regulates R-type anion currents in *Arabidopsis thaliana* guard cell protoplasts. The voltage range of R-type channel activity is shifted to more positive voltages what could be caused by direct blockage or channel phosphorylation (Figure 12, Section 4.1.2). To distinguish between these two possible ATP interactions with R-type currents, further experiments were conducted. Furthermore, two ecotypes with a significantly different ratio in *ALMT12/ALMT13* expression

level - WS and Col0 - were included to analyse the influence to ATP modulation of R-type anion channels. The measurements were essentially carried out in the presence of standard bath solution (**Table 1, Section 3.2.10**) and 75 mM  $\text{SO}_4^{2-}$  in pipette solution, which additionally contained 195 nM free  $\text{Ca}^{2+}$  and 5 mM ATP, 5 mM AMP-PNP or 0 mM ATP (**Table 4 R6-R8, Section 3.2.10**). With pipette solution lacking ATP, voltage pulses (+90 mV to -240mV with 10 mV steps) and positive holding potential (+70 mV) were applied (**Figure 7B, Section 3.2.8**). For both ecotypes, voltage-dependent current responses were recorded. In the presence of ATP, R-type anion currents showed peak-current at -90 mV (**Figure 20A and B**). The values of the measured peak current density for Col0 and WS in the presence of ATP were  $-63 \pm 11$  pA/pF and  $-56 \pm 10$  pA/pF, respectively (**Figure 20A and B**). Removal of ATP from the pipette solution resulted in a change of peak current position from -90 mV to about -170 mV, the shift of R-type channel activity to more negative voltages and a rise in peak current. However, these differences were not significant between ecotypes (**Figure 20A and B**). AMP-PNP cannot be used for phosphorylation, but still has a geometric structure similar to ATP (Yount R. G., 1975). The presence of 5 mM AMP-PNP in the pipette solution resulted in peak current and R-type channel activity that was between the presence and lack of ATP in position and size, but also without significant differences between ecotypes (**Figure 20A and B**). The patch clamp experiments performed for Col0 and WS did not show any significant differences between the R-type current responses in the presence of ATP and its derivatives for both ecotypes. Cytosolic AMP-PNP and ATP can modulate R-type currents with different effects. The above results suggest that ATP influence R-type anion channels by direct block and phosphorylation.

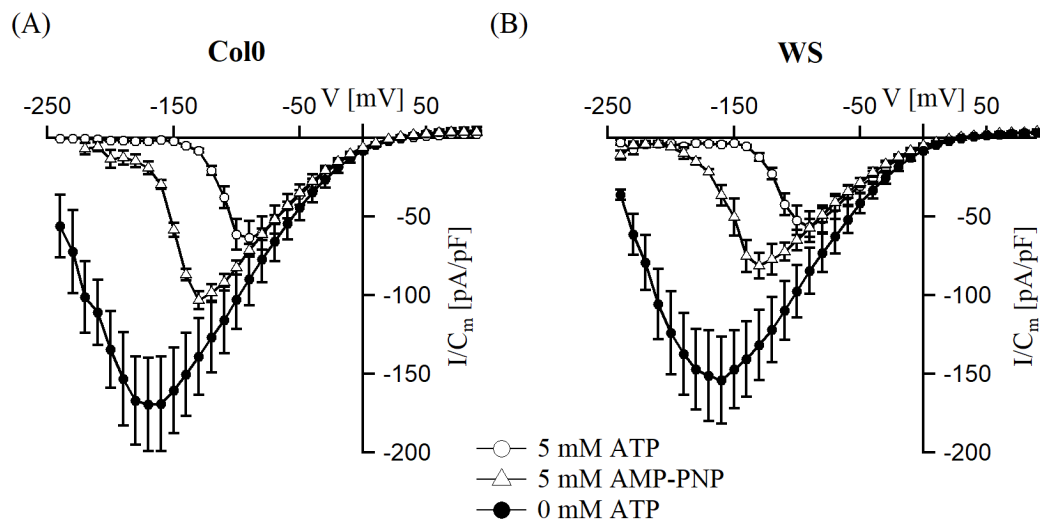


**Figure 20. R-type anion channel response of guard cell protoplasts of *Columbia* (Col0) and *Wassilewskija* (WS) ecotypes to cytosolic ATP or AMP-PNP.**

(A) and (B) Steady-state current density ( $I_{ss}/C_m$ ) plotted against corresponding voltages for (A) Col0 and (B) WS. Data points represent mean of (A) 5-6 and (B) 3-5 experiments with SEM. Measurement in A and B were performed in whole – cell configuration.

## 5. Discussion

### 5.1. *ALMT13* and *ALMT14* as genes involved in the generation of R-type anion currents

The stomatal pore width is regulated in response to environmental signals, which allows plants to control gas exchange and water loss (Sirichandra C. et al., 2009, Voss L. J. et al., 2018). Release of  $K^+$ ,  $Cl^-$  and organic ions (e.g. malate) results in increased water potential, water efflux from guard cells and finally stomatal closure (Hedrich R. et al., 1990, Pandey S. et al., 2007). The R-type and S-type anion channels, together with outward-rectifying  $K^+$  channels, participate in this process. In *Arabidopsis thaliana* plant S-type anion channels are encoded by genes that belong to the *SLAC* family (Vahisalu T. et al., 2008). R-type anion currents in *Arabidopsis thaliana* are partly assigned to AtALMT12 (Meyer S. et al., 2010, Sasaki T. et al., 2010). However, the knock out mutant of this plasma membrane-localized channel still show a high level of R-type-like currents, which suggests that ALMT12 is not the only component of the R-type currents encoded by members of the *ALMT* gene family (Meyer S. et al., 2010). Kovermann and co-workers in 2007 subdivided the *Arabidopsis ALMT* gene family into three clades: I to III. *ALMT12* together with three other genes - *ALMT11*, *ALMT13* and *ALMT14* - were allocated to clade number III, making them promising candidates for additional QUAC (quick-activating anion channel) current components (Kovermann P. et al., 2007). The patch clamp characterization of residual R-type currents present in the *almt12* loss-of-function mutant under different solute conditions revealed its significant similarities to wild type R-type anion currents e.g. strong voltage dependency, the same voltage range activity, peak current position and effect of ATP supplementation to cytosol (**Figure 10A, B and C, Section 4.1.1; Figure 12B and C, Section 4.1.2**). These similarities suggest that residual R-type currents measured in the *almt12* loss-of-function mutant are generated instead by one or more channels belonging to the *ALMT* family rather than other gene families. Study of ALMT gene expression levels revealed transcripts of *AtALMT1*, *AtALMT3*, *AtALMT4*, *AtALMT5*, *AtALMT6*, *AtALMT9*, *AtALMT12*, *AtALMT13* and *AtALMT14* in Col0 guard cell protoplasts.

Simultaneously, the *almt12* mutant showed *AtALMT3*, *AtALMT4*, *AtALMT5*, *AtALMT6*, *AtALMT9* and *AtALMT13* transcripts (**Figure 14, Section 4.1.4; Figure S2, Section 12**). According to the literature, *AtALMT3*, *AtALMT4*, *AtALMT5*, *AtALMT6* and *AtALMT9* are targeted to the tonoplast (Kovermann P. et al., 2007, Meyer S. et al., 2011, Zhang J., 2014, Eisenach C. et al., 2017). Furthermore, endoplasmic reticulum localization of *AtALMT5* was reported (Kovermann P. et al., 2007). The aforementioned localization data and similar expression level of *AtALMT3* to 6 and *AtALMT9* in Col0 and *almt12* makes it very unlikely that channels coded by these genes could generate QUAC current (**Figure S2, Section 12**). *AtALMT1*, *AtALMT13* and *AtALMT14* are localized in plasma membrane, similar to *AtALMT12* (Hoekenga O. A. et al., 2006, Gutermuth T. et al., 2018). R-type current reduction in the *almt12* mutant could be, in principle, caused by channels encoded by *AtALMT1*, *AtALMT13* and *AtALMT14*, but expression of *AtALMT1* in wild type was measured in marginal amounts (**Figure 14, Section 4.1.4; Figure S2, Section 12**). In the literature, *AtALMT1* is described as an  $Al^{3+}$ -activated channel, responsible for malate release in *Arabidopsis thaliana* roots, where it is specifically expressed (Hoekenga O. A. et al., 2006). Additionally, malate in the physiological range present in the chloride-based pipette solution did not reveal bell-shaped currents or any differences between wild type and the *almt12* mutant, which suggests that the *ALMT1* channel does not contribute to the reduction showed for *almt12* R-type currents compared to wild type (**Figure 11B, Section 4.1.1**). Altogether, this indicates that *AtALMT13* and *AtALMT14* are good candidates to participate in R-type-like anion currents.

**To validate the hypothesis that *ALMT13* and *ALMT14* participate in R-type currents**, two double loss-of-function mutants: *almt12/almt13* and *almt12/almt14* were studied. Patch clamp study performed for both mentioned mutants showed R-type currents with typical features - strong voltage dependency, the same voltage range activity, and peak current position as for wild type and the *almt12* mutant (**Figure 15B, Section 4.2; Figure 10B, Section 4.1.1; Figure S4, Section 12**). Both double mutants had similar peak current density to the *almt12* mutant, which is reduced compared to Col0 under 195 nM free cytosolic calcium conditions (**Figure 15C, Section 4.2**). Quantitative real time PCR revealed, as predicted, *ALMT13* transcript in the *almt12/almt14* mutant, but surprisingly, expression of *ALMT14* in *almt12/almt13* was also discovered (**Figure 15A, Section 4.2**). This expression data supports

the conclusion that ALMT13 and ALMT14 could participate in QUAC current, in addition to ALMT12, in *Arabidopsis thaliana* guard cell protoplasts. Nevertheless, one cannot fully exclude the possibility that other channels outside the ALMT family are involved in the generation of R-type currents. To test this hypothesis, the *almt12/almt13/almt14* triple loss-of-function mutant is necessary. Generation of this mutant is impeded by the localization of *ALMT13* and *ALMT14* genes on the same chromosome. In a future study, the CRISPR/Cas9 technique could be used to overcome this difficulty.

## **5.2. A rise in cytosolic ATP reduces R-type anion currents in *A.thaliana* guard cells**

The ATP supplementation to the pipette solution reduced R-type anion channel activity in all studied *Arabidopsis thaliana* plant lines (WS, Col0 and *almt12*) (**Figure 20A and B, Section 4.3.4; Figure 12B and C, Section 4.1.2**). The negative regulation of R-type anion currents caused by cytosolic ATP is also observed for *Arabidopsis thaliana* hypocotyl protoplasts. In both, guard cell protoplasts as well as in hypocotyl protoplasts, ATP modulates peak current position and causes a reduction peak size (Thomine S., et al., 1997). Absence of ATP in the cytosol of *A. thaliana* guard cell protoplasts shifts peak current around 80 mV to more negative voltages (from -90 mV to -170 mV) and keeps R-type channel active at hyperpolarized membrane potentials e.g. -250 mV (**Figure 20A and B, Section 4.3.4; Figure 12B and C, Section 4.1.2**). A bell shape is an intrinsic features of *A. thaliana* R-type currents and therefore of the current generated by the AtALMT12 channel (**Figure 20A and B, Section 4.3.4; Figure 12B and C, Section 4.1.2**, Hedrich R. et al., 1990, Thomine S. et al., 1997, Meyer S. et al., 2010). However, AtALMT9, a member of the ALMT family, did not show bell-shaped current in the absence of ATP (Zhang J. et al., 2014). Thus, Zhang J. and colleagues concluded that bell-shaped current is an effect of the ATP blockage (Zhang J. et al., 2014). This described difference between AtALMT12 and AtALMT9 is most likely related to the pulse protocol, which did not exceed -180 mV for AtALMT9 (Zhang J. et al., 2014). It could be that this was not sufficient to record the possible bell-shaped current for the AtALMT9 channel. It is highly possible that the peak current of AtALMT9, similarly to AtALMT12 in absence of cytosolic ATP, is located at a potential lower than -180 mV (**Figure 20A, Section 4.3.4**).



It is a matter of debate how ATP interacts with channels involved in R-type (QUAC) current generation. On the one hand, Thomine et al. in 1997 showed direct blockage of R-type channels by ATP for *Arabidopsis thaliana* hypocotyl protoplasts. They included non-hydrolysable forms of ATP (e.g. AMP-PNP) in the study and showed that these derivatives can block R-type channels with the same or higher efficiency than ATP (Thomine S. et al., 1997). An ATP-dependent direct block has also been shown for the AtALMT9 channel localized in guard cell vacuoles. This ALMT family member is involved in stomatal opening in *A. thaliana* (De Angeli A. et al., 2013). Lys-193 from AtALMT9, which creates a complex with ATP, is conserved in AtALMT12 (Lys-155), which suggests that this could also be the ATP binding site in AtALMT12 (Prof. Dirk Becker, University of Würzburg, personal communication, Zhang J. et al., 2014). The Lysine-193-ATP complex is located in the channel pore region and does not allow ions to flow through the AtALMT9 channel (Zhang J. et al., 2014). To test the possible role of ATP as a direct blocker of the *Arabidopsis thaliana* ALMT12 channel, mutagenesis of the codon coding Lys155 in the gene needs to be performed and electrophysiologically examined.

However, supplementation of AMP-PNP to the *Arabidopsis thaliana* guard cell cytosol caused a reduction in R-type currents, which did not achieve levels observed in response to cytosolic ATP elevation (**Figure 20A and B, Section 4.3.4**). These data suggest regulation of *Arabidopsis thaliana* QUAC currents occurs not only by direct block but also by phosphorylation. Deactivation of the R-type-like anion channels via phosphorylation has been already shown for AtALMT4. Eisenach C. and co-workers (2017) showed that AtALMT4 is deactivated via phosphorylation of serine in position 382. The SerPro di-peptide motif is a target for MPK4 and MPK6 kinases (mitogen-activated protein kinases) (Eisenach C. et al., 2017). Analogues of Ser-382 and the subsequent proline exist also in AtALMT12 amino acid sequence, which creates a possible ATP-dependent deactivation mechanism, driven by the phosphorylation of ALMT12 (Eisenach C. et al., 2017). Leung J. et al. (2006) showed that the *mpk6* loss-of-function mutant has a hypersensitive response to ABA compared to wild type. However, the *mpk6* loss-of-function mutant shows unaltered stomatal closure, which suggests involvement of MPK6 in stomatal opening rather than stomatal closure (Montillet J. et al., 2013). Furthermore, it was shown that ABA induces expression of HAI phosphatases, which dephosphorylate and inactivate MPK6 kinase (Mine A. et al., 2017). This suggests that active

MPK6 could participate in the inactivation of AtALMT12 through the phosphorylation of Ser-355, but ABA as an indirect, negative regulator of MPK6 leads to AtALMT12 activation. This hypothesis is in line with data published by Mumm P. et al. (2013), where authors examined several serine-alanine mutants in the C-terminus of AtALMT12 (S372A, S376A and S384A), which did not affect channel activity (Mumm P. et al., 2013). However, to finally test the hypothesis about ALMT12 deactivation via phosphorylation, a serine-glutamate ALMT12 mutant (imitating the phosphorylation state of ALMT12) need to be examined.

Regulation of R-type anion channels in *Arabidopsis thaliana* via phosphorylation was also postulated by Imes D. and co-workers (2013). They measured R-type anion current reduction in the *ost1-2* loss-of-function mutant and observed physical interaction between AtALMT12 and AtOST1 via bimolecular fluorescence complementation (BiFC) performed in the oocyte system. Together that lead them to the conclusion that AtALMT12 is activated via OST1-dependent phosphorylation (Imes D. et al., 2013). Nevertheless, the OST1 phosphorylation site is still unknown. Therefore, one could speculate that MPK6 and OST1 could regulate AtALMT12 via phosphorylation sites located in different places of the protein. It is interesting that knock-out of the *OST1* gene did not abolish the entire R-type current, which suggests that not all R-type channels are under the control of OST1 (Imes D. et al., 2013). This hypothesis is supported by the inability of OST1 to activate AtALMT13, but not AtALMT12 in *Xenopus* oocytes (Dr. Kai Konrad, University of Würzburg, personal communication, Gutermuth T. et al., 2018).

Finally, R-type anion currents recorded for the *Arabidopsis thaliana* ecotype Col0 and the *almt12* loss-of-function mutant have similar features compared to *Vicia faba* R-type anion currents – fast activation and deactivation, and a characteristic V-shape of the current-voltage relationship (**Figure 10A and B, Section 4.1.1**, Hedrich R. et al., 1990, Meyer S. et al., 2010). However, the ATP differently regulate R-type anion currents in *Arabidopsis thaliana* and *Vicia faba* guard cell protoplasts (Hedrich R. et al., 1990). *Vicia faba* R-type anion currents are activated by cytosolic ATP (Hedrich R. et al., 1990). However, this discrepancy in the literature can be attributed to a lack of knowledge about the channels underlying *Vicia faba* R-type currents. One could speculate also about possible differences in the number of subunits or regulatory factors between *Arabidopsis thaliana* R-type channels and *Vicia faba* R-type channels.

### 5.3. Residual QUAC current in the *almt12* mutant is dependent on cytosolic calcium

Studies performed for different plant species showed that calcium plays an important role in ABA- and CO<sub>2</sub>-induced stomatal closure via modulation of guard cell anion currents (Hedrich R. et al., 1990, Pei et al., 1997, Grabov et al., 1997, Mori I. et al., 2006, Siegel R. S. et al., 2009, **Section 1.2**). Increased cytosolic concentration of this secondary messenger causes activation of R-type anion channels, which was elegantly shown by Prof. Rainer Hedrich and co-workers in *Vicia faba* (Hedrich R. et al., 1990). This patch clamp study revealed that the activity of R-type anion channels in *Vicia faba* guard cell protoplasts increases together with increased cytosolic calcium concentration (Hedrich R. et al., 1990). Notwithstanding, there is no complex knowledge about the calcium dependency of R-type anion currents in the model plant *Arabidopsis thaliana* and residual R-type anion currents in the *almt12* mutant. Surprisingly, R-type currents recorded in the Col0 ecotype remained unaltered after the rise in cytosolic calcium. The Col0 ecotype showed exactly the same current response – around -86 pA/pF – under both cytosolic calcium conditions (**Figure 13A and C, Section 4.1.3**). However, knock out of ALMT12, a channel known to be partially responsible for the R-type anion currents in the Col0 ecotype, was sufficient to yield calcium-dependent behaviour. Residual R-type current in the *almt12* loss-of-function mutant showed a significant increase in peak current density (about 1.4-fold) associated with the rise in free cytosolic calcium concentration (**Figure 13B and C, Section 4.1.3**). A similar calcium-dependent R-type current variation was noticed for *almt12/almt14*, but not *almt12/almt13* double mutants (**Figure 16C, Section 4.2**).

This calcium related conversion of R-type current activity can be correlated with expression patterns of the ALMT gene family. This makes it possible to hypothesise that several expressed genes belonging to the ALMT family stands behind the calcium-independent or calcium-dependent R-type currents measured for Col0, the *almt12* mutant and both double mutants (**Section 5.1**). One may propose that ALMT12 is a dominant gene in the Col0 ecotype and current generated via this channel is calcium-independent, while ALMT13 is a calcium-dependent R-type anion channel that generates residual R-type current in the *almt12* mutant. This hypothesis is further supported by patch clamp data obtained for the *almt12/almt14* double mutant, which has the same ALMT gene expression pattern and

calcium-dependent behaviour as the *almt12* single mutant. Furthermore, similarly to the *ALMT12* gene in wild type, *ALMT14* expressed in the *almt12/almt13* loss-of-function mutant is related to the calcium-independent behaviour of R-type anion currents for this double mutant (**Figure 16C, Section 4.2**). Direct calcium regulation was shown for the ALMT channel localized in the vacuolar membrane, where activity of AtALMT6, but not AtALMT9 is regulated by cytosolic calcium concentration (Meyer S. et al., 2011, De Angeli A. et al., 2013). In addition to direct calcium regulation, indirect calcium regulation of the ALMT family via CPKs was also suggested (Gutermuth T. et al., 2018).

It is common knowledge that calcium can modulate channel activity via binding to "EF-hands" (Konrad K. R. et al., 2018). The canonical EF-hand consist of 12-residues that build a calcium binding loop, which starts with aspartate and ends with glutamate (Grabarek Z., 2006). Calcium ligands X, Y, Z, -X, -Y, -Z form an orthogonal coordinate system with a centrally-located  $\text{Ca}^{2+}$  ion (Grabarek Z., 2006). Typical binding of  $\text{Ca}^{2+}$  to the EF-hand leads to conformational changes. These changes can result in either modulation of activity or ability to interact with other proteins, which can finally modulate protein function or activity (Day I. S. et al., 2002, Konrad K. R. et al., 2018). Modulation of the activity and/or functionality via  $\text{Ca}^{2+}$  binding has been presented for calcium-permeable channels e.g. channels from the CNGC family and TPC1 in *Arabidopsis* (Dadacz-Narloch B. et al., 2011, Schulze C. et al., 2011, Jammes F. et al., 2011). Alignment of the AtALMT12, AtALMT13 and AtALMT14 amino acid sequence revealed a possible EF-hand-like motif in the AtALMT13 protein (**Figure 21**). Negatively charged amino acids start with Asp at position 247 and end with Glu at position 258. Interestingly this motif is missing in AtALMT12 and AtALMT14, which supports the idea of calcium-dependent and independent ALMT channels (**Figure 21**). This data leads to the conclusion that the ALMT13 channel could participate in QUAC current as a calcium-dependent component. Nonetheless, the lack of calcium dependency of Col0 QUAC currents indicates that ALMT13 is not a key player when *ALMT12* is overwhelmingly expressed. *ALMT13* and *ALMT14* genes have relatively low expression in *ALMT* mutants, however increased cytosolic calcium levels result in non-significantly different R-type current compared to wild type (**Figure 16A and B, Section 4.2**). That could suggest that ALMT12-14 channels all fulfil the same function in stomatal closure and can complement each other. Differences in susceptibility to calcium support the hypothesis that ALMT12, ALMT13 and ALMT14 could be involved in different signaling

cascades, which leads to stomatal closure e.g. calcium-dependent (with or without participation of other calcium-dependent proteins) and calcium-independent.

	X	Y	Z	-Y	-X	-Z	
AtALMT13	YFEEKLN	NETSD	SES	DD	ELIYNGYNTVLDSKSADEALAMYAKWEP	RRRCNKFPSQQ	299
AtALMT12	YFEEKEKEKT	-----	DSK	RIYEGYQAVLDSKSTDETLALYANWEP	RHLRCHRFP	PCQQ	290
AtALMT14	YFEEEEKDEETS	---	LSE	DIYNGYKTVLDSKSADEALAMYASWEP	RHRHCHRFP	PWKH	295

**Figure 21. Sequence alignment of AtALMT12, AtALMT13 and AtALMT14.**

Sequence alignment of AtALMT12, AtALMT13 and AtALMT14. Possible EF-hand in AtALMT13 and adequate sequence of AtALMT12 and AtALMT14 were marked with red bars. Amino acids which could be involved in Ca<sup>2+</sup> binding are highlighted with red frame (designated X, Y, Z, -X, -Y and -Z). Alignments were prepared with used of Clustel Omega (<https://www.ebi.ac.uk/Tools/msa/clustalo/>).

In the early 90s S. Gilroy and co-workers observed that guard cells that did not show a rise in cytosolic Ca<sup>2+</sup> still closed normally (Gilroy S. et al., 1991). This observation was one of the first suggestion for Ca<sup>2+</sup>-independent anion channel activation leading to stomatal closure. Since then, evidence for Ca<sup>2+</sup>-independent, as well as Ca<sup>2+</sup>-dependent activation of the S-type anion channels in *Arabidopsis thaliana*, *Nicotiana tobacco* and *Vicia faba* has been published (Levchenko V. et al., 2005, Marten H. et al., 2007, Geiger D. et al., 2010). In addition to S-type anion channels, activation of R-type anion channels also influences effective stomatal closure. Thus it is reasonable that R-type anion channels should also be involved in both Ca<sup>2+</sup>-dependent and Ca<sup>2+</sup>-independent stomatal closure. According to data presented by Brandt B. et al. (2012), a ABA-evoked, calcium-independent pathway can be mainly mediated by OST1, which can activate ALMT12 and ALMT14 but not ALMT13 (Brandt B. et al., 2012, Gutermuth T. et al., 2018, Dr. Kai Konrad, University of Würzburg, personal communication). There is no evidence for indirect activation of AtALMT13 by CPKs, in contrast to what has been shown for AtALMT12 and AtALMT14 (Gutermuth T. et al., 2018).

Briefly concluding, ALMT13 probably is a direct target of cytosolic calcium and cannot participate in Ca<sup>2+</sup>-independent stomatal closure, while ALMT12 and ALMT14 participate in both mentioned pathways, leading to stomatal closure and sensing a cytosolic calcium rise via the activation of CPKs (Gutermuth T. et al., 2018).

## 5.4. Chloride permeability of *A. thaliana* R-type anion channels in the native environment

Pioneering patch clamp research performed on *Vicia faba* guard cells showed that R-type anion channels are permeable for many anions - e.g.  $\text{NO}_3^-$ ,  $\text{Cl}^-$ , malate (Hedrich R. and Marten I., 1993). Further studies on *Arabidopsis thaliana* hypocotyl cells confirmed the possible composition of R-type anion currents for these anions, with slightly different selectivity ratios (Frachisse J. M. et al., 1999). In 2010, it was obvious that Col0 guard cells express the *ALMT12* gene, and the encoded AtALMT12 belongs to the R-type anion channels (Meyer S. et al., 2010, Sasaki T. et al., 2010). Then, questions about the ALMT12 channel permeability become interesting. Study performed in the heterologous oocyte system revealed that AtALMT12 is permeable for sulphate, chloride and malate (Meyer S. et al., 2010, Imes D. et al., 2013, Malcheska F. et al., 2017). However, patch clamp recordings did not reveal chloride as a conductive anion for R-type anion channels in *Arabidopsis thaliana* guard cell protoplasts in the thesis of P.Mumm (2010), or in the present thesis (**Figure 19A and C, Section 4.3.3**). One could conclude that discrepancies in the AtALMT12 channel conductance for cytosolic chloride between the heterologous oocyte expression system and native guard cell environment are related to various regulatory factors, which are either present or absent in plants.

Malate is a well-known modulator of the R-type channels in *Vicia faba* as well as an activator of AtALMT9 (Hedrich R. and Marten I., 1993, De Angeli A. et al., 2013). However, its presence from either the apoplastic, or the cytosolic side, did not trigger permeation of *Arabidopsis thaliana* R-type channels for chloride ions (**Figure 11B, Section 4.1.1; Figure 19C, Section 4.3.3**). It was shown that sulphate could also fulfil a function of positive modulator for R-type anion channels in *Arabidopsis thaliana* hypocotyls (Frachisse J. M. et al., 1999). Supplementation of 1 mM sulphate into chloride cytosolic solution resulted in noticeable differences in background currents between Col0 and the *almt12* mutant (**Figure 11A, Section 4.1.1**), which not exists under homogenous cytosolic chloride conditions and probably are related to voltage-independent, chloride-conductive channel activity (Sasaki T, et al., 2010). Furthermore, bell-shaped inward current was observed with significantly higher peak current density for the *almt12* mutant than Col0 (**Figure 11A, Section 4.1.1; Figure S6, Section 12**), which is a surprising result taking into account the higher Col0 peak current density compared to the *almt12* mutant at 75 mM cytosolic sulphate (**Figure 10A and B, Section 4.1.1**). Most

likely this behaviour is associated with *ALMT13* function in the *almt12* mutant and predominant the *ALMT12* gene expression in *Arabidopsis thaliana* Col0 guard cells (**Figure 14, Section 4.1.4**). The recorded ratio between the described peak current densities suggest modulation of the *ALMT13* channel by sulphate (**Figure 10A and Figure 11A, Section 4.1.1**). Similar effect has already been observed in *Arabidopsis thaliana* hypocotyls, where sulphate upregulates R-type current in cytosolic chloride conditions (Frachisse J. M. et al., 1999). However, that also can be explained by an altered *ALMT13* permeability ratio to  $\text{Cl}^-$  or  $\text{SO}_4^{2-}$  caused by the sulphate modulation in comparison to the *ALMT12* channel. This idea is further supported by the shift of reversal potential to more positive voltages (chloride-like) in the *almt12* mutant compared to wild type. Nevertheless, one cannot fully exclude that this shift of the reversal potential is partially mediated by chloride-permeable S-type anion channels.

F. Malcheska and co-workers (2017) suggest that sulphate, as a xylem-delivered chemical signal, can trigger stomatal closure in response to drought, which is in line with early reports assigning sulphate to stomatal closure (Goodger J. Q. et al., 2005, Ernst L. et al., 2010, Malcheska F. et al., 2017). Sulphate is transported from xylem to the apoplast via  $\text{H}^+/\text{SO}_4^{2-}$  co-transporters from the SULTR family and it mainly goes to plastids, where it promotes stress-induced cysteine synthesis related to ABA synthesis (Cao M-J. et al., 2012, Batool S. et al., 2018, Chen Z. et al., 2019). Sulphate can trigger stomatal closure not only via the ABA pathway but also via direct modulation of the R-type anion channels. Presented patch clamp data showed sulphate-dependent increase in *ALMT13* absolute open probability and/or permeability for sulphate and chloride (**Figure 11A, Section 4.1.1**). Thus, it is possible that *ALMT13* has higher R-type anion currents at lower cytosolic sulphate concentration than *ALMT12*. Therefore, it can be involved in early response to sulphate-mediated stomatal closure under drought conditions. Following this idea, At*ALMT12* and At*ALMT13* could be involved in stomatal closure under different cytosolic sulphate concentrations, which is associated with water availability.

## 5.5. Col0 versus WS - features of anion currents associated with expression of the S- and R-type channels

Ozone as an air pollutant causes differing levels of leaf damage among natural *Arabidopsis thaliana* accessions (Brosché M. et al., 2010). This phytotoxic substance penetrates the leaf mostly via open stomata and causes its closure (Kerstiens G. and Lenzian K. J., 1989, Kollist H. et al., 2000, Kangasjärvi J. et al., 2005, Brosché M. et al., 2010, Hoshika Y. et al., 2018). Together, this suggests that variations in ion channel activity involved in the mechanism of stomatal closure. Col0 and WS are *Arabidopsis thaliana* ecotypes, which significantly differ in ozone sensitivity and revealed variation for the most prominent S-type and R-type anion channels (**Figure 17A and B, Section 4.3.1**). Analysis of the Col0 ecotype revealed expression of three genes belonging to the *ALMT* family (*ALMT12*, *ALMT13* and *ALMT14*), with *ALMT12* being the most highly expressed, whereas the WS ecotype did not show *ALMT14* expression and had significantly higher the *ALMT13* gene expression compared with Col0 (**Figure 17A, Section 4.3.1**).

Recently, Zhang A. and co-workers (2016) showed the relationship between SLAC1, SLAH3 and KAT1, where S-type channels negatively regulate the K<sup>+</sup> inward channel via protein-protein interaction. Both S-type anion channels have no effect on KAT1 expression or localization. Nevertheless, their co-expression with KAT1 in the heterologous oocyte system results in lower inward K<sup>+</sup> currents. Researchers proved that SLAC1 and SLAH3, participating as inhibitors of KAT1, can still conduct anions (Zhang A. et al., 2016). Therefore, there might be a similar interaction between *ALMT12* and *ALMT13* R-type channels, with additional negative regulation of *ALMT12* activity by *ALMT13*. This hypothesis is supported by similar expression of *AtALMT12* in both ecotypes with significantly higher expression of *ALMT13* in the WS ecotype (**Figure 17A, Section 4.3.1**). Furthermore, patch clamp measurements revealed lower peak current densities of R-type currents for WS compared to Col0 and cytosolic calcium-dependent behaviour of the WS ecotype (**Figure 18A and B, Section 4.3.2**). There is no differences in the amino acid sequence of *ALMT12* and *ALMT13* between Col0 and WS (Dr. Felix Bemm, University of Würzburg, data not shown), which assigns a calcium-dependent behaviour to the *ALMT13* channel and reinforces patch clamp data obtained for *almt12* and *almt12/almt14* mutants (**Figure 13B and C, Section 4.1.3; Figure 16C, Section 4.2**). However, peak current densities for WS and calcium-dependent *almt* mutants are not identical at



different cytosolic calcium concentrations, which suggests the importance of *ALMT12/ALMT13* expression ratio (**Figure 13B and C, Section 4.1.3; Figure 16C, Section 4.2; Figure 18B, Section 4.3.2**). Interaction between ALMTs and other proteins are further supported by the resting (holding) potential as a factor equalizing *Arabidopsis thaliana* R-type currents in both ecotypes (**Figure S5, Section 12**). To support the postulated ALMT-interaction hypothesis, bimolecular fluorescence complementation and electrophysiological evaluation of different *ALMT12/ALMT13* ratios in a heterologous expression system (e.g. the oocyte system) should be performed.

The WS ecotype showed significantly smaller linear inward chloride currents compared to Col0, but rose to Col0 levels after cytosolic malate supplementation (**Figure 19C and D, Section 4.3.3**). These features differentiate both ecotypes. Cytosolic chloride is not permeable for *Arabidopsis thaliana* R-type anion channels in guard cell protoplasts (Mumm P., 2010). Recently, Wang C. et al. (2018) published that cytosolic malate can activate S-type anion channels in *Arabidopsis thaliana* guard cell protoplasts, similar to the WS ecotype (**Figure 19D, Section 4.3.3**). Furthermore, *SLAC1* and *SLAH3* transcript levels were found in guard cells of both ecotypes (**Figure 17B, Section 4.3.1**). In light of this data, one can assume that the measured linear component is generated by S-type anion channels, which are permeable for chloride (Roelfsema M. R. et al., 2004, Geiger D. et al., 2009, Cubero-Font P. et al., 2016). It is interesting that this linear component is affected by cytosolic malate only in WS, but not in Col0, which was observed by Wang C. et al (2018). However, the external solution that was used by Wang C. and colleagues did not contain malate, which could show an apoplastic malate-dependent modulation of S-type channels in Col0 but not in the WS ecotype. R-type anion channels in *Arabidopsis thaliana* could participate in the uptake of apoplastic malate, which suggests outward linear current for both ecotypes (**Figure 19C and D, Section 4.3.3**). Furthermore, the release of cytosolic malate via R-type channels cannot be fully excluded. Lack of characteristic bell-shaped currents may be caused cumulatively by low cytosolic malate concentration and malate permeability (Frachisse J. M. et al., 1999, **Figure 19C and D, Section 4.3.3**).

## 5.6. The role of ALMT12-14 in stomatal closure during drought stress

Stomatal pore width changes via shrinking and swelling of the guard cells in response to environmental factors (Sano T. et al., 2008). In the open stomata state under normal water conditions, ALMT12-14 are switched to the deactivated state, probably by low cytosolic calcium, negative membrane potential, ATP direct blockage and MPK6-dependent phosphorylation (**Figure 22; Figure 21, Section 5.3; Figure 12A and B, Section 4.1.2**, Schroeder J. I. and Keller B. U., 1992, Eisenach C. et al. 2017). Drought stress triggers stomatal closure to prevent water loss (Geiger D. et al., 2011, Malcheska F. et al., 2017, Batool S. et al., 2018). Early response to drought is assigned to sulphate as a chemical signal, which is transported from roots into shoots by SULTR transporters (Malcheska F. et al., 2017). Higher sulphate concentration promotes ABA synthesis (**Figure 22**, Batool S. et al., 2018). ABA present in the cytosol can trigger expression of HAI phosphatases, which repress MPK6 (Mine A. et al., 2017). Furthermore, ABA allows the autophosphorylation of OST1 kinase by inactivating ABI1/ABI2 phosphatases (**Figure 22**, Geiger D. et al., 2009, 2010, 2011, Hedrich R., 2012). Active OST1 can phosphorylate ALMT12 and ALMT14 (**Figure 22**, Imes D. et al., 2013, Gutermuth T. et al., 2018). ALMT12 and ALMT14 can also be indirectly activated in a calcium-dependent manner via CPK- (e.g. CPK21-) driven phosphorylation (**Figure 22**, Gutermuth T. et al., 2018). ALMT13 activity seems to be directly related to cytosolic calcium concentration (**Figure 22, Figure 13B, Section 4.1.3**). Furthermore, it can not be activated by OST and CPKs in oocytes (Gutermuth T. et al., 2018, Dr. Kai Konrad, University of Würzburg, personal communication).

Active ALMT12 and ALMT14 mediates sulphate efflux out of the cell. Active ALMT13 seems to be able to mediate associated sulphate and chloride efflux (**Figure 22**). Anion efflux mediated by R-type channels leads to an increase in the water potential in the cytosol, which causes guard cell shrinkage and finally stomatal closure.

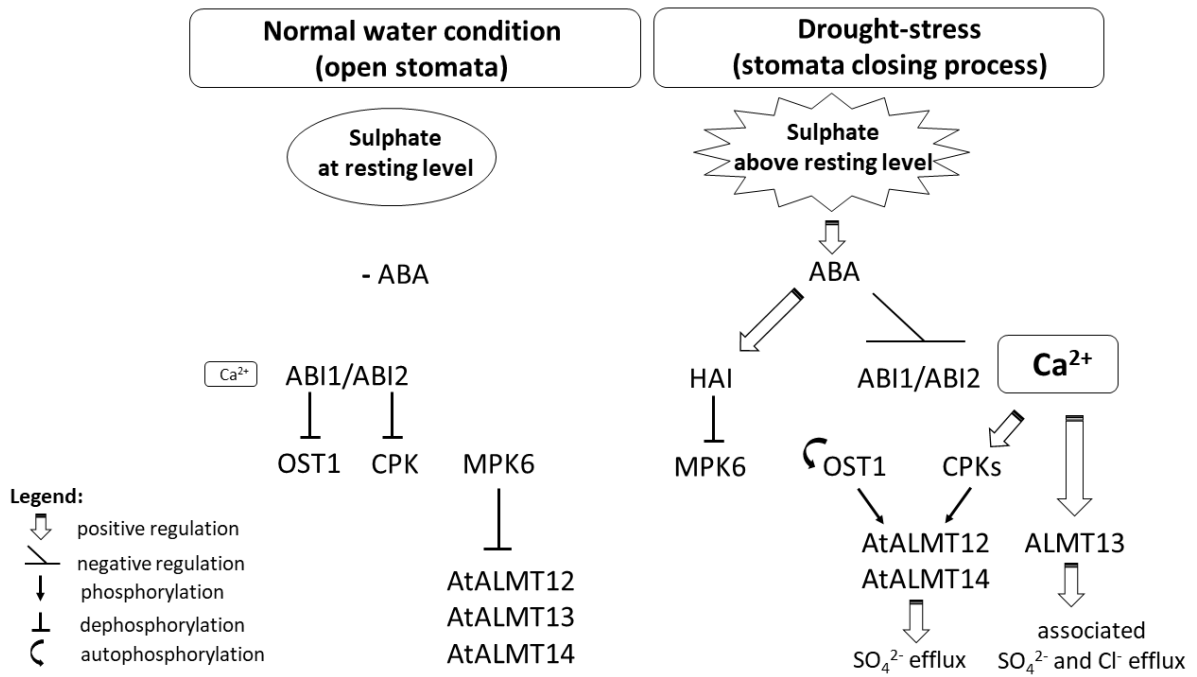


**Figure 22. Model of ALMT12, ALMT13 and ALMT14 regulation during stomatal movement.**

Model of stomatal movement under different water conditions including ALMT12, ALMT13, ALMT14 regulation and function. For more details see the main text.

## 6. Summary

In contrast to the well described molecular basis for S-type anion currents, the genes underlying R-type anion currents were unknown until 2010. Meyer S. and colleagues (2010) showed that, localized in the guard cell plasma membrane, AtALMT12 is an R-type anion channel involved in stomatal closure. However, knocking out AtALMT12 did not fully shut down R-type currents; the *almt12* loss-of-function mutant has residual R-type-like currents indicating that *ALMT12* is not the only gene encoding *Arabidopsis thaliana* R-type channels (Meyer S. et al., 2010). This PhD thesis is focussed on understanding the properties, regulation and molecular nature of the R-type channels in *Arabidopsis thaliana* plants. To fulfil these aims, the patch clamp technique was used to characterize electrical features of R-type currents in various conditions such as the presence/absence of ATP, variation in cytosolic calcium concentration or the presence of cytosolic chloride. Electrophysiological study revealed many similarities between the features of *Arabidopsis thaliana* R-type currents (Col0) and residual R-type currents (the *almt12* loss-of-function mutant). Strong voltage dependency, channel activity in the same voltage range, position of maximal recorded current and blockage by cytosolic ATP all pointed to a shared phylogenetic origin of the channels underlying these R-type currents. Expression patterns of the *ALMT* family members for Col0 and the *almt12* mutant revealed *ALMT13* and *AMT14* as potential candidates of the R-type channels. Electrical characterization of Col0, *almt12* and the two double loss-of-function mutants (*almt12/almt13* and *almt12/almt14*) strongly suggest that *ALMT13* mediates the calcium-dependent R-type current component that is directly regulated by cytosolic calcium. Additionally, similarly to *ALMT12*, *ALMT14* could participate as a calcium-independent R-type anion channel. Differences in response to the cytosolic calcium concentration between *ALMT12*, *ALMT13* and *ALMT14* suggest their possible involvement in different signalling pathways leading to stomatal closure. Moreover, a study performed for the two *Arabidopsis thaliana* ecotypes Col0 and WS showed drastically increased *ALMT13* expression for WS, which is related to R-type current properties. The WS ecotype has calcium-dependent R-type current behaviour, while it is calcium-independent in Col0. Furthermore, this plant line showed lower peak current densities compared to Col0 and *almt* mutants. These facts strongly suggest interaction between *ALMT12* and *ALMT13*, with *ALMT13* as a repressor of the

ALMT12. Acquired patch clamp data revealed sulphate-dependent increases in ALMT13 current. This could be caused by changes in absolute open probability and/or permeability for sulphate and possibly chloride and links ALMT13 with sulphate-mediated stomatal closure under drought stress. It was then confirmed that ATP affects R-type currents. In contrast to *Vicia faba*, ATP was identified as a negative regulator of the *Arabidopsis thaliana* R-type anion channels. The effect of ATP is ambiguous but there is a high probability that it is a result of direct block and phosphorylation. However, the phosphorylation site and place of ATP binding needs further investigation.

The story of the ALMT family, as examined in this thesis, sheds light on the complexity of the stomatal closure process.

## 7. Zusammenfassung

Im Gegensatz zu den gut beschriebenen S-Typ Anionenströmen, die durch Kanäle der SLAC1 Familie vermittelt werden, waren die Gene, die für R-Typ Anionenkanäle kodieren bis 2010 unbekannt (Negi J. et al., 2008, Vahisalu T. et al., 2008). In diesem Jahr identifizierten Meyer S. und Kollegen AtALMT12 als R-Typ Anionenkanal, der in der Plasmamembran von Schließzellen lokalisiert und am Stomaschluss beteiligt ist. In *almt12* Verlustmutanten sind jedoch restliche R-Typ Ströme messbar, die darauf hinweisen, dass *ALMT12* nicht das einzige Gen ist, das in *Arabidopsis thaliana* für R-Typ Anionenkanäle kodiert (Meyer S. et al., 2010). Diese Dissertation konzentriert sich auf die Analyse der Eigenschaften, der Regulation und der molekularen Natur der R-Typ Kanäle in *Arabidopsis thaliana* Pflanzen. Dafür wurde die Patch Clamp Technik angewandt, um den Einfluss verschiedener Faktoren wie z.B. das Fehlen/Vorhandensein von ATP, Unterschiede in der zytosolischen Kalziumkonzentration oder das Vorhandensein von zytosolischem Chlorid auf die elektrische Eigenschaften der R-Typ Ströme der verschiedene Kanäle zu untersuchen. Die elektrophysiologischen Untersuchungen zeigten viele Ähnlichkeiten zwischen den Eigenschaften von R-Typ Ströme in Wildtyp Pflanzen (Col0) und den noch vorhandenen Strömen in der Verlustmutante *almt12*. Beide sind stark spannungsabhängig, zeigen Kanalaktivität im gleichen Spannungsbereich und werden durch zytosolisches ATP inhibiert, was auf einen gemeinsamen phylogenetischen Ursprung der R-Typ Anionenkanäle hinweist. Die Expressionsanalyse der Gene der *ALMT*-Familie zeigte, dass *ALMT13* und *ALMT14* weitere potenzielle Kandidaten für Anionenkanäle des R-Typs sind. Die elektrophysiologische Charakterisierung von Col0, *almt12* und den beiden zweifachen Verlustmutanten *almt12/almt13* und *almt12/almt14* ermöglichte es, die durch *ALMT13* vermittelten Ströme als kalziumabhängige Komponente der R-Typ Ströme zu spezifizieren. Dabei wird *ALMT13* direkt durch zytosolisches Kalzium reguliert. *ALMT14* vermittelt dagegen kalziumunabhängige Ströme, ähnlich wie *ALMT12*. Unterschiede in der Reaktion auf die zytosolische Kalziumkonzentration zwischen *ALMT12*, *ALMT13* und *ALMT14* deuten auf eine mögliche Beteiligung an verschiedenen Signalwegen hin, die zum Stomaschluss führen. Darüber hinaus wurde eine Studie für zwei *Arabidopsis thaliana* Ökotypen durchgeführt. Pflanzen des Ökotyps WS zeigten eine erhöhte Expression von *ALMT13* im Vergleich zu Col0 Pflanzen, während die Expression von *ALMT12* in beiden vergleichbar ist. Diese Unterschiede

wirken sich auf die R-Typ Ströme aus, die nur in WS-Pflanzen kalziumabhängig sind und eine geringere Amplitude haben. Diese Fakten deuten stark auf eine Interaktion zwischen ALMT12 und ALMT13 hin, bei der ALMT13 als Repressor von ALMT12 wirkt. Die Auswertung der Patch-Clamp-Daten zeigte außerdem eine sulfatabhängige Zunahme der durch ALMT13 vermittelten R-Typ Ströme. Diese wird wahrscheinlich durch eine Änderung der Offenwahrscheinlichkeit und/oder der Permeabilität für Sulfat und möglicherweise für Chlorid verursacht, und die darauf hinweist, dass ALMT13 für frühe Antworten im sulfatvermittelten Stomaschluss bei Trockenstress eine Rolle spielt. Außerdem wurde gezeigt, dass ATP die R-Typ Ströme beeinflusst. In *Arabidopsis thaliana* Pflanzen wirkt ATP als negativer Regulator der Anionenkanäle vom R-Typ, nicht jedoch in *Vicia faba* (Hedrich R. et al., 1990). Der Mechanismus, über den ATP wirkt ist nicht eindeutig geklärt, aber es wird davon ausgegangen, dass es sich um eine direkte Inhibierung und Phosphorylierung handelt. Die Phosphorylierungsstelle und der Ort der ATP-Bindung bedürfen jedoch weiterer Untersuchungen.

Die Geschichte der ALMT-Familie, wie sie in dieser Arbeit untersucht wird, wirft ein Licht auf die Komplexität des stomatalen Verschlussprozesses.

## 8. Table list

TABLE 1. COMPOSITION OF BATH SOLUTION. ....	32
TABLE 2. COMPOSITION OF SULPHATE-BASED PIPETTE SOLUTIONS.....	32
TABLE 3. COMPOSITION OF CHLORIDE-BASED PIPETTE SOLUTIONS. ....	33
TABLE 4. PIPETTE SOLUTION COMPOSITION USED TO STUDY ATP EFFECT ON R-TYPE ANION CHANNELS.....	33
TABLE 5. PRIMERS FOR THE QUANTITATIVE REAL-TIME POLYMERASE CHAIN REACTION. ....	37
TABLE 6. CYCLER-PROGRAM FOR QUANTITATIVE REAL-TIME POLYMERASE CHAIN REACTION. ....	38
TABLE 7. PRIMERS USED FOR GENOTYPING LOSS-OF-FUNCTION MUTANTS. ....	40
TABLE 8. CYCLER-PROGRAM FOR GENOTYPING LOSS-OF-FUNCTION MUTANTS.....	41



## 9. Figure list

FIGURE 1. MORPHOLOGICAL TYPES OF STOMATA. ....	2
FIGURE 2. PROTEIN CASCADE OF QUICK ABA RESPONSE LEADING TO STOMATAL CLOSURE. ....	6
FIGURE 3. PHYLOGENETIC TREE OF THE ARABIDOPSIS THALIANA SHAKER FAMILY POTASSIUM CHANNELS. ....	8
FIGURE 4. PHYLOGENETIC TREE OF THE ARABIDOPSIS THALIANA S-TYPE GENE FAMILY. ....	10
FIGURE 5. PHYLOGENETIC TREE OF THE ARABIDOPSIS THALIANA ALMT FAMILY. ....	12
FIGURE 6. GENERATION OF THE FOUR EXPERIMENTAL PATCH CLAMP CONFIGURATIONS. ....	23
FIGURE 7. VOLTAGE PULSE PROTOCOLS USED FOR MEASUREMENTS OF R-TYPE ANION CHANNEL CURRENTS. ....	28
FIGURE 8. ANALYSIS OF R-TYPE CURRENT MEASUREMENTS. ....	29
FIGURE 9. ANALYSIS OF R-TYPE TAIL CURRENTS. ....	30
FIGURE 10. R-TYPE ANION CHANNEL RESPONSE IN GUARD CELL PROTOPLASTS OF COLUMBIA (COLO) AND THE ALMT12 LOSS-OF-FUNCTION MUTANT. ....	44
FIGURE 11. R-TYPE ANION CHANNEL RESPONSE IN GUARD CELL PROTOPLASTS OF COLO AND THE ALMT12 LOSS-OF-FUNCTION MUTANT TO DIFFERENT CYTOSOLIC CONDITIONS. ....	45
FIGURE 12. R-TYPE ANION CHANNEL RESPONSE OF GUARD CELL PROTOPLASTS OF THE COLUMBIA (COLO) ECOTYPE AND THE ALMT12 LOSS-OF-FUNCTION MUTANT TO CYTOSOLIC ATP. ....	47
FIGURE 13. R-TYPE ANION CHANNEL RESPONSE IN GUARD CELL PROTOPLASTS OF COLO AND THE ALMT12 LOSS-OF-FUNCTION MUTANT UNDER DIFFERENT CYTOSOLIC CALCIUM CONDITIONS. ....	49
FIGURE 14. EXPRESSION OF ALMT12, ALMT13 AND ALMT14 IN GUARD CELL PROTOPLASTS OF COLUMBIA (COLO) AND THE ALMT12 LOSS-OF-FUNCTION MUTANT. ....	50
FIGURE 15. R-TYPE ANION CHANNEL RESPONSE IN GUARD CELL PROTOPLASTS OF COLUMBIA (COLO) AND ALMT12/ALMT13, ALMT12/ALMT14 LOSS-OF-FUNCTION MUTANTS. ....	52
FIGURE 16. R-TYPE ANION CHANNEL RESPONSE IN GUARD CELL PROTOPLASTS OF COLO AND ALMT12/ALMT13 AND ALMT12/ALMT14 LOSS-OF-FUNCTION MUTANTS UNDER DIFFERENT CYTOSOLIC CALCIUM CONDITIONS. ....	53
FIGURE 17. EXPRESSION OF ALMT12, ALMT13, ALMT14, SLAC1 AND SLAH3 IN GUARD CELL PROTOPLASTS OF COLUMBIA (COLO) AND WASSILEWSKIJA (WS) ECOTYPES. ....	55
FIGURE 18. VOLTAGE-INDUCED MACROSCOPIC R-TYPE ANION CURRENTS OF GUARD CELL PROTOPLASTS FROM COLUMBIA (COLO) AND WASSILEWSKIJA (WS) ECOTYPES. ....	56
FIGURE 19. R-TYPE ANION CHANNEL RESPONSE IN GUARD CELL PROTOPLASTS OF COLUMBIA (COLO) AND WASSILEWSKIJA (WS) ECOTYPES TO DIFFERENT CYTOSOLIC CONDITIONS. ....	58
FIGURE 20. R-TYPE ANION CHANNEL RESPONSE OF GUARD CELL PROTOPLASTS OF COLUMBIA (COLO) AND WASSILEWSKIJA (WS) ECOTYPES TO CYTOSOLIC ATP OR AMP-PNP. ....	60
FIGURE 21. SEQUENCE ALIGNMENT OF ATALMT12, ATALMT13 AND ATALMT14. ....	68
FIGURE 22. MODEL OF ALMT12, ALMT13 AND ALMT14 REGULATION DURING STOMATAL MOVEMENT. ....	74

## 10. References

- Ache P., Becker D., Ivashikina N., Dietrich P., Roelfsema M. R., Hedrich R., 2000,** GORK, a delayed outward rectifier expressed in guard cells of *Arabidopsis thaliana*, is a K<sup>+</sup>-selective, K<sup>+</sup>-sensing ion channel, *FEBS Letters* 486, 93-98
- Anderson J. A., Huprikar S. S., Kochian L. V., Lucas W. J., Gaber R. F., 1992,** Functional expression of a probable *Arabidopsis thaliana* potassium channel in *Saccharomyces cerevisiae*, *Proceedings of the National Academy of Sciences of the United States of America*, 89, 3736–3740
- Barbier–Brygoo H., De Angeli A., Filleur S., Frachisse J – M., Gambale F., Thomine S., Wege S., 2011,** Anion channels / transporters in plants: from molecular bases to regulatory networks, *Annual Review of Plant Biology*, 62, 25–51
- Batool S., Uslu V. V1., Rajab H., Ahmad N., Waadt R., Geiger D., Malagoli M., Xiang C. B., Hedrich R., Rennenberg H., Herschbach C., Hell R., Wirtz M., 2018,** Sulfate is incorporated into cysteine to trigger ABA production and stomatal closure, *Plant Cell*, 30, 2973-2987
- Bauer H., Ache P., Lautner S., Fromm J., Hartung W., Al-Rasheid K. A., Sonnewald S., Sonnewald U., Kneitz S., Lachmann N., Mendel R. R., Bittner F., Hetherington A. M., Hedrich R., 2013,** The stomatal response to reduced relative humidity requires guard cell-autonomous ABA synthesis, *Current Biology*, 23, 53–57
- Bertl A., Blumwald E., Coronado R., Eisenberg R., Findlay G., Gradmann D., et al., 1992,** Electrical measurements on endomembranes, *Science*, 258, 873-874
- Biemelt S, Tschiersch H, Sonnewald U. (2004)** Impact of altered gibberellin metabolism on biomass accumulation, lignin biosynthesis, and photosynthesis in transgenic tobacco plants, *Plant Physiology*, 135, 254–265
- Blatt M. R. and Armstrong F., 1993,** K<sup>+</sup> channels of stomatal guard cells: abscisic acid – evoked control of the outward rectifier mediated by cytoplasmic pH, *Planta*, 191, 330–341
- Boursiac Y., Leran S., Corratge-Faillie C., Gojon A., Krouk G., Lacombe B., 2013,** ABA transport and transporters, *Trends in Plant Science*, 18, 325–333

**Brandt B., Brodsky D. E., Xue S., Negi J., Iba K., Kangasjärvi J., Ghassemian M., Stephan A. B., Hu H., Schroeder J. I.**, 2012, Reconstitution of abscisic acid activation of SLAC1 anion channel by CPK6 and OST1 kinases and branched ABI1 PP2C phosphatase action, *Proceedings of the National Academy of Sciences of the United States of America*, 109, 10593–10598

**Brearley J., Venis M. A., Blatt M. R.**, 1997, The effect of elevated CO<sub>2</sub> concentrations on K<sup>+</sup> and anion channels of *Vicia faba L.* guard cells, *Planta*, 203, 145-154

**Briggs W. R., Beck C. F., Cashmore A. R., Christie J. M., Hughes J., Jarillo J. A., Kagawa T., Kanegae H., Liscum E., Nagatani A., Okada K., Salomon M., Rüdiger W., Sakai T., Takano M., Wada M., Watson J. C.**, 2001, The phototropin family of photoreceptors, *Plant Cell*, 13, 993–997

**Brosché M., Merilo E., Mayer F., Pechter P., Puzõrjova I., Brader G., Kangasjärvi J., Kollist H.**, 2010, Natural variation in ozone sensitivity among *Arabidopsis thaliana* accessions and its relation to stomatal conductance, *Plant Cell Environment*, 33, 914–925

**Bruggemann L., Dietrich P., Becker D., Dreyer I., Palme K., Hedrich R.**, 1999, Channel – mediated high – affinity K<sup>+</sup> uptake into guard cells from *Arabidopsis*, *Proceedings of the National Academy of Sciences of the United States of America*, 96, 3298–3302

**Buchner P., Takahashi H., Hawkesford M. J.**, 2004, Plant sulphate transporters: co-ordination of uptake, intracellular and long-distance transport, *Journal of Experimental Botany*, 55, 1765–1773

**Cao M - J., Wang Z., Wirtz M., Hell R., Oliver D. J., Xiang C. B.**, 2012, SULTR3;1 is a chloroplast-localized sulfate transporter in *Arabidopsis thaliana*, *The Plant Journal*, 73, 607-616

**Cao Y., Ward J. M., Kelly W. B., Ichida A. M., Gaber R. F., Anderson J. A., Uozumi N., Schroeder J. I., Crawford N. M.**, 1995, Multiple genes, tissue specificity, and expression-dependent modulation contribute to the functional diversity of potassium channels in *Arabidopsis thaliana*, *Plant Physiology*, 109, 1093–1106

**Chen Y-H., Hu L., Punta M., Bruni R., Hillerich B., Kloss B., Rost B., Love J., Siegelbaum S., Hendrickson W.**, 2010, Homologue structure of the SLAC1 anion channel for closing stomata in leaves, *Nature*, 467, 1074–1080

**Chen Z., Zhao P – X., Miao Z – Q., Qi G – F., Wang Z., Yuan Y., Ahmad N., Cao M – J., Hell R., Wirtz M., Xiang C – B.,** 2019, SULTR3s function in chloroplast sulfate uptake and affect ABA biosynthesis and the stress response, *The Plant Physiology*, DOI: <https://doi.org/10.1104/pp.18.01439>

**Christie J. M.,** 2007, Phototropin blue-light receptors, *Annual Review of Plant Biology*, 58, 21-45

**Christie J. M., Salomon M., Nozue K., Wada M., Briggs W. R.,** 1999, LOV (light, oxygen, or voltage) domains of the blue-light photoreceptor phototropin (*nph1*): binding sites for the chromophore flavin mononucleotide, *Proceedings of the National Academy of Sciences of the United States of America*, 96, 8779-8783

**Collins N. C., Shirley N. J., Saeed M., Pallotta M., Gustafson J. P.,** 2008, An ALMT1 gene cluster controlling aluminium tolerance at the Alt4 locus of rye (*Secale cereale L*), *Genetics*, 179, 669-682

**Cubero-Font P., Maierhofer T., Jaslan J., Rosales M. A., Espartero J., Díaz-Rueda P., Müller H. M., Hürter A - L., Al - Rasheid K. A., Marten I., Hedrich R., Colmenero - Flores J.M., Geiger D.,** 2016, Silent S-type anion channel subunit SLAH1 gates SLAH3 open for chloride root-to-shoot translocation, *Current Biology*, 26, 2213–2220

**Curmi J. P., Premkumar L. S., Birnir B., Gage P. W.,** 1993, The influence of membrane potential on chloride channels activated by GABA in rat cultured hippocampal neurons, *The Journal of Membrane Biology*, 136, 273-280

**Dadacz-Narloch B., Beyhl D., Larisch C., Lo´pez-Sanjurjo E. J., Reski R., Kuchitsu K., Müller T. D., Becker D., Schönknecht G., Hedrich R.,** 2011, A novel calcium binding site in the slow vacuolar cation channel TPC1 senses luminal calcium levels, *The Plant Cell*, 23, 2696–2707

**Davis A. R. and Gunning B. E. S.,** 1992, The modified stomata of the floral nectary of *Vicia faba* L.1. Development, anatomy and ultrastructure, *Protoplasma*, 166, 134–152

**Day I. S., Reddy V. S., Shad Ali G., Reddy S. S. N.,** Analysis of EF-hand-containing proteins in *Arabidopsis*, 2002, *Genome Biology*, 3, research0056.1–research0056.24

**De Angeli A., Baetz U., Francisco R., Zhang J., Chaves M. M., Regalado A.,** 2013, The vacuolar channel VvALMT9 mediates malate and tartrate accumulation in berries of *Vitis vinifera*, *Planta*, 238, 283-291

**De Angeli A., Zhang J., Meyer S., Martinoia E.,** 2013, AtALMT9 is a malate-activated vacuolar chloride channel required for stomatal opening in *Arabidopsis*, *Nature Communications*, 4: 1804. Doi: 10. 1038/ncomms2815

**Delhaize E., Craig S., Beaton C. D., Bennet R. J., Jagadish V. C., Randall P J.,** 1993a, Aluminium tolerance in wheat (*Triticum aestivum* L.) (I. uptake and distribution of aluminium in root apice), *Plant Physiology*, 103, 685–693

**Delhaize E., Ryan P. R., Randall P J.,** 1993b, Aluminium tolerance in wheat (*Triticum aestivum* L.) (II. aluminium-stimulated excretion of malic acid from root apices), *Plant Physiology*, 103, 695–702

**DeSilva D. L. R., Cox R. C., Hetherington A. M., Mansfield T.A.,** 1985, Suggested involvement of calcium and calmodulin in the responses of stomata to abscisic acid, *New Phytologist*, 101, 555-563

**DeSilva D. L. R., Hetherington A. M., Mansfield T. A.,** 1985, Suggested involvement of calcium and calmodulin in the responses of stomata to abscisic – acid, *New Phytologist*, 100, 473-483

**Dietrich P. and Hedrich R.,** 1998, Anions permeate and gate GCAC1, a voltage – dependent guard cell anion channel, *Plant Journal*, 76, 825–835

**Eisenach C., Baetz U., Huck N.V., Zhang J., De Angeli A., Beckers G. J. M., Martinoia E.,** 2017, ABA-induced stomatal closure involves ALMT4, a phosphorylation-dependent vacuolar anion channel of *Arabidopsis*, *The Plant Cell*, 29, 2552–2569

**Emi T., Kinoshita T., Shimazaki K.,** 2001, Specific binding of vf14-3-3a isoform to the plasma membrane H<sup>+</sup>-ATPase in response to blue light and fusicoccin in guard cells of broad bean, *Plant Physiology*, 125, 1115-1125

**Engineer C. B., Hashimoto-Sugimoto M., Negi J., Israelsson-Nordström M., Azoulay-Shemer T., Rappel W. J., Iba K., Schroeder J. I.,** 2016, CO<sub>2</sub> sensing and CO<sub>2</sub> regulation of stomatal conductance: advances and open questions, *Trends in Plant Science*, 21, 16-30

- Epstein E.**, 1953, Mechanism of ion absorption by roots, *Nature*, 171, 83–84
- Ernst L., Goodger J.Q., Alvarez S., Marsh E. L., Berla B., Lockhart E., Jung J., Li P., Bohnert H. J., Schachtman D. P.**, 2010, Sulphate as a xylem-borne chemical signal precedes the expression of ABA biosynthetic genes in maize roots, *Journal Experimental Botany* 61, 3395-3405
- Finkelstein R.**, 2013, Abscisic Acid synthesis and response, *Arabidopsis Book*, 11, e0166
- Fitzsimons P. J., Weyers J. D. B.**, 1986, Volume changes of *Commelina communis* guard cell protoplasts in response to K<sup>+</sup>, light and CO<sub>2</sub>, *Physiologia Plantarum*, 66, 463–468
- Fonoteca G., Silva-Navas J., Benito C., Mestres M. A., Espino F. J., Hernández-Riquer M. V., Gallego F. J.**, 2007, Candidate gene identification of an aluminium-activated organic acid transporter gene at the Alt4 locus for aluminum tolerance in rye (*Secale cereale L.*), *Theoretical and Applied Genetics*, 114, 249-260
- Frachisse J. M., Thomine S., Colcombet J., Guern J., Barbier-Brygoo H.**, 1999, Sulfate is both a substrate and an activator of the voltage-dependent anion channel of Arabidopsis hypocotyl cells, *Plant Physiology*, 121, 263–262
- Franklin K. A., Lerner V. S., Whitelam G. C.**, 2005, The signal transducing photoreceptors of plants, *The International Journal of Developmental Biology*, 49, 653-664
- Franks P. J. and Farquhar G. D.**, 2007, The mechanical diversity of stomata and its significance in gas-exchange control, *Plant Physiology*, 143, 78–87
- Freudenberger H.**, 1940, Die Reaktion der Schliesszellen auf Kohlensäure und Sauerstoffentzug, *Protoplasma*, 35, 15–34
- Gage P. W. and Chung S – H.**, 1994, Influence of membrane potential on conductance sublevels of chloride channels activated by GABA, *Proceedings of the Royal Society B: Biological Sciences*, 255, 167–172
- Gamble F. and Uozomi N.**, 2006, Properties of Shaker – type potassium channel in higher plants, *The Journal of Membrane Biology*, 210, 1-19
- Gao X. Q., Li C. G., Wei P. C., Zhang X. Y., Chen J., Wang X. C.**, 2005, The dynamic changes of tonoplasts in guard cells are important for stomatal movement in *Vicia faba*, *Plant Physiology*, 139, 1207–1216

**Gaymard F., Pilot G., Lacombe B., Bouchez D., Bruneau D., Boucherez J., Michaux-Ferriere N., Thibaud J. B., Sentenac H., 1998, Identification and disruption of a plant shaker – like outward channel involved in K<sup>+</sup> release into the xylem sap, *Cell*, 94, 647-655**

**Geiger D., Scherzer S., Mumm P., Marten I., Ache P., Matschi S., Liese A., Wellmann C., Al-Rasheid K. A. S., Grill E., Romeis T., Hedrich R., 2010, Guard cell anion channel SLAC1 is regulated by CDPK protein kinases with distinct Ca<sup>2+</sup> affinities, *Proceedings of the National Academy of Sciences of the United States of America*, 107, 8023–8028**

**Geiger D., Scherzer S., Mumm P., Stange A., Marten I., Bauer H., Ache P., Matschi S., Liese A., Al-Rasheid K. A. S., Romeis T., Hedrich R., 2009, Activity of guard cell anion channel SLAC1 is controlled by drought – stress signaling kinase – phosphatase pair, *Proceedings of the National Academy of Sciences of the United States of America*, 106, 21425–21430**

**Geiger D., Becker D., Vosloh D., Gambale F., Palme K., Rehers M., Anschuetz U., Dreyer I., Kudla J., Hedrich R., 2009, Heteromeric AtKC1-AKT1 channels in *Arabidopsis* roots facilitate Growth under K<sup>+</sup> - limiting conditions, *Journal of Biological Chemistry*, 284, 21288-21295**

**Geiger D., Maierhofer T., Al-Rasheid K. A. S., Scherzer S., Mumm P., Liese A., Peter A., Wellmann C., Marten I., Grill E., Romeis T., Hedrich R., 2011, Stomatal closure by fast abscisic acid signaling is mediated by the guard cell anion channel SLAH3 and the receptor RCAR1, *Science Signaling*, 4, ra32**

**Geisler M. J., Deppong D. O., Nadeau J. A., Sack F. D., 2003, Stomatal neighbour cell polarity and division in *Arabidopsis*, *Planta*, 216, 571-579**

**Gilroy S., Fricker M. D., Read N. D., Trewavas A. J., 1990, Elevation of cytoplasmic calcium by caged calcium or caged inositol triphosphate initiates stomatal closure, *Nature*, 346, 769 – 771**

**Gilroy S., Fricker M. D., Read N. D., Trewavas A.J., 1991, Role of calcium in signal transduction of *Commelina* guard cells, *Plant Cell*, 3, 333–344**

**Goodger J. Q., Sharp R. E., Marsh E. L., Schachtman D. P., 2005, Relationships between xylem sap constituents and leaf conductance of well-watered and water-stressed maize across three xylem sap sampling techniques, *Journal Experimental Botany* 56, 2389-2400**

**Grabarek Z.**, 2006, Structural basis for diversity of the EF-hand calcium-binding proteins, *Journal of Molecular Biology*, 359, 509-525

**Grabov A. and Blatt M. R.**, 1998, Membrane voltage initiates Ca<sup>2+</sup> waves and potentiates Ca<sup>2+</sup> increases with abscisic acid in stomatal guard cells, *Proceedings of the National Academy of Sciences of the United States of America*, 95, 4778-4783

**Grabov A., Leung J., Giraudat J., Blatt M. R.**, 1997, Alteration of anion channel kinetics in wild-type and *abi1-1* transgenic *Nicotiana benthamiana* guard cells by abscisic acid, *Plant Journal*, 12, 203-213

**Grobler J., Bauer F., Subden R. E., Van Vuuren H. J.**, 1995, The *mae1* gene of *Schizosaccharomyces pombe* encodes a permease for malate and other C4 dicarboxylic acids, *Yeast*, 11, 1485–1491

**Gruber B. D., Delhaize E., Richardson A. E., Roessner U., James R. A., Howitt S. M., Ryan P. R.**, 2011, Characterisation of HvALMT1 function in transgenic barley plants, *Functional Plant Biology*, 38, 163–175

**Gutermuth T., Herbell S., Lassig R., Brosché M., Romeis T., Feijó J. A., Hedrich R., Konrad K. R.**, 2018, Tip-localized Ca<sup>2+</sup>-permeable channels control pollen tube Growth via kinase-dependent R- and S-type anion channel regulation, *New Phytologist*, 218, 1089–1105

**Hamill O. P., Marty A., Neher E., Sakmann B., Sigworth F. J.**, 1981, Improved patch clamp techniques for high-resolution current recording from cells and cell-free membrane patches, *Pflügers Archiv: European Journal of Physiology* 391, 85-100

**Heath O. V. S.**, 1948, Control of stomatal movement by a reduction in the normal carbon dioxide content of the air, *Nature*, 161, 179–181

**Hedrich R. and Becker D.**, 1994, Green circuits: the potential of plant specific ion channels, *Plant Molecular Biology*, 26, 1637–1650

**Hedrich R. and Marten I.**, 1993, Malate – induced feedback regulation of plasma membrane anion channels could provide a CO<sub>2</sub> sensor to guard cells, *The EMBO Journal*, 12, 897-901

**Hedrich R.**, 2012, Ion channels in plants, *Physiological Reviews*, 92, 1777–1811



**Hedrich R., Busch H., Raschke K.**, 1990, Ca<sup>2+</sup> and nucleotide dependent regulation of voltage dependent anion channels in the plasma membrane of guard cells, *The EMBO Journal*, 9, 3889-3892

**Hedrich R., Marten I., Lohse G., Dietrich P., Winter H., Lohaus G., Heldt H – W.**, 1994, Malate-sensitive anion channels enable guard cells to sense changes in the ambient CO<sub>2</sub> concentration, *Plant Journal*, 6, 741–748

**Hetherington A. M. and Woodward F. I.**, 2003, The role of stomata in sensing and driving environmental change, *Nature*, 424, 901–908

**Hill B.**, 1992, *Ionic channel of excitable membranes*, Sinauer. Sunderland, MA

**Hirsch R. E., Lewis B. D., Spalding E. P., Sussman M. R.**, 1998, A role for the AKT1 potassium channel in plant nutrition, *Science*, 280, 918–921

**Hoekenga O. A., Maron L. G., Piñeros M. A., Cançado G. M., Shaff J., Kobayashi Y., Ryan P. R., Dong B., Delhaize E., Sasaki T., Matsumoto H., Yamamoto Y., Koyama H., Kochian L.V.**, 2006, AtALMT1, which encodes a malate transporter, is identified as one of several genes critical for aluminum tolerance in *Arabidopsis*, *Proceedings of the National Academy of Sciences of the United States of America*, 103, 9738–9743

**Hoffland E., Findenegg G. R., Nelemans J. A.**, 1989, Solubilization of rock phosphate by rape, *Plant and Soil*, 113, 155–160

**Hoshika Y., Watanabe M., Carrari E., Paoletti E., Koike T.**, 2017, Ozone-induced stomatal sluggishness changes stomatal parameters of Jarvis-type model in white birch and deciduous oak, *Plant Biology*, 20, 20–28

**Hosy E., Vavasseur A., Mouline K., Dreyer I., Gaymard F., Poree F., Boucherez J., Lebaudy A., Bouchez D., Very AA., Simonneau T., Thibaud J. B., Sentenac H.**, 2003, The *Arabidopsis* outward K<sup>+</sup> channel GORK is involved in regulation of stomatal movements and plant transpiration, *Proceedings of the National Academy of Sciences of the United States of America*, 100, 5549–5554

**Iino M., Ogawa T., Zeiger E.**, 1985, Kinetic properties of the blue-light response of stomata, Proceedings of the National Academy of Sciences of the United States of America, 82, 8019–8023

**Imes D., Mumm P., Böhm J., Al-Rasheid K. A., Marten I., Geiger D., Hedrich R.**, 2013, Open stomata 1 (OST1) kinase controls R-type anion channel QUAC1 in Arabidopsis guard cells, The Plant Journal, 74, 372-382

**Irving H. R., Gehring C. A., Parish R. W.**, 1992, Changes in cytoplasmic pH and calcium of guard cells precede stomatal movements, Proceedings of the National Academy of Sciences of the United States of America, 89, 1790–1794

**Ivashikina N., Becker D., Ache P., Meyerhoff O., Felle H. H., Hedrich R.**, 2001, K<sup>+</sup> channel profile and electrical properties of *Arabidopsis* root hairs, FEBS Letters, 508, 463-469

**Jammes F., Hu H. C., Villiers F., Bouten R., Kwak J. M.**, 2011, Calcium-permeable channels in plant cells, The FEBS Journal, 278, 4262–4276

**Kangasjärvi J., Jaspers P., Kollist H.**, 2005, Signalling and cell death in ozone-exposed plants, Plant, Cell and Environment, 28, 1021–1036

**Keller B. U., Hedrich R., Raschke K.**, 1989, Voltage – dependent anion channels in the plasma membrane of *Vicia faba* guard cells, Nature, 341, 250–253

**Kerstiens G. and Lenzian K. J.**, 1989, Interactions between ozone and plant cuticles. I. Ozone deposition and permeability, New Phytologist, 112, 13–19

**Kim T. H., Bohmer M., Hu H., Nishimura N., Schroeder J. I.**, 2010, Guard cell signal transduction network: advances in understanding abscisic acid, CO<sub>2</sub>, and Ca<sup>2+</sup> signaling, Annual Review of Plant Biology, 61, 561–591

**Kinoshita T., Doi M., Suetsugu N., Kagawa T., Wada M., Shimazaki K.**, 2001, Phot1 and phot2 mediate blue light regulation of stomatal opening, Nature, 414, 656-660

**Kinoshita T., Emi T., Tominaga M., Sakamoto K., Shigenaga A., Doi M., Shimazaki K.**, 2003, Blue-light- and phosphorylation-dependent binding of a 14-3-3 protein to phototropins in stomatal guard cells of broad bean, Plant Physiology, 133, 1453–1463

**Kinoshita T., Nishimura M., Shimazaki K. I.**, 1995, Cytosolic concentration of Ca<sup>2+</sup> regulates the plasma membrane H<sup>+</sup>-ATPase in guard cells of fava bean, *Plant Cell*, 7, 1333-1342

**Kinoshita T., Shimazaki K.**, 2002, Biochemical evidence for the requirement of 14-3-3 protein binding in activation of the guard-cell plasma membrane H<sup>+</sup>-ATPase by blue light, *Plant Cell Physiology*, 43, 1359-1365

**Kline K. G., Barrett – Wilt G. A., Sussman M. R.**, 2010, In planta changes in protein phosphorylation induced by the plant hormone abscisic acid, *Proceedings of the National Academy of Sciences of the United States of America*, 107, 15986–15991

**Kollist H., Moldau H., Mortensen L., Rasmussen S. K., Jorgensen L. B.**, 2000, Ozone flux to plasmalemma in barley and wheat is controlled by stomata rather than by direct reaction of ozone with cell wall ascorbate, *Journal of Plant Physiology*, 156, 645–665

**Kollist, T., Moldau, H., Rasulov, B., Oja, V., Rämme, H., Hüve, K., Jaspers, P., Kangasjärvi, J. and Kollist, H.**, 2007, A novel device detects a rapid ozone-induced transient stomatal closure in intact *Arabidopsis* and its absence in *abi2* mutant, *Plant Physiology*, 129, 796–803

**Kollist H., Nuhkat M., Roelfsema M. R. G.**, 2014, Closing gaps: linking elements that control stomatal movement, *New Phytologist*, 203, 44-62

**Kong S. K. and Lee C. Y.**, 1995, The use of fura 2 for measurement of free calcium concentration, *Biochemical Education*, 23

**Konrad K. R., Maierhofer T., Hedrich R.**, 2018, Spatio-temporal aspects of Ca<sup>2+</sup> signalling: lessons from guard cells and pollen tubes, *Journal of Experimental Botany*, 69, 4195–4214

**Kopcewicz J. and Lewak S.**, 2002, *Fizjologia roślin*, Polskie Wydawnictwo Naukowe

**Kourie J. and Goldsmith M. H.**, 1992, K<sup>+</sup> channels are responsible for an inwardly rectifying current in the plasma membrane of mesophyll protoplasts of *Avena sativa*, *Plant Physiology*, 98, 1087–1097

**Kovermann P., Meyer S., Hörtensteiner S., Picco C., Scholz-Starke J., Ravera S., Lee Y., Martinoia E.**, 2007, The *Arabidopsis* vacuolar malate channel is a member of the ALMT family, *Plant Journal*, 52, 1169–1180

**Kwak J. M., Mori I. C., Pei Z-M., Leonhardt N., Torres M. A., Dangl J. L., Bloom R. E., Bodde S., Jones J. D., Schroeder J. I., 2003, NADPH oxidase AtrbohD and AtrbohF genes function in ROS – dependent ABA signaling in *Arabidopsis*, The EMBO Journal, 22, 2623–2633**

**Kwak J. M., Murata Y., Baizabal-Aguirre V. M., Merrill J., Wang M., Kemper A., Hawke S. D., Tallman G., Schroeder J. I., 2001, Dominant negative guard cell K<sup>+</sup> channel mutants reduce inward-rectifying K<sup>+</sup> currents and light-induced stomatal opening in *Arabidopsis*, Plant Physiology, 127, 473–485**

**Lagarde D., Basset M., Lepetit M., Conejero G., Gaymard F., Astruc S., Grignon C., 1996, Tissue-specific expression of *Arabidopsis* AKT1 gene is consistent with a role in K<sup>+</sup> nutrition, Plant Journal, 9, 195-203**

**Lebaudy A., Very A. A., Sentenac H., 2007, K<sup>+</sup> channels activity in plants: genes, regulations, and functions, FEBS Letters., 581, 2357–2366**

**Lee D. M. and Assmann S. M., 1992, Stomatal responses to light in the facultative Crassulacean acid metabolism species, *Portulacaria afra.*, Plant Physiology, 85, 35-42**

**Lee S. C., Lan W., Buchanan B.B., Luan S., 2009, A protein kinase-phosphatase pair interacts with an ion channel to regulate ABA signaling in plant guard cells, Proceedings of the National Academy of Sciences of the United States of America, 106, 21419-21424**

**Lemitri C. F. and MacRobbie E. A. C., 1994, Role of calcium in the modulation of *Vicia* guard cell potassium channels by abscisic acid: a patch clamp study, The Journal of Membrane Biology, 137, 99-107**

**Leonhardt N., Vavasseur A., Forestier C., 1999, ATP binding cassette modulators control abscisic acid – regulated slow anion channels in guard cells, Plant Cell, 11, 1141–1152**

**Leung J., Orfanidi S., Cheddor F., Mészáros T., Bolte S., Mizoguchi T., Shinozaki K., Giraudat J., Bögre L., 2006, Antagonistic interaction between MAP kinase and protein phosphatase 2C in stress recovery, Plant Science, 171, 596–606**

**Levchenko V., Konrad K. R., Dietrich P., Roelfsema M. R. G., Hedrich R., 2005, Cytosolic abscisic acid activates guard cell anion channels without preceding Ca<sup>2+</sup> signals, Proceedings of the National Academy of Sciences of the United States of America, 102, 4203–4208**

- Li J., Wang X. Q., Watson M. B., Assmann S. M., 2000,** Regulation of abscisic acid – induced stomatal closure and anion channels by guard cell AAPK kinase, *Science*, 287, 300-303
- Li W., de Ollas C., Dodd I. C., 2018,** Long-distance ABA transport can mediate distal tissue responses by affecting local ABA concentrations, *Journal of Integrative Plant Biology*, 60, 16–33
- Ligaba A., Katsuhara M., Ryan P. R., Shibasaka M., Matsumoto H., 2006,** The BnALMT1 and BnALMT2 genes from rape encode aluminum-activated malate transporters that enhance the aluminum resistance of plant cells, *Plant Physiology*, 142, 1294–1303
- Ligaba A., Maron L., Shaff J., Kochian L., Piñeros M., 2012,** Maize ZmALMT2 is a root anion transporter that mediates constitutive root malate efflux, *Plant Cell Environment*, 35, 1185-1200
- Linder B. and Raschke K., 1992,** A slow anion channel in guard – cells, activating at large hyperpolarization, may be principal for stomatal closing, *FEBS Letters*, 313, 27–30
- Lisei de Sá M. E., Conceição Lopes M. J., de Araújo Campos M., Vilela Paiva L., Amorim dos Santos R. M., Aparecida Beneventi M., Pereira Firmino A. A., Grossi de Sá M. F., 2012,** Transcriptome analysis of resistant soybean roots infected by *Meloidogyne javanica*, *Genetics and Molecular Biology*, 35, 272-282
- Logemann J., Schell J., Willmitzer L., 1987,** Improved method for the isolation of RNA from plant tissues, *Analytical Biochemistry*, 163, 16–20
- Ma J. F., Zheng S. J., Matsumoto H., 1997,** Specific secretion of citric acid induced by Al stress in *Cassia tora*, L. *Plant Cell Physiology*, 38, 1019–1025
- Ma Y., Szostkiewicz I., Korte A., Moes D., Yang Y., Christmann A., Grill E., 2009,** Regulators of PP2C phosphatase activity function as abscisic acid sensors, *Science*, 324, 1064-1068
- MacKinnon R., 2003,** Potassium channels, *FEBS Letters.*, 555, 62-65
- MacRobbie E. A. C., 1980,** Osmotic measurements on stomatal cells of *Commelina communis*, *Journal of Membrane Biology*, 53, 189–198

**MacRobbie E. A. C.**, 2000, ABA activates multiple Ca<sup>2+</sup> fluxes in stomatal guard cells, triggering vacuolar K<sup>+</sup> (Rb<sup>+</sup>) release, *Proceedings of the National Academy of Sciences of the United States of America*, 97, 12361-12368

**Maierhofer T., Lind C., Hüttl S., Scherzer S., Papenfuß M., Simon J., Al - Rasheid K. A., Ache P., Rennenberg H., Hedrich R., Muller T. D., Geiger D.**, 2014, A single-pore residue renders the *Arabidopsis* root anion channel SLAH2 highly nitrate selective, *Plant Cell*, 26, 2554–2567

**Malcheska F., Ahmad A., Batool S., Müller H. M., Ludwig-Müller J., Kreuzwieser J., Randewig D., Hänsch R., Mendel R. R., Hell R., Wirtz M., Geiger D., Ache P., Hedrich R., Herschbach C., Rennenberg H.**, 2017, Drought-enhanced xylem sap sulfate closes stomata by affecting ALMT12 and guard cell ABA synthesis, *Plant Physiology*, 174, 798-814

**Marten H., Konrad K. R., Dietrich P., Roelfsema M. R., Hedrich R.**, 2007, Ca<sup>2+</sup>-dependent and -independent abscisic acid activation of plasma membrane anion channels in guard cells of *Nicotiana tabacum*, *Plant Physiol.*, 143, 28–37

**McAdam S. A. M., Manzib M., Rossa J. J., Brodribba T. J., Gomez-Cadenas A.**, 2016, Uprooting an abscisic acid paradigm: shoots are the primary source, *Plant Signaling and Behavior*, 11

**McAinsh M. R., Brownlee C., Hetherington A. M.**, 1990, Abscisic acid-induced elevation of guard cell cytosolic Ca<sup>2+</sup> precedes stomatal closure, *Nature*, 343, 186-188

**Medeiros D. B., Martins S. C. V., Cavalcanti J. H. F., Daloso D. M., Martinoia E., Nunes-Nesi A., DaMatta F. M., Fernie A. R., Araujo W. L.**, 2016, Enhanced photosynthesis and Growth in *atquac1* knockout mutants are due to altered organic acid accumulation and an increase in both stomatal and mesophyll conductance, *Plant Physiology*, 170, 86–101

**Merilo E., Laanemets K., Hu H., Xue S., Jakobson L., Tulva I., Gonzalez-Guzman M., Rodriguez P. L., Schroeder J. I., Broschè M., Kollist H.**, 2013, PYR/RCAR receptors contribute to ozone-, reduced air humidity-, darkness-, and CO<sub>2</sub>-induced stomatal regulation, *Plant Physiology*, 162, 1652–1668

**Meyer S., Mumm P., Imes D., Endler A., Weder B., Al-Rasheid K. A., Geiger D., Marten I., Martinoia E., Hedrich R.**, 2010, AtALMT12 represents an R-type anion channel required for stomatal movement in *Arabidopsis* guard cells, *Plant Journal*, 63, 1054-1062

**Meyer S., Scholz-Starke J., De Angeli A., Kovermann P., Burla B., Gambale F., Martinoia E.,** 2011, Malate transport by the vacuolar AtALMT6 channel in guard cells is subject to multiple regulation, *Plant Journal*, 67, 247-257

**Michard E., Dreyer I., Lacombe B., Sentenac H., Thibaud J. B.,** 2005 Inward rectification of the AKT2 channel abolished by voltage-dependent phosphorylation, *Plant Journal*, 44, 783–797

**Mine A., Berens M.L., Nobori T., Anver S., Fukumoto K., Winkelmüller T.M., Takeda A., Becker D., Tsuda K.,** 2017, Pathogen exploitation of an abscisic acid- and jasmonate-inducible MAPK phosphatase and its interception by *Arabidopsis* immunity, *Proceedings of the National Academy of Sciences of the United States of America*, 114: 7456–7461

**Montillet J.-L. Leonhardt N., Mondy S., Tranchimand S., Rumeau D., Boudsocq M., Garcia A. V., Douki T., Bigeard J., Laurière C., Chevalier A., Castresana C., Hirt H.,** 2013, An abscisic acid-independent oxylipin pathway controls stomatal closure and immune defense in *Arabidopsis*, *PLoS Biol.* 11: e1001513

**Moran N., Ehrenstein G., Iwasa K., Bare C., Mischke C.,** 1984, Ion channels in plasmalemma of wheat protoplasts, *Science*, 126, 835-838

**Mori I. C., Murata Y., Yang Y., Munemasa S., Wang Y-F., Andreoli S., Tiriack H., Alonso J. M., Harper J. F., Ecker J. R., Kwak J. M., Schroeder J. I.,** 2006, CDPKs CPK6 and CPK3 function in ABA regulation of guard cell S-type anion- and Ca<sup>2+</sup>-permeable channels and stomatal closure, *PLoS Biol.* 4 (10), e327

**Mott K.A.,** 1988, Do stomata respond to CO<sub>2</sub> concentrations other than intercellular? *Plant Physiology*, 86, 200–203

**Muir C. D.,** 2015, Making pore choices: repeated regime shifts in stomatal ratio, *Proceedings of the Royal Society B: Biological Sciences*, 282, 20151498

**Mumm P.,** 2010, Electrophysiological analysis of ion fluxes and their regulation in stomatal cell of *Zea mays* and guard cells of *Arabidopsis thaliana*, University of Würzburg, urn: nbn:de: bvb:20-opus-49267

- Mustilli A. C., Merlot S., Vavasseur A., Fenzi F., Giraudat J., 2002, *Arabidopsis* OST1 protein kinase mediates the regulation of stomatal aperture by abscisic acid and acts upstream of reactive oxygen species production, *Plant Cell*, 14, 3089-3099**
- Nadeau J. A. and Sack F. D., 2003, Stomatal development: cross talk puts mouths in place, *TRENDS in Plant Science*, 8, 6**
- Negi J, Matsuda O, Nagasawa T, Oba Y, Takahashi H, Kawai-Yamada M, Uchimiya H, Hashimoto M, Iba K., 2008, CO<sub>2</sub> regulator SLAC1 and its homologues are essential for anion homeostasis in plant cells, *Nature*, 452, 483-486**
- Neher E. and Sakmann B., 1976, Single-channel currents recorded from membrane of denervated frog muscle fibres, *Nature*, 260, 799–802**
- Neher E., 1992, Correction for liquid junction potentials in patch clamp experiments, *Methods in Enzymology*, 207, 123-131**
- Nelson M. and Rinzel J., HH convention, in: Bower J. M. and Beeman D., *The Book of GENESIS: Exploring Realistic Neural Models with the GEneral NEural Simulation System*, 1998, Springer, 35-36**
- Ogasawara Y., Kaya H., Hiraoka G., Yumoto F., Kimura S., Kadota Y., Hishinuma H., Senzaki E., Yamagoe S., Nagata K., Nara M., Suzuki K., Tanokura M., Kuchitsu K., 2008, Synergistic activation of the *Arabidopsis* NADPH oxidase AtrbohD by Ca<sup>2+</sup> and phosphorylation, *Journal of Biological Chemistry*, 283, 8885-8892**
- Pandey S., Zhang W., Assmann S. M., 2007, Roles of ion channels and transporters in guard cell signal transduction, *FEBS Letters*, 581, 2325–2336**
- Park S-Y., Fung P., Nishimura N., Jensen D. R., Fujii H., Zhao Y., Lumba S., Santiago J., Rodrigues A., Chow T. F., Alfred S. E., Bonetta D., Finkelstein R., Provart N. J., Desveaux D., Rodriguez P.L., McCourt P., Zhu J-K., Schroeder J. I., Volkman B. F., Cutler S. R., 2009, Abscisic acid inhibits type 2C protein phosphatases via the PYR/PYL family of START proteins, *Science*, 324, 1068–1071**
- Paton J. A. and Pearce J. V., 1957, The occurrence, structure and functions of the stomata in British bryophytes, *Transactions of the British Bryological Society*, 3, 228-259**



**Pei Z-M., Kuchitsu K., Ward J. M., Schwarz M., Schroeder J. I.,** 1997, Differential abscisic acid regulation of guard cell slow anion channels in *Arabidopsis* wild – type and *abi1* and *abi2* mutants, *Plant Cell*, 9, 409-423

**Pei Z-M., Murata Y., Benning G., Thomine S., Kluesener B., Allen G., Grill E., Schroeder J. I.,** 2000, Calcium channels activated by hydrogen peroxide mediate abscisic acid signalling in guard cells, *Nature*, 406, 731-734

**Peng W., Wu W., Peng J., Li J., Lin Y., Wang Y., Tian J., Sun L., Liang C., Liao H.,** 2018, Characterization of the soybean GmALMT family genes and the function of GmALMT5 in response to phosphate starvation, *Journal of Integrative Plant Biology*, 60, 216–231

**Peterson F. C., Burgie E. S., Park S. Y., Jensen D. R., Weiner J. J., Bingman C. A., Chang C. E. A., Cutler S. R., Phillips G. N., Volkman B. F.,** 2010, Structural basis for selective activation of ABA receptors, *Nature Structural & Molecular Biology.*, 17, 1109–1113

**Piñeros M. A., Cançado G. M., Kochian L. V.,** 2008, Novel properties of the wheat aluminum tolerance organic acid transporter (TaALMT1) revealed by electrophysiological characterization in *Xenopus Oocytes*: functional and structural implications, *Plant Physiology*, 147, 2131–2146

**Piñeros M. A., Cançado G. M., Maron L. G., Lyi S. M., Menossi M., Kochian L. V.,** 2008, Not all ALMT1-type transporters mediate aluminum-activated organic acid responses: the case of ZmALMT1 - an anion-selective transporter, *The Plant Journal*, 53, 352-367

**Raschke K. and Fellows M. P.,** 1971, Stomatal movement in *Zea mays*: shuttle of potassium and chloride between guard cells and subsidiary cells, *Planta*, 101, 296-316

**Raschke K.,** 1979, Movements of stomata, In Haupt, W. and Feinleib, E. (eds), *Encyclopedia of Plant Physiology*, 7, 384-441

**Raschke K., Hedrich R., Reckmann U., Schroeder J. I.,** 1988, Exploring biophysical and biochemical components of the osmotic motor that drives stomatal movement, *Botanica Acta*, 101, 283-294

- Raschke K., Shabahang M., Wolf R.**, 2003, The slow and the quick anion conductance in whole guard cells: their voltage-dependent alternation, and the modulation of their activities by abscisic acid and CO<sub>2</sub>, *Planta*, 217, 639-650
- Rasmussen R., Morrison T., Herrmann M., Wittwer C.**, 1998, Quantitative PCR by continuous fluorescence monitoring of a double strand DNA specific binding dye, *Biochemica*, 2, 8-11
- Raven J. A.**, 2002, Selection pressures on stomatal evolution, *New Phytologist*, 153, 371–386
- Reintanz B., Szyroki A., Ivashikina N., Ache P., Godde M., Becker D., Palme K., Hedrich R.**, 2002, AtKC1 a silent *Arabidopsis* potassium channel  $\alpha$ - subunit modulates root hair K<sup>+</sup> influx, *Proceedings of the National Academy of Sciences of the United States of America*, 99, 4079–4084
- Richardson F., Timothy J. Brodribb, Gregory J. Jordan**, 2017, Amphistomatic leaf surfaces independently regulate gas exchange in response to variations in evaporative demand, *Tree Physiology*, 37, 869–878
- Roelfsema M. R. G. and Hedrich R.**, 2004, In the light of stomatal opening: new insights into 'the Watergate', *New Phytologist*, 167, 665-691
- Roelfsema M. R. G. and Hedrich R.**, 2016, Do stomata of evolutionary distant species differ in sensitivity to environmental signals?, *New Phytologist*, 211, 767–770
- Roelfsema M. R. G., Hedrich R., Geiger D.**, 2012, Anion channels: master switches of stress responses, *Trends in Plant Science*, 17, 221-229
- Roelfsema M. R. G., Levchenko V., Hedrich R.**, 2004, ABA depolarizes guard cells in intact plants, through a transient activation of R- and S-type anion channels, *The Plant Journal*, 37, 578–588
- Roy A. K., Sharma A., Talukder G.**, 1988, Some aspects of aluminum toxicity in plants, *The Botanical Review*, 54, 145–178
- Ruszala E. M., Beerling D. J., Franks P. J., Chater C., Casson S. A., Gray J. E., Hetherington A. M.**, 2011, Land plants acquired active stomatal control early in their evolutionary history, *Current Biology*, 21, 1030–1035

**Ryan P. R., Skerrett M., Findlay G. P., Delhaize E., Tyerman S. D.**, 1997, Aluminum activates an anion channel in the apical cells of wheat roots, *Proceedings of the National Academy of Sciences of the United States of America*, 94, 6547–6552

**Sano T., Kutsuna N., Hasezawa S., Tanaka Y.**, 2008, Membrane trafficking in guard cells during stomatal movement, *Plant Signaling and Behavior*, 3, 233-235

**Sasaki T, Mori IC, Furuichi T, Munemasa S, Toyooka K, Matsuoka K, Murata Y, Yamamoto Y.**, 2010, Closing plant stomata requires a homolog of an aluminum-activated malate transporter, *Plant Cell Physiology*, 52, 354-365

**Sasaki T., Tsuchiya Y., Ariyoshi M., Nakano R., Ushijima K., Kubo Y., Mori I. C., Higashiizumi E., Galis I., Yamamoto Y.**, 2016, Two members of the aluminum-activated malate transporter family, SIALMT4 and SIALMT5, are expressed during fruit development, and the overexpression of SIALMT5 alters organic acid contents in seeds in tomato (*Solanum lycopersicum*), *Plant Cell Physiology*, 57, 2367–2379

**Sasaki T., Yamamoto Y., Ezaki B., Katsuhara M., Ahn S. J., Ryan P. R., Delhaize E., Matsumoto H.**, 2004, A wheat gene encoding an aluminum-activated malate transporter, *Plant Journal*, 37, 645-653

**Schachtman D. P., Schroeder J. I., Lucas W. J., Anderson J. A., Gaber R. F.**. 1992, Expression of an inward – rectifying potassium channel by the *Arabidopsis* KAT1 cDNA, *Science*, 258, 1654-1658

**Schmidt C., Schelle I., Liao Y. J., Schroeder J. I.**, 1995, Strong regulation of slow anion channels and abscisic acid signaling in guard cells by phosphorylation and dephosphorylation events, *Proceedings of the National Academy of Sciences of the United States of America*, 92, 9535–9539

**Schmidt C., Schroeder J. I.**, 1994, Anion selectivity of slow anion channels in the plasma membrane of guard cells (large nitrate permeability), *Plant Physiology*, 106, 383–391

**Schroeder J. I. and Keller B. U.**, 1992, Two types of anion channel currents in guard cells with distinct voltage regulation, *Proceedings of the National Academy of Sciences of the United States of America*, 89, 5025-5029

- Schroeder J. I.**, 1988, K<sup>+</sup> transport properties of K<sup>+</sup> channels in the plasma membrane of *Vicia faba* guard cells, *The Journal of General Physiology*, 92, 667–683
- Schroeder J. I., Allen G. J., Hugouvieux V., Kwak J. M., Waner D.**, 2001, Guard cell signal transduction, *Annual review of plant physiology and plant molecular biology*, 52, 627-658
- Schroeder J. I., Hagiwara S.**, 1989, Cytosolic calcium regulates ion channels in the plasma membrane of *Vicia faba* guard cells, *Nature*, 338, 427–430
- Schroeder J. I., Hedrich R., Fernandez J. M.**, 1984, Potassium selective single channels in guard cell protoplasts of *Vicia faba*, *Nature*, 312, 361-362
- Schroeder J. I., Raschke K., Neher E.**, 1987, Voltage dependence of K<sup>+</sup> channels in guard cell protoplasts, *Proceedings of the National Academy of Sciences of the United States of America*, 84, 4108–4112
- Schroeder J. I., Schmidt C., Sheaffer J.**, 1993, Identification of high-affinity slow anion channel blockers and evidence for stomatal regulation by slow anion channels in guard cells, *The Plant Cell*, 5, 1831-1841
- Schulze C., Sticht H., Meyerhoff P., Dietrich P.**, 2011, Differential contribution of EF-hands to the Ca<sup>2+</sup>-dependent activation in the two-pore channel TPC1, *The Plant Journal*, 68, 424–432
- Schwartz A.**, 1985, Role of Ca<sup>2+</sup> and EGTA on stomatal movements in *Commelina communis* L., *Plant Physiology*, 79, 1003-1005
- Schwarz M., Schroeder J. I.**, 1998, Abscisic acid maintains S – type anion channels activity in ATP – depleted *Vicia faba* guard cells, *FEBS Letters*, 428, 177–182
- Sentenac H., Bonnaeud N., Minet M., Lacroute F., Salmon J – M., Gaymard F., Grignon C.**, 1992, Cloning and expression in yeast of a plant potassium ion transport system, *Science*, 256, 663–665
- Shope J. C., DeWald D. B., Mott K. A.**, 2003, Changes in surface area of intact guard cells are correlated with membrane internalization, *Plant Physiology*, 133, 1314–1321
- Siegel R. S., Xue S., Murata Y., Yang Y., Nishimura N., Wang A., Schroeder J. I.**, 2009, Calcium elevation-dependent and attenuated resting calcium-dependent abscisic acid induction of

stomatal closure and abscisic acid-induced enhancement of calcium sensitivities of S-type anion and inward-rectifying K<sup>+</sup> channels in *Arabidopsis* guard cells, *Plant Journal*, 59, 207-220

**Sirichandra C., Gu D., Hu H. C., Davanture M., Lee S., Djaoui M., Valot B., Zivy M., Leung J., Merlot S., Kwak J. M.**, 2009, Phosphorylation of the *Arabidopsis* AtrbohF NADPH oxidase by OST1 protein kinase, *FEBS Letters*, 583, 2982–2986

**Sirichandra C., Wasilewska A., Vlad F., Valon C., Leung J.**, 2009, The guard cell as a single – cell model towards understanding drought tolerance and abscisic acid action, *Journal Experimental Botany*, 60, 1439–1463

**Smith F. W., Rae A. L., Hawkesford M. J.**, 2000, Molecular mechanisms of phosphate and sulphate transport in plants, *Biochemica et Biophysica Acta*, 1465, 236–245

**Staxén I., Pical C., Montgomery L. T., Gray J. E., Hetherington A. M., McAinsh M. R.**, 1999, Abscisic acid induces oscillations in guard-cell cytosolic free calcium that involve phosphoinositide-specific phospholipase C, *Proceedings of the National Academy of Sciences of the United States of America*, 96, 1779-1784

**Szyroki A., Ivashikina N., Dietrich P., Roelfema M. R., Ache P., Reintanz B., Deekan R., Godde M., Felle H., Steinmeyer R., Palme K., Hedrich R.**, 2001, KAT1 is not essential for stomatal opening, *Proceedings of the National Academy of Sciences of the United States of America*, 98, 2917–2921

**Takanashi K., Sasaki T., Kan T., Saida Y., Sugiyama A., Yamamoto Y., Yazaki K.**, 2016, A dicarboxylate transporter, LjALMT4, mainly expressed in nodules of *Lotus japonicus*, *Molecular Plant-Microbe Interactions Journal*, 29, 584–592

**Takemiya A., Kinoshita T., Asanuma M., Shimazaki K.**, 2006, Protein phosphatase 1 positively regulates stomatal opening in response to blue light in *Vicia faba*, *Proceedings of the National Academy of Sciences of the United States of America*, 103, 13549–13554

**Thomine S., Guern J., Barbier-Brygoo H.**, 1997, Voltage-dependent anion channel of *Arabidopsis* hypocotyls: nucleotide regulation and pharmacological properties, *The Journal of Membrane Biology*, 159, 71-82

**Torsethaugen G., Pell E. J., Assmann S. M.,** 1999, Ozone inhibits guard cell K<sup>+</sup> channels implicated in stomatal opening, *Proceedings of the National Academy of Sciences, USA*, 96, 13577–13582

**Vahisalu T., Kollist H., Wang Y. F., Nishimura N., Chan W. Y., Valerio G., Lamminmäki A., Brosché M., Moldau H., Desikan R., Schroeder J. I., Kangasjärvi J.,** 2008, SLAC1 is required for plant guard cell S – type anion channels function in stomatal signaling, *Nature*, 452, 487–491

**Vahisalu T., Puzõrjova I., Brosché M., Valk E., Lepiku M., Moldau H., Pechter P., Wang Y. S., Lindgren O., Salojärvi J., Loog M., Kangasjärvi J., Kollist H.,** 2010, Ozone-triggered rapid stomatal response involves the production of reactive oxygen species, and is controlled by SLAC1 and OST1, *Plant Journal*, 62, 442–453

**Van Kirk C. A. and Raschke K.,** 1978, Presence of chloride reduces malate production in epidermis during stomatal opening, *Plant Physiology*, 61, 361–364

**Vavasseur A. and Raghavendra A. S.,** 2005, Guard cell metabolism and CO<sub>2</sub> sensing, *New Phytologist*, 165, 665–682

**Vaultier M – N. and Jolivet Y.,** 2014, Ozone sensing and early signaling in plants: an outline from the cloud, *Environmental and Experimental Botany*, 114, 144-152

**Voss L. J., McAdam S. A. M., Knoblauch M., Rathje J. M., Brodribb T., Hedrich R., Roelfsema M. R. G.,** 2018, Guard cells in fern stomata are connected by plasmodesmata, but control cytosolic Ca<sup>2+</sup> levels autonomously, *New Phytologist*, 219, 206-215

**Walter E. G., Weiner J. H., Taylor D. E.,** 1991, Nucleotide sequence and overexpression of the tellurite resistance determinant from the IncHII plasmid pHH1508a, *Gene*, 101, 1-7

**Wang C., Zhang J., Wu J., Brodsky D. E., Schroeder J. I.,** 2018, Cytosolic malate and oxaloacetate activate S-type anion channels in Arabidopsis guard cells, *New Phytologist*, 220, 178-186

**Wang Y., Noguchi K., Ono N., Inoue S-I., Terashima I., Kinoshita T.,** 2014, Overexpression of plasma membrane H<sup>+</sup>-ATPase in guard cells promotes light-induced stomatal opening and enhances plant growth, *Proceedings of the National Academy of Sciences of the United States of America*, 111, 533–538

- Ward J. M., Mäser P., Schroeder J. I.**, 2009, Plant ion channels: gene families, physiology, and functional genomics analyses, *Annual Review of Physiology*, 71, 59-82
- Webb A. A. R. and Hetherington A. M.**, 1997, Convergence of the abscisic acid, CO<sub>2</sub>, and extracellular calcium signal transduction pathways in stomatal guard cells, *Plant Physiology*, 114, 1557-1560
- Webb A. A. R., McAinsh M. R., Mansfield T. A., Hetherington A. M.**, 1996, Carbon dioxide induces increases in guard cell cytosolic free calcium, *Plant Journal*, 9, 297–304
- Wilkinson S., Mills G., Illidge R. Davies W. J.**, 2012, How is ozone pollution reducing our food supply ?, *Journal of Experimental Botany*, 63, 527–536
- Wille A. and Lucas W. J.**, 1984, Ultrastructural and histochemical studies on guard cells, *Planta*, 160, 129-142
- Willmer C. M. and Fricker M.**, 1996, *Stomata*, Springer
- Wilson J. A., Ogunkanmi A. B., Mansfield T. A.**, 1978, Effects of external potassium supply on stomatal closure induced by abscisic acid, *Plant, Cell and Environment*, 1, 199-201
- Xu J., Li H. D., Chen L. Q., Wang Y., Liu L. L., He L., Wu W. H.**, 2006, A protein kinase, interacting with two calcineurin B-like proteins, regulates K<sup>+</sup> transporter AKT1 in *Arabidopsis*, *Cell*, 125, 1347–1360
- Xu M., Gruber B. D., Delhaize E., White R. G., James R. A., You J., Yang Z., Ryan P. R.**, 2015, The barley anion channel, HvALMT1, has multiple roles in guard cell physiology and grain metabolism, *Plant Physiology*, 153, 183–193
- Yamaguchi M. and Kasamo K.**, 2001, Modulation in the activity of purified tonoplast H<sup>+</sup>-ATPase by tonoplast glycolipids prepared from cultured rice (*Oryza sativa L. var. Boro*) cells, *Plant Cell Physiology*, 42, 516-523
- Yamaguchi M., Sasaki T., Sivaguru M., Yamamoto Y., Osawa H., Ahn S. J., Matsumoto H.**, 2005, Evidence for the plasma membrane localization of Al-activated malate transporter (ALMT1), *Plant Cell Physiology*, 46, 812–816
- Young J. J., Mehta S., Israelsson M., Godoski J., Grill E., Schroeder J.I.**, 2006, CO<sub>2</sub> signaling in guard cells: calcium sensitivity response modulation, a Ca<sup>2+</sup>-independent phase, and CO<sub>2</sub>

insensitivity of thegca2 mutant, Proceedings of the National Academy of Sciences of the United States of America, 103, 7506-7511

**Yount R. G.**, 1975, Advances in Enzymology and Related Areas of Molecular Biology, 43, 1-56

**Zeevaart J. A. D.**, 1999, Biochemistry and molecular biology of plant hormones, New Comprehensive Biochemistry, 8

**Zeiger E. and Hepler P., K.**, 1977, Light and stomatal function: blue light stimulates swelling of guard cell protoplasts, Science, 196, 887–889

**Zhang A., Ren H-M., Tan Y-Q., Qi G-N., Yao F-Y., Wu G-L., Yang L-W., Hussain J., Sun S-J., Wang Y-F.**, 2016, S-type anion channels SLAC1 and SLAH3 function as essential negative regulators of inward K<sup>+</sup> channels and stomatal opening in *Arabidopsis*, The Plant Cell, 28, 949-965

**Zhang J.**, 2014, Functional and structural characterization of the vacuolar anion channels AtALMT9 and AtALMT4 in *Arabidopsis thaliana*, Zurich Open Repository and Archive, University of Zurich

**Zhang J., Baetz U., Krugel U., Martinoia E., De Angeli A.**, 2013, Identification of a probable pore forming domain in the multimeric vacuolar anion channel AtALMT9, Plant Physiology, 163, 830-843

**Zhang J., Martinoia E., De Angeli A.**, 2014, Cytosolic nucleotides block and regulate the *Arabidopsis* vacuolar anion channel AtALMT9, Journal of Biological Chemistry, 289, 25581–25589

**Zhang X. C. and Li H.**, 2018, Interplay between the electrostatic membrane potential and conformational changes in membrane proteins, Protein Science, 28, 502-512

**Zheng X., He K., Kleist T., Chen F., Luan S.**, 2015, Anion channel SLAH3 functions in nitrate-dependent alleviation of ammonium toxicity in *Arabidopsis*, Plant Cell Environment, 38, 474-486



## 11. Glossary

<b>ABA</b>	Absciscic Acid
<b>ABC</b>	<b>ATP binding cassette</b>
<b>ABI1</b>	ABA-insensitive 1
<b>ABI2</b>	ABA-insensitive 2
<b>AKT1</b>	<i>Arabidopsis thaliana</i> <b>K<sup>+</sup> Transporter 1</b>
<b>AKT2</b>	<i>Arabidopsis thaliana</i> <b>K<sup>+</sup> Transporter 2</b>
<b>ALMT</b>	<b>Aluminum activated Malate Transporter</b>
<b>Al<sup>3+</sup></b>	Aluminum Cation
<b>ATP</b>	Adenosine Triphosphate
<b>Ca<sup>2+</sup></b>	Calcium Cation
<b>CO<sub>2</sub></b>	Carbon dioxide
<b>CBL</b>	<b>Calcineurin B-Like protein</b>
<b>CIPK 23</b>	<b>CBL-Interacting Protein Kinase 23</b>
<b>Cl<sup>-</sup></b>	Chloride Anion
<b>GORK</b>	<b>Guard cell outward rectifying K<sup>+</sup> channel</b>
<b>H<sup>+</sup></b>	Hydrogen Cation
<b>H<sub>2</sub>O<sub>2</sub></b>	Hydrogen peroxide
<b>K<sup>+</sup></b>	Potassium Cation
<b>KAT1</b>	<b>K<sup>+</sup> Channel <i>Arabidopsis thaliana</i> 1</b>
<b>KAT2</b>	<b>K<sup>+</sup> Channel <i>Arabidopsis thaliana</i> 2</b>
<b>KC1</b>	<b>K<sup>+</sup> Rectifying Channel 1</b>

<b>NADPH</b>	Nicotinamide adenine dinucleotide phosphate
<b>nm</b>	Nanometer
<b>OH<sup>-</sup></b>	Hydroxide Anion
<b>OST1</b>	<b>Open Stomata</b>
<b>PHOT1</b>	<b>Phototropin 1</b>
<b>PHOT2</b>	<b>Phototropin 2</b>
<b>PAR</b>	<b>Photosynthetic Active Radiation</b>
<b>PP1</b>	<b>Protein Phosphatase 1</b>
<b>PP2C</b>	<b>Protein Phosphatase 2C</b>
<b>PYR/PYL/RCAR</b>	Pyrabactin Resistance / PYR1 Like / Regulatory Component of ABA Receptor
<b>ROS</b>	<b>Reactive Oxygene Species</b>
<b>RT – PCR</b>	<b>Real time polymerase chain reaction</b>
<b>R-type</b>	<b>Rapid Anion Channel</b>
<b>SKOR</b>	<b>Stelar K<sup>+</sup> outward rectifier</b>
<b>SLAC1</b>	<b>Slow Anion Channel 1</b>
<b>SnRK</b>	<b>SNF1 Related Kinase</b>
<b>S-type</b>	<b>Slow Anion Channel</b>

## 12. Supplementary information

**Table S1. Values of half activation potential ( $V_{\text{half}}$ ) and charge movement ( $Z_q$ ) received from tail analyses of R-type currents measured for Col0, WS, *almt12*, *almt12/almt13*, *almt12/almt14* under 195 nM and 1850 nM free cytosolic calcium concentration.**

<i>Arabidopsis</i> plant line	Cytosolic free calcium concentration in [nM]	$V_{\text{half}} \pm \text{SEM}$ in [mV]	$Z_q$	Number of experiments
Col0	195	$-115 \pm 1$	$2.02 \pm 0.07$	6
Col0	1850	$-113 \pm 1$	$2.07 \pm 0.09$	10
WS	195	$-118 \pm 1$	$1.86 \pm 0.07$	5
WS	1850	$-112 \pm 1$	$1.98 \pm 0.06$	6
<i>almt12</i>	195	$-116 \pm 1$	$2.05 \pm 0.06$	9
<i>almt12</i>	1850	$-114 \pm 1$	$2.07 \pm 0.06$	12
<i>almt12/almt13</i>	195	$-118 \pm 2$	$1.79 \pm 0.03$	4
<i>almt12/almt13</i>	1850	$-113 \pm 1$	$1.94 \pm 0.06$	7
<i>almt12/almt14</i>	195	$-120 \pm 2$	$2.14 \pm 0.21$	4
<i>almt12/almt14</i>	1850	$-114 \pm 1$	$1.99 \pm 0.06$	3

Measurements were performed under standard bath solution in presence of 5 mM cytosolic ATP and 195 nM or 1850 nM free cytosolic  $\text{Ca}^{2+}$  (Table 1 and Table 2 R1 and R2, Section 3.2.10).  $V_{\text{half}}$  and  $Z_q$  parameters are presented as a means of values calculated by Boltzmann equation from tail currents of individual experiments.

**Table S2. Expression of *ALMT1*, *ALMT3*, *ALMT4*, *ALMT5*, *ALMT6* and *ALMT9* in guard cell protoplasts of Columbia (Col0) and different loss-of-function mutants.**

<i>Arabidopsis</i> plant line	Gen	Mean value of ALMT transcript per 10.000 actin molecules ± SEM
Col0	<i>ALMT1</i>	10 ± 3
Col0	<i>ALMT3</i>	23 ± 4
Col0	<i>ALMT4</i>	366 ± 40
Col0	<i>ALMT5</i>	178 ± 21
Col0	<i>ALMT6</i>	423 ± 35
Col0	<i>ALMT9</i>	317 ± 18
<i>almt12</i>	<i>ALMT3</i>	15 ± 7
<i>almt12</i>	<i>ALMT4</i>	355 ± 70
<i>almt12</i>	<i>ALMT5</i>	254 ± 42
<i>almt12</i>	<i>ALMT6</i>	367 ± 77
<i>almt12</i>	<i>ALMT9</i>	333 ± 50
<i>almt12/almt13</i>	<i>ALMT1</i>	8 ± 4
<i>almt12/almt13</i>	<i>ALMT3</i>	25 ± 7
<i>almt12/almt13</i>	<i>ALMT4</i>	213 ± 13
<i>almt12/almt13</i>	<i>ALMT5</i>	200 ± 29
<i>almt12/almt13</i>	<i>ALMT6</i>	313 ± 20
<i>almt12/almt13</i>	<i>ALMT9</i>	364 ± 14
<i>almt12/almt14</i>	<i>ALMT1</i>	9 ± 3
<i>almt12/almt14</i>	<i>ALMT3</i>	27 ± 5
<i>almt12/almt14</i>	<i>ALMT4</i>	190 ± 30
<i>almt12/almt14</i>	<i>ALMT5</i>	179 ± 23
<i>almt12/almt14</i>	<i>ALMT6</i>	353 ± 88
<i>almt12/almt14</i>	<i>ALMT9</i>	375 ± 25

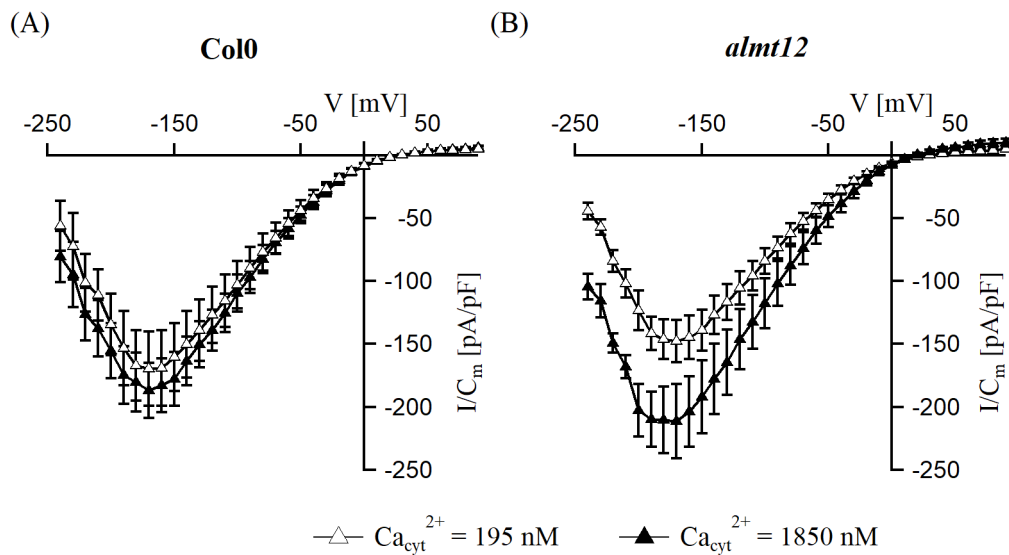


**Figure S1. R-type anion channel response in guard cell protoplasts of Col0 and the *almt12* loss-of-function mutant to 0 mM of the cytosolic ATP concentration under different free cytosolic  $Ca^{2+}$ .**

Steady-state current density ( $I_{ss}/C_m$ ) plotted against corresponding voltages of (A) Col0 and (B) *almt12*. Data points represent mean 5-6 experiments with SEM. Measurements were performed under sulphate conditions in whole – cell configuration.

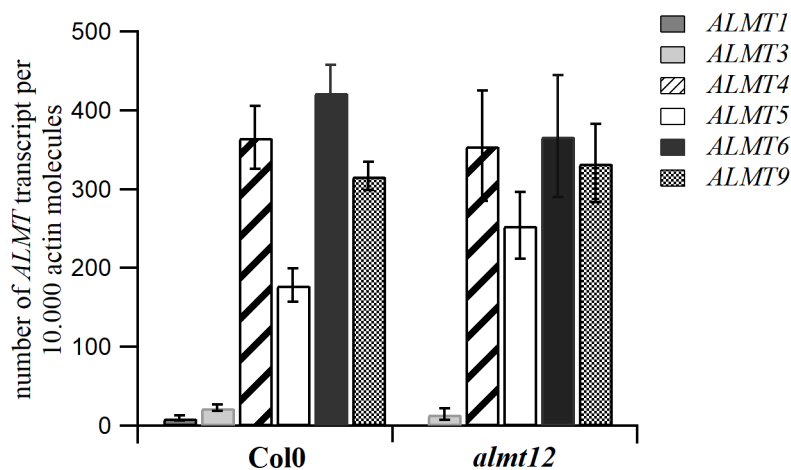


**Figure S2. Expression of ALMT1, ALMT3, ALMT4, ALMT5, ALMT6 and ALMT9 in guard cell protoplasts of Columbia (Col0) and the *almt12* loss-of-function mutant.**

Transcript levels of ALMT1, ALMT3, ALMT4, ALMT5, ALMT6 and ALMT9 in Col0 and the *almt12* loss-of-function mutant. Data represents means  $\pm$  SEMs. The number of independent biological repetition was  $n = 3$ , total number of examined samples was  $n = 7-10$ . Data of ALMT3, ALMT4, ALMT5, ALMT6 and ALMT9 expression were analysed by Dr. Heike Müller (University of Würzburg).

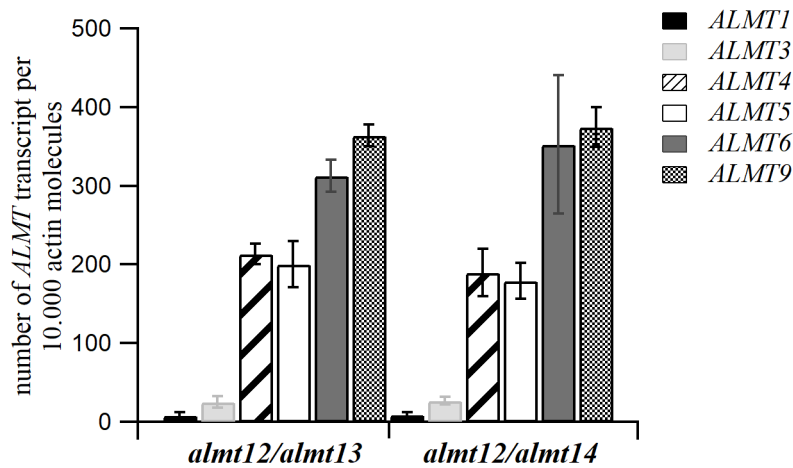


**Figure S3. Expression level of ALMT1, ALMT3, ALMT4, ALMT5, ALMT6 and ALMT9 in guard cell protoplasts of *almt12/almt13* and *almt12/almt14* loss-of-function mutants.**

Transcript levels of ALMT1, ALMT3, ALMT4, ALMT5, ALMT6 and ALMT9 in *almt12/almt13* and *almt12/almt14* loss-of-function mutants. Data represents means  $\pm$  SEMs. The number of independent biological repetition was  $n = 3$ , total number of examined samples was  $n = 7-8$ . Data of ALMT3, ALMT4, ALMT5, ALMT6 and ALMT9 expression were analysed by Dr. Heike Müller (University of Würzburg).

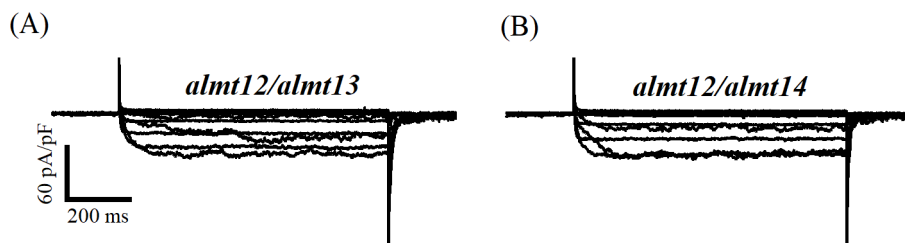


**Figure S4. R-type anion channel response in guard cell protoplasts of *almt12/almt13* and *almt12/almt14* loss-of-function mutants.**

Current traces recorded for R-type anion channels of different ALMTs loss-of-function mutants in response to depolarizing voltage pulses in the range of  $-170$  mV to  $+70$  mV. The voltage pulses were applied in  $+20$  mV increments from holding voltage of  $-170$  mV.

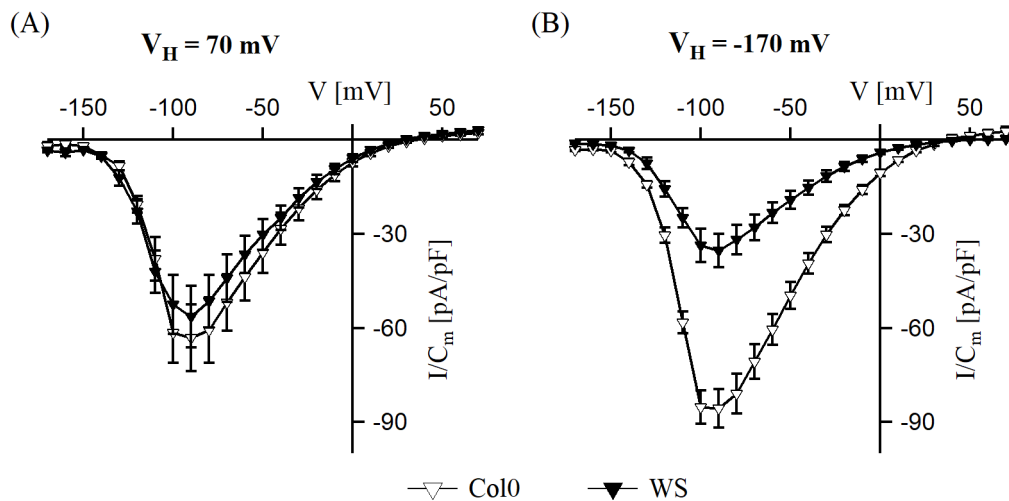


**Figure S5. R-type anion channel response in guard cell protoplasts of Columbia (Col0) and Wassilewskija (WS) ecotypes to different holding potential.**

Steady-state current density ( $I_{ss}/C_m$ ) plotted against corresponding voltages for (A) Col0 and (B) WS. Data points represent mean 5-6 experiments with SEM. Measurements in A and B were done under holding +70 mV or -170 mV respectively. Measurements in A and B were performed in whole – cell configuration Peak current data presented in B are significantly different (\*\*,  $P < 0.01$ , Two-Way Anova followed by Bonferroni test).

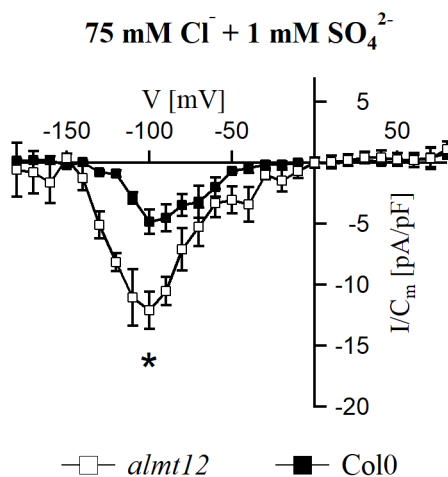


**Figure S6. R-type anion channel response in guard cell protoplasts of Columbia (Col0) and the *almt12* loss-of-function mutant.**

Comparison of steady-state currents density ( $I_{ss}/C_m$ ) plotted against respective voltages, between Col0 and the *almt12* loss-of-function mutant after subtraction of linear component performed by line fit. Data points represents mean of 3 experiments with SEM. Measurement were performed in whole – cell configuration. To quantify significant differences between peak currents - \*,  $P < 0.05$ , One-Way Anova followed by Bonferroni test were used.

## 13. Curriculum Vitae



<b><u>PERSONAL DETAILS</u></b>		
<b>name:</b>	<b>Justyna Joanna Jaślan</b>	
<b>birth name</b>	<b>Kędzierska</b>	
<b>nationality:</b>	Polish	
<b>date of birth:</b>	23 March 1988	
<b>marital status:</b>	married	
<b><u>EDUCATION</u></b>		
<b>2012 - 2016</b>	Experimental work for PhD thesis of Biology at the Julius-Maximilian-Universität in Würzburg	
<b>2011 - 2013</b>	Master studies of Chemistry on the faculty of Chemistry in Maria Curie – Skłodowska University in Lublin, speciality: analytical chemistry	
<b>2010 - 2012</b>	Master studies of Physics on the faculty of Mathematic, Physics and Computer Science in Maria Curie – Skłodowska University in Lublin, speciality: experimental physics an applied	
<b><u>EXPERIENCE</u></b>		
<b>2016 - present</b>	Part-time co-worker in BETAHIEMIS project at the Julius-Maximilian-Universität in Würzburg	
<b><u>PERSONAL QUALITIES</u></b>		
- computer literate	- adaptable	- organized
- quick learner	- ability to work well under stress	
- ambitious		
<b><u>LANGUAGES</u></b>		
Polish - native, English - fluent, German – intermediate, Italian - basic		



## 14. Publication list

- 1) Cubero-Font P., Maierhofer T., **Jaslan J.**, Rosales M. A., Espartero J., Díaz-Rueda P., Müller H. M., Hürter A. L., Al-Rasheid K. A., Marten I., Hedrich R., Colmenero-Flores J. M., Geiger D., 2016, Silent S-Type Anion Channel Subunit SLAH1 Gates SLAH3 Open for Chloride Root-to-Shoot Translocation, *Current Biology*, 26 (16), 2213-2220
- 2) Guzel-Deger A., Scherzer S., Nuhkat M., **Kedzierska J.**, Kollist H., Brosché M., Unyayar S., Boudsocq M., Hedrich R., Roelfsema M. R., 2015, Guard cell SLAC1-type anion channels mediate flagellin-induced stomatal closure, *New Phytologist*, 208 (1), 162-173

## 15. Acknowledgements

*I give heartfelt thanks to my doctoral supervisor  
**Prof. Dr. Rainer Hedrich**  
for sharing knowledge, dedicated time and all important tips.*

*I would like to thank **Prof. Dr. Erhard Wischmeyer**  
for the time he invested as my second referee.*

*I am grateful to **Prof. Dr. Irene Marten**  
for help during measurements, dedicated time and correction of this work.*

*I would like to thank **Dr. Rosalia Deeken, Dr. Kai Konrad**  
and **Dr. M. Rob G. Roelfsema**  
for fruitful discussions and dedicated time.*

*Thanks to all my colleagues in **Botanik I**  
for the friendly atmosphere and Institute life.*

*I heartily thank  
**my Mum, Dad and Brother**  
for your encouragement in all my decisions.*

*Last but not least, special thanks to my husband, **Dawid**,  
for providing support at every difficult moment.*

## 16. Affidavit in English and German

I hereby confirm that my thesis entitled **R-type currents in *Arabidopsis* guard cells: properties and molecular nature** is the result of my own work. I did not receive any help or support from commercial consultants. All sources and / or materials applied are listed and specified in the thesis.

Furthermore, I confirm that the thesis has not yet been submitted as part of another examination process neither in identical nor in similar form.

.....

Place, date

.....

Signature (Justyna Jaślan)

Hiermit erkläre ich an Eides statt, die **R-type Ströme in *Arabidopsis* Schließzellen: Eigenschaften und molekularer Hintergrund**. Eigenständig, d.h. insbesondere selbstständig und ohne Hilfe eines kommerziellen Promotionsberaters, angefertigt und keine anderen als die von mir angegebenen Quellen und Hilfsmittel verwendet zu haben.

Ich erkläre außerdem, dass die Dissertation weder in gleicher noch in ähnlicher Form bereits in einem anderen Prüfungsverfahren vorgelegen hat.

.....

Ort, Datum

.....

Unterschrift (Justyna Jaślan)